Dissertation
with the aim of achieving the degree
doctor rerum naturalium

Characterization of structural requirements for ER export and analysis of turnover of the Golgi-resident *N*-acetylglucosamin-1-phosphotransferase

submitted by

Mine Franke

at the Department of Biology,
Faculty of Mathemathics, Informatics and Natural Sciences,
University of Hamburg

2013 in Hamburg

Genehmigt vom Fachbereich Biologie
der Fakultät für Mathematik, Informatik und Naturwissenschaften
an der Universität Hamburg
auf Antrag von Priv.-Doz. Dr. S. STORCH
Weiterer Gutachter der Dissertation:
Priv.-Doz. Dr. E. KRAMER
Tag der Disputation: 31. Januar 2014

Hamburg, den 16. Januar 2013

Professor Dr. C. Lohr
Vorsitzender des
Fach-Promotionsausschusses Biologie

THE
SCRIPPS
RESEARCH
INSTITUTE

10550 North Torrey Pines Road
La Jolla, California 92037

January 9, 2014

Fachbereich Biologie
Universität Hamburg
Biozentrum Klein Flottbek
- Studienbüro –
Ohnhorststr. 18
D-22609 Hamburg
Germany

Certification of correctness of language
Bestätigung der Korrektheit der englischen Sprache

Dear Sir or Madam,

I certify as a native English speaker that the thesis by Mine Franke titled "Characterization of structural requirements for ER export and analysis of turnover of the Golgi-resident N-acetylglucosamin-1-phosphotransferase" is written in grammatically correct English.

Christopher M Baskerville

Christopher Baskerville, Ph.D.
Staff Scientist, Teyton Lab, IMM-23

Academic advisor
1. Gutachter: PD Dr. rer. nat. Stephan Storch

Co-advisor
2. Gutachter: PD Dr. rer. nat. Edgar Kramer

Date of disputation:
Tag der Disputation: 31. Januar 2014

Eidesstattliche Versicherung

Hiermit erkläre ich an Eides statt, dass ich die vorliegende Dissertationsschrift selbst verfasst und keine anderen als die angegebenen Quellen und Hilfsmittel benutzt habe.

Declaration on oath

I hereby declare, on oath, that I have written the present dissertation by my own and have not used other than the acknowledged resources and aids.

Hamburg, den — Unterschrift

Hamburg, — Signature

Aileme

Contents

1 INTRODUCTION

Eukaryotic cells evolved membrane delineated compartments, like the nucleus, the mitochondria, the peroxisomes and the compartments of the endocytic pathway: the endoplasmic reticulum (ER), the Golgi apparatus, the endosomes and the lysosomes. These organelles provide distinct internal microenvironments with concentrated enzymes, cofactors and substrates to favor particular macromolecular interactions. To integrate activities of the organelles for the benefit of the whole cell, mechanisms are required to transport material between compartments and across the membranes that surround them. Many functional pathways require processes of vesicular trafficking, involving budding of vesicles from one membrane bounded compartment followed by fusion with another.

1.1 Protein folding and quality control in the ER

The ER and the Golgi apparatus constitute early parts of the secretory membrane system. Lipids and proteins are synthetized in the ER, modified in the Golgi apparatus and delivered to the secretory pathway, the cell surface or endosomal system. The ER is the largest of membrane bound intracellular compartments. It is the site of phospholipid and sterol synthesis, as well as the major Ca^{2+} storage site, regulating intracellular Ca^{2+} levels and signaling (Koch, 1990; van Meer, 2005). It consists of an extended array of a three dimensional network of tubules and flat saccules, stretching from the nuclear envelope to the cell surface, providing expanded membrane surface for protein and lipid biosynthesis (Pendin et al, 2011). The rough ER is studded with ribosomes on its cytoplasmic surface, defining areas that are specialized for protein synthesis, folding and degradation (Bravo et al, 2013). The smooth ER is composed of tubular elements lacking ribosomes. It is dedicated to enzymes involved in drug metabolism, lipid and steroid synthesis or calcium uptake and release (Pendin et al, 2011). Other ER regions that lack ribosomes are the nuclear envelope, which surrounds the nucleus, and the ER export sites (ERES), also referred to as transitional ER, which consist of tubular membranes that bud during export of secretory cargo to the Golgi apparatus (Bravo et al, 2013; Budnik & Stephens, 2009). Large multi domain Sec16 proteins localize to ERES and serve as scaffold proteins, concentrating, organizing and stabilizing the coat protein complex II formation (Brandizzi & Barlowe, 2013; Zanetti et al, 2012).

About one third of newly synthetized proteins are translocated from the cytoplasm through the ER membrane into the lumen of the ER or integrated into its membranes by the Sec61 complex, including secretory proteins, ER- and Golgi-resident proteins as well as proteins of endosomes, lysosomes and the plasma membrane. To deliver nascent proteins to the ER membrane the signal recognition particle (SRP) binds a signal sequence as it engages from the ribosome and to the ribosome (ribosome nascent chain complex, RNC), arresting the protein biosynthesis. Signals that mediate translocation into the ER lumen or insertion into the ER membrane are highly divergent in length and shape. The RNC-SRP complex is recruited by the SRP-receptor (SR) to the ER membrane, followed by transfer of the RNC from the SR-SRP to the Sec61 translocon. Subsequently protein synthesis is restarted and the nascent chain is translocated through the pore, while the SRP dissociates from the SR (Nyathi et al, 2013). Concomitant with translocation, signal peptidase cleaves the signal peptide and oligosaccharyltransferase transfers preassembled oligosaccharides on selected asparagine residues, that are specified by the consensus sequence NXS/T (X can be any amino acids/aa except proline) of the polypeptide chain (Aebi, 2013; Nyathi et al, 2013).

The preformed oligosaccharide precursor of glycoproteins is composed of 14 monosaccharides: two *N*-acetylglucosamines, nine mannoses, and three glucoses (GlcNAc2Man9Glc3, Aebi, 2013). It is synthesized in a stepwise manner on the membrane associated carrier molecule dolichol phosphate, a long chained phosphorylated isoprenoid. The initial seven steps of oligosaccharide biosynthesis are executed at the cytosolic side of the ER membrane, after which the molecule is flipped inwards, now facing the ER lumen (Aebi, 2013; Hagiwara & Nagata, 2012). *N*-glycosylation stabilizes the folding of proteins and prevents aggregation (Beers et al, 2013). The ER lumen bears a dense meshwork of chaperones and other modifying enzymes, like calnexin, calreticulin, binding immunoglobulin protein (BiP) and protein disulfide isomerase (PDI) that catalyze the folding and assembly of synthetized proteins (Csala et al, 2012). The ER inherent quality control ensures that only functional correctly folded proteins exit the ER. Markers for misfolding are: exposed hydrophobicity regions, unpaired cysteine residues or aggregation (Ellgaard & Helenius, 2003). Best characterized is the glycan code. *N*-glycans can be sequentially modified by glycosidases I and II resulting in monoglycosylated intermediates. Soluble monoglucosylated glycoproteins associate with calnexin and calreticulin, whereas membrane bound glycoproteins bind to calnexin only. Thereby the proteins are sequestered, preventing their aggregation and exposed to the thiosulfide oxidoreductase

ERp57 (ER protein 57), a member of the (PDI)-like family, which catalyzes intra-molecular disulfide bond interchange during the folding process (Chakrabarti et al, 2011). The oxidizing environment in the ER lumen favors disulfide bond formation, which helps to stabilize proteins (Hagiwara & Nagata, 2012). The chaperone BiP cooperates with the calnexin cycle. It assists in protein folding and oligomerization in the ER lumen by protecting hydrophobic surfaces found at subunit interfaces. The glycoproteins are released when glucosidase II removes the remaining glucose residue from the core glycan. In case the glycoproteins are fully folded they are free to leave the ER (Chakrabarti et al, 2011). Otherwise they are recognized and glycosylated by the folding sensor UDP-Glc-glycoprotein glucose transferase and re-enter the calnexin/calreticulin cycle (Parodi, 2000). If the glycoproteins fail to fold over a number of cycles the probability that terminal mannose residues are trimmed by α-1,2 mannosidase I increases, so that they can be recognized by ER degradation enhancing α-mannosidase (EDEM)-like proteins. EDEMs trim the *N*-glycans extensively to allow efficient ER-associated degradation (ERAD, Vembar & Brodsky, 2008). The misfolded proteins and glycoproteins are targeted to the retranslocation machinery located in the ER membranes. During the translocation into the cytsosol lysine residues of misfolded proteins are modified with polyubiqitin (poly-Ub) chains by the concerted action of E1-Ub-activating-enzymes, E2 Ub-conjugating enzymes and E3 Ub-ligases. Polyubiquitylated proteins are then extracted from the membrane and targeted to the proteasome where they are finally degraded into peptide fragments (Chakrabarti et al, 2011; Gidalevitz et al, 2013).

Accumulation of misfolded proteins in the ER can trigger the unfolded protein response (UPR) by activating expression of specific genes to modify or destroy the misfolded proteins and compensate for decreased capacity of the ER folding (Vembar & Brodsky, 2008). The UPR is mediated by three signal transduction pathways via the double stranded RNA-activated protein kinase (PKR)-like ER kinase (PERK), the activating transcription factor 6 (ATF6) and the inositol requiring kinase 1 (IRE1). All pathways are initiated by dissociation of BIP from those signal transduction components, due to its higher affinity to unfolded proteins. PERK transduces pro- and anti-apoptotic signals by slowing down the translation rate through phosphorylation of eukaryotic initiation factor 2α (elF2α). ATF6 induces expression of chaperones as BIP and apoptosis signals like CCAAT/-enhancer-binding protein homologous protein (CHOP). And finally IRE1 bears endoribonuclease

and serine-threonine kinase activity, transducing pro-apoptotic signals (Chakrabarti et al, 2011).

1.2 ER-Golgi trafficking

Membrane traffic between the ER and Golgi is bidirectional. Anterograde transport of transmembrane cargo proteins from the ER to the ER-Golgi intermediate compartment (ERGIC) and the Golgi apparatus is mediated by ER export motifs present in their cytoplasmic domains, which interact with components of the coat protein complex II (COPII) transport machinery (Bonifacino & Glick, 2004). The COPII coat is composed of five cytosolic proteins (Sar1, Sec23/Sec24 complex, Sec13/Sec31 complex) that are sequentially recruited to the ER membranes (Lord et al, 2013). In vertebrates two Sar1 (Sar1A and B), two Sec23 (Sec23A and B), four Sec24 (Sec24A-D) and two Sec31 (Sec31A and B) paralogs exist (Venditti et al, 2013). In the first step the small GTPase Sar1 (sorting-associated Ras-related 1) is activated by the exchange of GDP by GTP catalyzed by the guanine nucleotide exchange factor (GEF) Sec12 (Fig. 1.1). GTP-bound Sar1 exposes a long N-terminal amphipathic helix which mediates association to ER membranes. Sar1 recruits the Sec23/Sec24 complex. The cargo adaptor Sec24 directly interacts with sorting signals present in the cytosolic domains of transmembrane cargo proteins thereby forming the prebudding complex (Lord et al, 2013). Some cargo enters also unspecifically the COPII-coated vesicles by bulk flow (Martinez-Menarguez et al, 1999; Thor et al, 2009). The prebudding complexes are clustered by the Sec13/Sec31-subcomplex generating COPII-coated vesicles (Fig. 1.1). After fission from ER membranes the COPII coat is released and the vesicles fuse with membranes of the ERGIC (Lord et al, 2013).

Directionality and fidelity of COPII-coated vesicle fusion is mediated by Rab GTPases, tethering factors and integral membrane soluble *N*-ethymaleimide-sensitive factor attachment protein receptor (SNARE) proteins. Rab GTPases interact with extended coiled-coil domain proteins, as p115, *cis*-Golgi matrix proteins of 130 kDa (GM130) and Golgi reassembly stacking protein of 65 kDa (GRASP65). They are recruited by Rab1 GTP to tether vesicles to the acceptor membrane. Rab GTPases interact also with the 170 kDa transport protein particle I (TRAPPI) complex comprising Bet3, Bet5, TRAPP-subunit (TRS) 20, TRS23, TRS31 and TRS33, which exerts GEF activity towards Rab1. Fusion of COPII-coated vesicles with ERGIC membranes depends on a set of four tail anchored

integral membrane SNARE proteins STX5, membrin (GOSR2), Bet1 and Sec22B, that drive membrane bilayer fission (Brandizzi & Barlowe, 2013; Rendon et al, 2013).

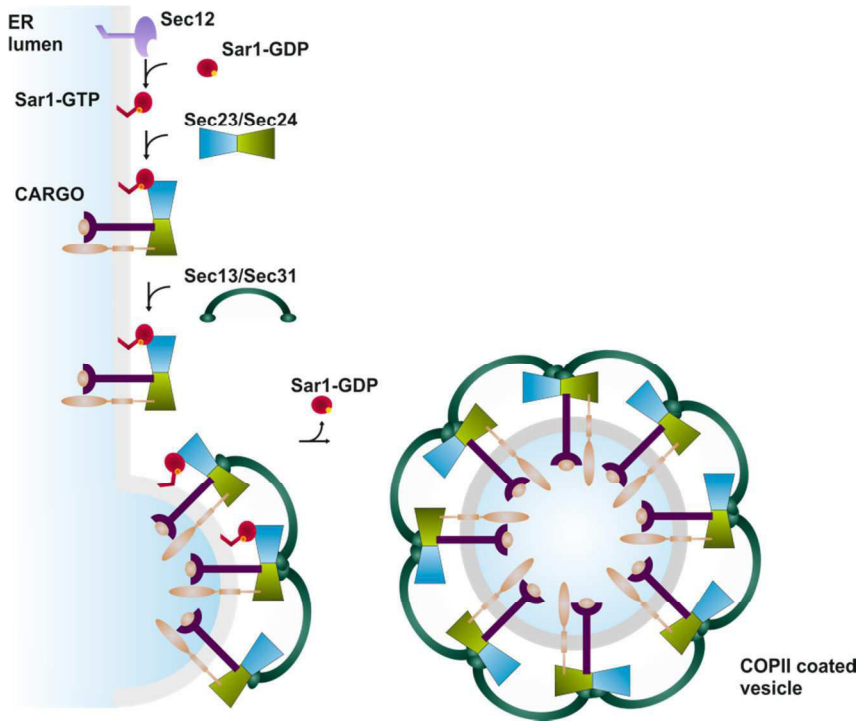

Figure 1.1: Formation of COPII-coated vesicles. ER-resident Sec12 activates the Ras like GTPase Sar1 by facilitating the exchange of GDP by GTP. Subsequently Sar1-GTP associates to the ER membrane and recruits the Sec23/Sec24 heterodimer from the cytosol. Cytoplasmic sorting signals of transmembrane cargo proteins are recognized by Sec24. Finally association of the Sec13/Sec31 heterodimer with the pre-budding complex leads to membrane fission and vesicle formation.

After fusion with membranes of the ERGIC, transmembrane cargo is sorted to the Golgi apparatus by coat protein complex I (COPI)-coated vesicles (Zanetti et al, 2012). The COPI-coated vesicles also mediate the recycling of proteins back to the ER and sorting within the Golgi apparatus. The COPI coat complex, which consists of α-, β-, β'-, γ-, δ-, ε- and ζ-COP and the GTPase ARF1, has a similar morphology as COPII (Popoff et al, 2011). Multisubunit DSL1 and TRAPPII tethering complexes direct SNARE-mediated membrane fission of COPI-coated vesicles with the ER. TRAPPII complexes function as GEF for Rab1, but do not interact directly with SNAREs (Brandizzi & Barlowe, 2013; Rendon et al, 2013). The incorporation in COPI-coated vesicles for retrograde transport to the ER is mediated by dilysine-based KKXX and KXKXX sorting motifs, where X is any amino acid, in the C terminus of type I membrane proteins (Popoff et al, 2011). ER-resident soluble proteins are retrieved from the Golgi apparatus by binding to KDEL receptors via their KDEL motifs (Popoff et al, 2011).

1.3 ER export motifs

Two main classes of ER export motifs have been identified in the C-terminal domains of type I and type III membrane proteins: diacidic motifs which conform to the consensus sequence (DE)X(DE), where X can be any aa and short hydrophobic motifs, like LL, IL, FY, YYM and FF (Barlowe, 2003). Furthermore several unconventional ER export signals have been characterized in N-terminal domains of transmembrane cargo proteins. The N-terminal sequence of the bovine anion exchanger 1 contains an ER export signal with the consensus sequence ΦXΦXΦ, where Φ is a hydrophobic amino acid and X is any amino acid (Otsu et al, 2013). Dibasic motifs which conform to the consensus sequence (RK)X(RK) have been identified in the N-terminal domains of Golgi-resident type II membrane proteins (Giraudo & Maccioni, 2003). A triple arginine motif in the third intracellular loop of the α_{2B} adrenergic receptor functions as a novel ER export signal (Dong et al, 2012). Many proteins contain combinatorial signals composed of any of the above described sorting signals or unconventional signals (Sato & Nakano, 2007). The N-terminal domain of the adiponectin receptor contains a combinatorial ER export motif composed of a $F(X)_3F(X)_3F$ and a $D(X)_3LL$ motif (Juhl et al, 2012). Furthermore heteroligomeric association of Emp46/47 and the Erv41/46 complexes has been shown to be required for efficient ER export (Otte & Barlowe, 2002). In eukaryotic cells four different Sec24 isoforms (Sec24A-D) exist. The Sec24A/B and C/D paralogs are functionally redundant (Wendeler et al, 2007). Sec24 contains at least three different binding sites, which interact with sorting signals and are named "A-site", "B-site" and "R342-site" (Miller et al, 2003; Mossessova et al, 2003). Luminal, soluble cargo proteins, which cannot interact directly with COPII, but also GPI-anchored proteins and some transmembrane proteins rely on transmembrane receptors or adaptors that interact with Sec24 (Venditti et al, 2013). Interaction of Sec24 with transmembrane cargo proteins can be regulated by cargo phosphorylation (Jakobsen et al, 2013) and the assembly state of oligomeric cargoes (Horak et al, 2008; Nufer et al, 2003)

1.4 Structure and functions of the Golgi apparatus in processing and sorting of proteins

The Golgi apparatus provides a platform, connecting anterograde and retrograde protein flow within the secretory pathway (Rendon et al, 2013). It is a dynamic structure composed

of three to nine stacked flat cisternae which can be divided into *cis*-, *medial*-, *trans*-Golgi compartments, surrounded by tubulovesicular elements (Klumperman, 2011). The Golgi matrix connects cisternae and transport vesicles, regulating the membrane traffic and maintaining the Golgi structure.

Newly synthetized proteins and lipids from the ER enter the *cis*-Golgi cisternae and exit from the *trans*-side, taking about 10 to 20 minutes (Rendon et al, 2013). *N*-linked oligosaccharides of proteins and lipids are processed in a protein, cell-type and species specific manner by Golgi-resident glycosyltransferases during their movement from *cis*- to *trans*-Golgi cisternae (Munro, 2011b). They can be modified with fucose, galactose, glucose, *N*-acetylgalactosamine, *N*-acetylglucosamine, glucuronic acid, iduronic acid, mannose, sialic acid and xylose, generating complex- or hybrid-type *N*-linked glycans (Moremen et al, 2012). Other posttranslational modifications include *O*-glycosylation, sulfation of glycans on proteins and glycosaminoglycans, phosphorylation and proteolysis of prohormones, proproteins and viral proteins (Munro, 2011b). The lipid bilayer is modified by the synthesis of sphingolipids/glycolipids and the increase of cholesterol content in the Golgi apparatus.

The *trans*-Golgi network (TGN) is located at the *trans*-side of the Golgi apparatus. It is a tubular vesicular cluster, executing final sorting to endosomes, lysosomes and to secretory granules (Brandizzi & Barlowe, 2013). Furthermore newly synthesized secretory proteins and transmembrane/GPI-anchored proteins are sorted to the extracellular space and to the plasma membrane, respectively (Anitei & Hoflack, 2011). In the TGN final steps in the processing of oligosaccharides, including sulfurylation and sialylation, serine linked *O*-phosphorylation and the proteolytic cleavage of hormone precursors are performed.

The functions of the Golgi-apparatus are mediated by Golgi-resident membrane proteins, for example glycosyltransferases, glycosidases, proteases, and nucleotide sugar transporters (Munro, 2011b). Glycosyltransferases which catalyze the transfer of specific monosaccharides from a sugar-nucleotide to monosaccharides of a growing glycan chain, are the predominant membrane proteins of the Golgi apparatus (Tu & Banfield, 2010). Only few of the Golgi-resident proteins are distributed homogenously. Likewise most proteins and lipids associated with Golgi function like matrix proteins, rab proteins, SNAREs, cholesterol and sphingolipids show a polarized distribution.

For the transport through the Golgi two models have been proposed, the stable cisternae model (Patterson et al, 2008) and the maturing cisternae model (Glick & Luini, 2011). In the first model cisternae are static and secretory cargo is transported forward from one cisterna to the next via vesicles or other intermediates, in the second model the cisternae mature from *cis* to *trans* while changing their composition and Golgi-resident proteins have to be recycled by retrograde vesicles or tubules in synchrony with cisternal progression (Rabouille & Klumperman, 2005). An alternative dual transport model was postulated, proposing that the first two models are complementary and work simultaneously (Rendon et al, 2013).

For vesicular transport in the Golgi apparatus both cytosolic (Rab-GTPases, COPI coat components) and membrane-associated tethering complexes (golgins, COG complexes) are important (Boncompain & Perez, 2013). Rab GTPases control budding, uncoating, mobility and transport of vesicles, by reversible association with sorting adaptors, tethering factors, kinases, phosphatases and motor proteins in their active GTP bound form (Hutagalung & Novick, 2011). Golgi-associated Rabs are Rab1 (ER to Golgi transport, Golgi ribbon maintenance), Rab2 (ER to Golgi transport), Rab6 (maintenance of the Golgi structure, regulation of Golgi in and out transport), Rab33B (Golgi to ER transport), Rab18 and Rab43. Tethering of vesicle is mediated by Golgin tethers or multiprotein COG complexes (Hutagalung & Novick, 2011). Golgins are coiled-coil tethers, which form the Golgi matrix and bind to Rab effectors, providing an initial specificity for membrane fusion and facilitate the formation of SNARE complexes which drives membrane fusion (Munro, 2011a). An example is p115. It interacts with Rab1, ER-Golgi SNARES, conserved oligomeric Golgi (COG) complex-subunits and other coiled-coil proteins, as GM130 or giantine. GM130 interacts with Rab1, Rab2, Rab33B, GRASP65, p115, and others. The multisubunit complex COG is a tether composed of eight different subunits (Miller & Ungar, 2012). It is located in *cis*- and *medial*-Golgi cisternae, where it contributes to recycling of Golgi-resident proteins by interacting with COPI components, syntaxin5 and coiled-coil tethers.

The retention of transmembrane proteins in the Golgi apparatus depends on protein-protein interactions, composition and length of transmembrane and cytosolic domains and on their binding affinity to coat complexes (Rendon et al, 2013). The length and

composition of transmembrane domains (TMD) have been shown to be required for the Golgi retention of SNARE protein syntaxin 5 (Watson & Pessin, 2001), GOLPH2 (Hu et al, 2011) and 1,4-β-galactosyltransferase (Cosson et al, 2013; Masibay et al, 1993). Comparison of the lengths of TMDs from single-spanning membrane proteins of the Golgi apparatus and plasma membrane revealed that the TMDs of Golgi protein are on average four amino acids shorter than those of plasma membrane proteins (Sharpe et al, 2010).

1.5 Lysosomes are major sites of intracellular degradation

Lysosomes are the major sites for intracellular degradative processes. They are organelles of heterogenous size and content that are surrounded by a single lipid bilayer. Lysosomes are biochemically characterized by an acidic pH of 4.7, high Ca^{2+} content, enrichment of lysosomal membrane proteins and the lack of mannose 6-phosphate receptors (MPR, Saftig & Klumperman, 2009). The acidic milieu in the lumen of lysosomes is maintained by the action of V-type H^{+}-ATPases, that transport two protons per hydrolysed ATP into lysosomes (Forgac, 1999). The main function of lysosomes is the degradation of intracellular and extracellular material, which is delivered via endocytosis, phagocytosis or autophagy (Saftig & Klumperman, 2009). They are important for numerous physiological functions including cholesterol homeostasis, plasma membrane repair, remodeling and regeneration of bone tissue, antigen presentation, pathogen defense, metabolic processes and signal transduction (Saftig & Klumperman, 2009; Settembre et al, 2013). Lysosomes contain about 60 different soluble lysosomal enzymes, glycosidases, lipases, nucleases, phosphatases, proteases and sulfatases, which have a pH optimum between 4.5 and 5.0 (Lübke et al, 2009). They contain more than 200 different membrane proteins, which are required for maintenance of the lysosomal membrane integrity, the acidification of the lysosomal lumen, the intracellular motion of lysosomes along microtubules, the selective transport of metabolites like amino acids, fatty acids and carbohydrates into the cytosol, as well as the homo and heterotypic fusion of lysosomes with other organelles (Schröder et al, 2010). Lysosomal proteins are highly glycosylated, which protects them against hydrolysis. In specialized cell types lysosome-related organelles like major histocompatibility complex (MHC) class II compartments, melanosomes, platelet-dense granules and lytic granules are found (Dell'Angelica et al, 2000).

1.6 Biosynthesis of the mannose 6-phosphate recognition marker on lysosomal enzymes

A continuous substitution of lysosomal hydrolases is essential for the biogenesis and function of lysosomes. Newly synthesized proteins must be transported from the ER through the Golgi apparatus and endosomes to the lysosomes. Transport of almost all newly synthesized soluble proteins to lysosomes depends on the presence of the M6P-recognition marker. Newly synthesized soluble lysosomal enzyme precursor proteins are translocated into the ER lumen, where selected asparagine residues are modified with preformed $GlcNAc_2Man_9Glc_3$ core oligosaccharides (Pohl et al, 2009). After processing of the oligosaccharide chains and transport of the lysosomal enzymes to the Golgi apparatus, the biosynthesis of the mannose 6-phosphate (M6P) recognition marker occurs in a two-step reaction (Fig. 1.2, Kollmann et al, 2010).

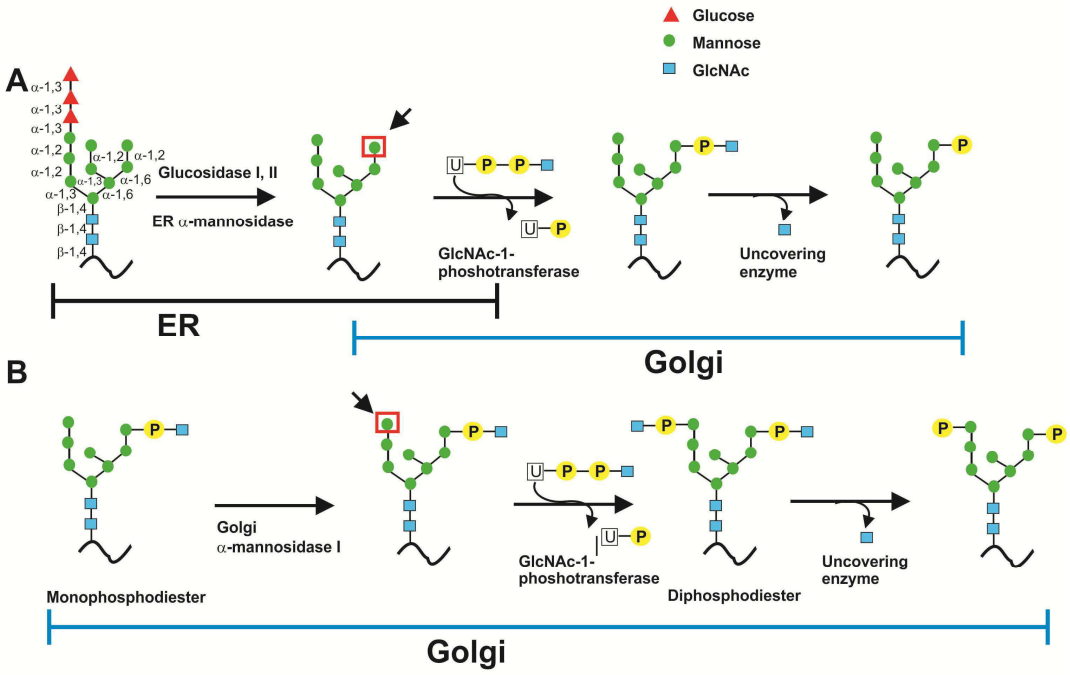

Figure 1.2: Schematic representation of the M6P-formation on *N*-linked glycans of newly synthesized lysosomal hydrolases. (A) High mannose-type *N*-linked oligosaccharides are sequentially modified by glucosidase I and glucosidase II, and ER α-mannosidase(s). In the *cis*-Golgi compartments GlcNAc-1-phosphotransferase transfers GlcNAc-phosphate on terminal mannose residues of the α-1,6 branch. Subsequently the GlcNAc residue is removed by the uncovering enzyme (UCE/GlcNAc-PD), uncovering the M6P-residue. (B) Some of the monophosphorylated oligosaccharides can be phosphorylated also in the α-1,3 branch (Pohl et al, 2009). (Abbrevations: GlcNAc*N*-Acetylglucosamin, U: Uridin).

In the first step, the Golgi-resident GlcNAc-1-phosphotransferase complex (EC 2.7.8.17, PT) transfers *N*-acetyl-glucosamin-1-phosphate (GlcNAc-1-phosphate) from UDP-GlcNAc to hydroxyl groups at position C6 of selected terminal mannose residues of high mannose-type oligosaccharides on lysosomal enzymes, generating a phosphodiester as intermediate product (Lazzarino & Gabel, 1989). In the second step, TGN-localized acetylglucosamin-1-phosphodiester α-*N*-acetylglucosaminidase (EC 3.1.4.45, uncovering enzyme, GlcNAc-1-PD) removes the GlcNAc generating the M6P monoester (Rohrer & Kornfeld, 2001; Waheed et al, 1981). The GlcNAc-1-PD is a 68 kDa type I transmembrane protein, which forms tetramers (Kornfeld et al, 1999). *N*-glycans of lysosomal enzymes might be structurally different and may contain one or two phosphate groups (Fig. 1.2). The generation of M6P residues requires specific recognition of the hydrolases by the GlcNAc-1-phosphotransferase complex. The recognition motif includes neighboring lysine residues on the surface of the hydrolases, which represent a three dimensional structure motif (Pohl et al, 2009).

M6P residues on lysosomal enzymes are bound by two types of M6P-receptors (MPR) in the TGN, the 300 kDa cation-independent MPR300 and the 46 kDa cation dependent MPR46, segregating lysosomal enzymes from the secretory pathway (Fig.1.3, Braulke & Bonifacino, 2009). The receptor ligand complexes are packed into clathrin coated vesicles, which bud from the TGN and fuse with endosomal compartments. Due to the low pH the receptor ligand complexes dissociate and the lysosomal enzyme precursors are further sorted to lysosomes whereas the MPRs recycle back to the TGN to mediate further rounds of transport (Ghosh et al, 2003). Some of the newly synthesized lysosomal enzymes escape binding to MPRs in the TGN and are secreted into the extracellular medium. They are bound by the cell surface-localized MPR300 and are re-internalized and finally delivered to lysosomes (Braulke & Bonifacino, 2009). In lysosomes the M6P residues are removed from lysosomal enzymes by the action of lysosomal acid phosphatases Acp2 or Acp5 and the lysosomal enzyme precursors are activated by proteolytic processing (Makrypidi et al, 2012).

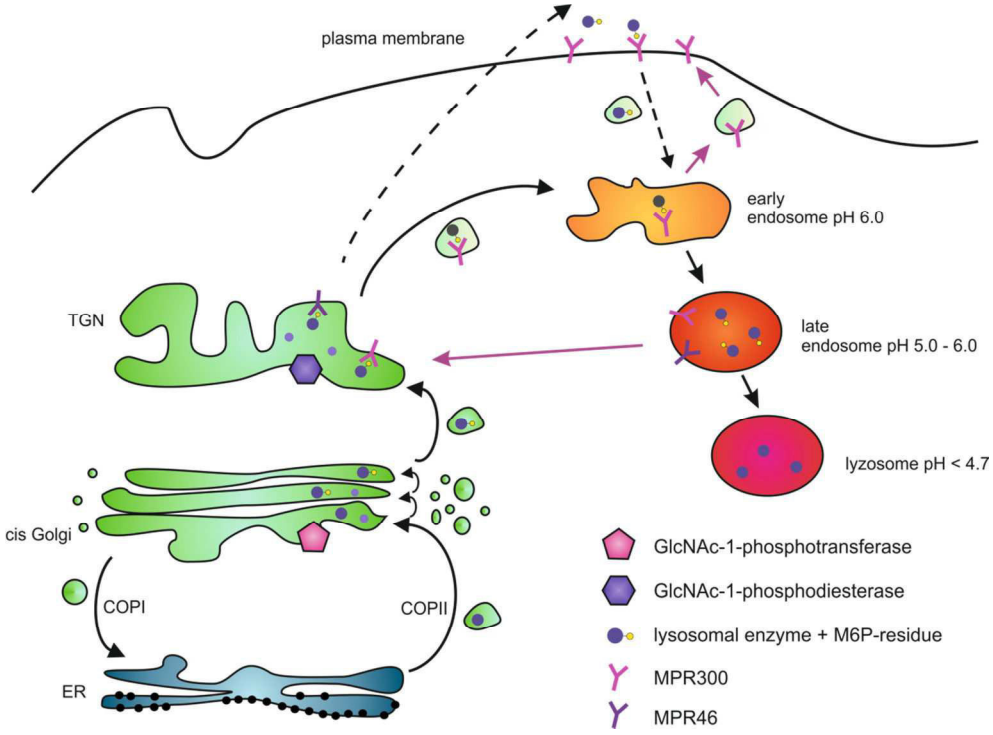

Figure 1.3: M6P-dependent transport of newly synthesized soluble proteins to lysosomes. Soluble lysosomal proteins are synthesized in the ER (blue) and are modified with *N*-linked oligosaccharides in their unfolded conformation. After processing of the oligosaccharide chains and transport to the Golgi apparatus (green), *N*-acetylglucosamin (GlcNAc)-1-phosphate residues are transferred to selected mannose residues by the GlcNAc-1-phosphotransferase. In the TGN the GlcNAc-residues are removed by the GlcNAc-1-phosphodiesterase and the M6P marker is exposed. The M6P receptors MPR300 and MPR46 bind lysosomal enzymes in the TGN and the receptor-ligand complexes are transported to endosomal compartments where they dissociate due to the lower pH. Lysosomal enzymes are further transported to lysosomes whereas the MPRs recycle back to the TGN to mediate further binding of lysosomal enzymes. 5-20% of lysosomal enzymes escape the binding by the MPRs in the TGN and are secreted. These enzymes can be bound by the MPR300 at the cell surface and further transported to lysosomes after internalization.

1.7 Structure and function of the GlcNAc-1-phosphotransferase complex

The 540 kDa bovine GlcNAc-1-phosphotransferase (PT) complex is proposed to contain three subunits, named α, β, and γ, and represents a heterohexameric complex having a $\alpha_2\beta_2\gamma_2$-stochiometry in its catalytically active conformation (Bao et al, 1996). The PT α- and γ-subunits are disulfide-linked homodimers, whereas the two β-subunits are associated non-covalently (Bao et al, 1996). The human Golgi-resident GlcNAc-1-phosphotransferase α/β is encoded by the *GNPTAB* gene (chromosomal localization 12q23.2) and is synthesized as a subunit precursor protein in the ER (Tiede et al, 2005b). The PT α/β-subunit precursor represents a type III membrane protein of 1256 amino acids with a large luminal domain (LD, 1170 aa) containing 20 potential *N*-glycosylation sites and two putative TMDs consisting of 23 aa each (Fig. 1.5, Tiede et al, 2005b). After transport to the Golgi apparatus the PT α/β-subunit precursor is proteolytically cleaved in its LD between residues arginine 928 and glutamine 929 by the site-1 protease (S1P, Fig. 1.4), generating

the mature α- and β-subunits (Kudo & Canfield, 2006; Marschner et al, 2011). S1P is a membrane anchored subtilisin related serine protease, which is located in the *cis*- and *medial*-Golgi compartments (Brown et al, 2000). The 928 amino acid mature PT α-subunit represents a type II membrane protein with a single TMD, 17 potential *N*-glycosylation sites and an N-terminal cytosolic domain of 19 aa. The mature PT β-subunit is a type I-membrane protein of 328 amino acids with three potential *N*-glycosylation sites, a single TMD and a C-terminal cytosolic domain of 21 aa.

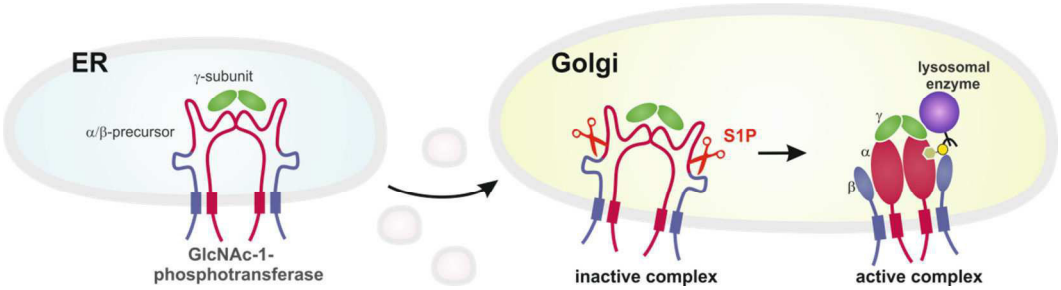

Figure 1.4: ER export and proteolytical activation of the PT complex in the Golgi apparatus. The hexameric PT complex is composed of two α-, two β- and two γ-subunits. The α- and β-subunits are synthethised as a precursor protein in the ER. After transport to the Golgi apparatus the PT α/β-subunit precursor protein is proteolytically activated by the membrane-bound site-1 protease (S1P).

The PT α/β-subunits contain sequence homologies to functionally active domains including four stealth domains, two Notch-repeat like domains and a DMAP binding-like domain and have been shown to carry the catalytic activity of the complex (Fig. 1.5, Qian et al, 2010; Tiede et al, 2005b). The DMAP domain of the PT α-subunit has been shown to bind newly synthesized lysosomal enzymes (Fig. 1.5, Qian et al, 2013). The functions of the soluble γ-subunit, encoded by the *GNPTG* gene (chromosomal localization 16p13.3) are less clear (Raas-Rothschild et al, 2000). The human PT γ-subunit contains 305 amino acids and two used *N*-glycosylation sites in positions 88 and 115 (Encarnacao et al, 2011). After cleavage of the 24 amino acid signal peptide two PT γ-subunits form a homodimer by disulfide bridge linkage of cysteine residues in position 245 that associate with the PT α/β subunits (Encarnacao et al, 2011; Raas-Rothschild et al, 2000).

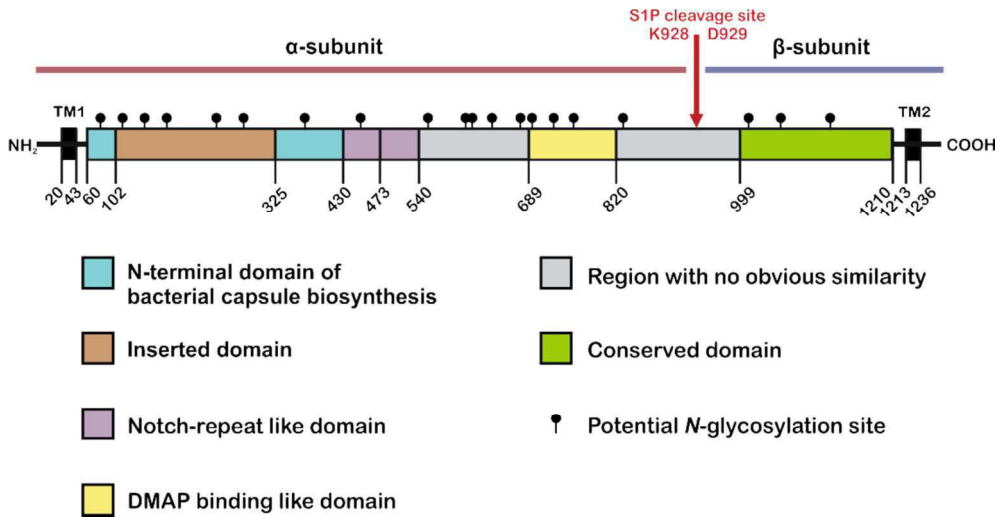

Figure 1.5: Domain organisation of the human PT α/β-subunit precursor protein. The positions and lengths of the domains, potential *N*-glycosylation and the S1P cleavage site (arrow) are indicated in the PT α/β-subunit precursor protein. Length of the mature PT-α and β-subunits are shown by the red and purple lines, respectively.

1.8 Mutations in the *GNPTAB* and *GNPTG* genes result in lysosomal storage disorders

Defects in the stability or the transport or activity of single or multiple lysosomal proteins lead to diseases called lysosomal storage disorders (LSDs), which are characterized by accumulation of non-degraded material and metabolites in the lysosomes (Futerman & van Meer, 2004). LSDs are rare diseases with an overall incidence of 1:5000 and are characterized by a broad spectrum of clinical phenotypes, which vary in their age of onset, the affected organs, the central nervous system manifestations, the severity of symptoms and the reduction of life time (Platt et al, 2012). Most of the LSDs are autosomal recessively inherited disorders and no therapy is available for the majority of those diseases. To date, more than 50 different LSDs are known which are caused by the defective activity of lysosomal proteins or non-lysosomal proteins important for their synthesis and trafficking (Ballabio & Gieselmann, 2009). The majority of mutations in the *GNPTAB* gene result in the severe autosomal recessive lysosomal storage disorder mucolipidosis II (MLII, I-cell disease), alpha/beta (OMIM #252500). To date, 127 different mutations in the *GNPTAB* gene have been described in MLII patients which mostly have nonsense, frame shift or splice site alterations in *GNPTAB* (Cathey et al, 2010). In these patients enzymatic activity is completely absent leading to a clinical phenotype which is characterized by reduced birth weight and length, severe skeletal abnormalities, cardiomegaly, coarse facial features, psychomotor retardation and premature death between

5 and 8 years of age (Braulke et al, 2013; Spranger, 2002). Biochemically the levels of lysosomal enzymes in the serum of patients are increased due to impaired lysosomal targeting and hypersecretion. Characteristic inclusions are present in the mesenchymal cells, especially fibroblasts (Cathey et al, 2010). In a mouse model for MLII carrying a missense mutation by insertion of a single cytosine into exon 16 of the mouse *Gnptab* gene (*Gnptab* $^{c.3082insC}$, pG1028RfsX16), growth retardation, progressive brain atrophy, skeletal abnormalities, elevated lysosomal enzyme activities in serum, lysosomal storage in fibroblasts and brain, infertility and a shortened life span were reported (Kollmann et al, 2012). Selected mutations in the *GNPTAB* gene and all mutations in the *GNPTG* gene lead to the less severe diseases, mucolipidosis III (MLIII) alpha/beta (OMIM # 252600; pseudo-Hurler polydystrophy) and MLIII gamma (OMIM #252605), respectively. MLIII patients retain a low level of phosphotransferase activity. MLIII gamma is a slowly progressive autosomal recessive disorder characterized by a milder phenotype with moderate dysostosis multiplex, progressive joint pain and stiffness, gradual mild coarsening of facial features, lacking psychomotor retardation, and survival into adulthood (Raas-Rothschild et al, 2000). Although the genetic basis for MLII and MLIII is well understood, the consequences of individual mutations present in the PT α-, β-, and γ-subunits on the assembly and stability of the PT complex, the interaction of the subunits, its posttranslational modifications and enzymatic activity, its ER export to the Golgi apparatus, its proteolytic processing and activation are poorly characterized.

1.9 Aims of the Study

The Golgi-resident hexameric GlcNAc-1-phosphotransferase (PT) complex is composed of three subunits, termed α, β and γ. It is the key enzyme in the formation of M6P-residues on newly synthesized soluble lysosomal proteins. The M6P-residue targets the lysosomal enzymes to the lysosomes. Mutations in the PT-coding genes *GNPTAB* and *GNPTG* lead to missorting of lysosomal enzymes to the extracellular space, followed by an accumulation of non-degraded material in the lysosomes, resulting in childhood onset lysosomal storage diseases called mucolipidosis type II and III. The membrane-bound PT α- and β-subunits contain the catalytic site and they recognize and bind the substrates UDP-GlcNAc and mannose residues of lysosomal enzymes. They are synthetized as a type III membrane protein subunit precursor, which is transported to the Golgi apparatus and cleaved by the S1P to the mature PT α- and β-subunits. The proteolytical activation is essential for the activation of the PT complex. Therefor the transport of the precursor protein from the ER to the Golgi apparatus is required.

In the first part of this study the structural requirements for the efficient ER export of the PT α/β subunit precursor protein and its transport to the Golgi apparatus were analyzed. The role of luminal, transmembrane, cytosolic domains and of posttranslational modifications of the PT α/β-subunit precursor protein for ER to Golgi transport was investigated. In the second part of intra-Golgi transport of the PT α/β subunit and the effect of MLIII mutations on the ER export, and the stability of the PT α/β subunit precursor were investigated. The second part of the study mechanisms contributing to the turnover of wild type and mutant Golgi-localized PT α- and β-subunits and the effects of mutations identified in MLIII alpha/beta on the ER export, intracellular localization and the turnover of the PT α/β-subunit precursor protein were studied.

2 Material and Methods

2.1 Material

2.1.1 Equipment, consumables and chemicals

Equipment, consumables and chemicals are listed in Table 2.1, 2.2. and 2.3 respectively.

Table 2.1: Equipment

Device	Model	Manufacturer
Autoclave	3850 EL	Systec, Wettenberg
Balance	AC100 (fine balance)	Mettler Toledo, Gießen
	TE2101	Sartorius, Göttingen
Block thermostat	Block Thermostat BT100	Kleinfeld Labortechnik, Gehrden
	TM130-6	HLC, Bovenden
β-Scintillation Counter	β-Counter LS3801	Beckman Counter, Krefeld
Centrifuge	5424R, 5418, 5415R and 5804R	Eppendorf, Hamburg
	Heraeus Minifuge RF	Thermo Scientific, Waltham, USA
CO_2 incubator	CO_2-Incubator	Sanyo, Bad Nenndorf
	Gasboy C20A	Labotect, Wiesbaden
	Innova CO-170	New Brunswick Scientific, Enfield, USA
Cryogenic freezing unit	Nalgene™ Cryo 1°C	Nalgene, Roskilde, Denmark
Developing machine	Curix 60	Agfa, Mortsel, Belgium
Electrophoresis chamber	Agagel Midi Wide	Biometra, Göttingen
	SE600 (SDS-PAGE)	Hoefer, Holliston, USA
Electrophoresis Power supply	EPS 1001	GE Healthcare, Munich
	Standard Power Pack P25	Biometra, Göttingen
Film developer	Curix 60	Agfa, Leverkusen
Fluorescence plate reader	POLAR star Optima	BMG LABTECH, Ortenberg
Gel dryer	GelAir Dryer	Bio-Rad, Munich
Ice machine	AF10	Scotsman, Herborn
Immunoblot imager	Chemi Doc XRS	Bio-Rad, Munich
Inverted microscope	Axiovert 25	Zeiss, Oberkochen
Laminar flow hoods	Heraeus Herasafe	Thermo Scientific, Waltham, USA
	Gelaire Flow Laboratories	Gelaire, Seven Hills, Australia
Liquid nitrogen cryogenic storage container	Arpege 55	Air Liquide, Düsseldorf
Magnetic stirrer	MSH-basic	IKA-Werke, Staufen

Multichannel electronic pipette	E4 XLS+	Rainin Instrument LLC, Oakland, USA
Confocal microscope	Leica DM IRE2	Leica, Wetzlar
Microwave	Promicro	Microwave Promicro Whirlpool, Stuttgart
pH meter	MP220	Mettler Toledo, Gießen
Photometer	BioPhotometer	Eppendorf, Hamburg
Pipettes	Research	Eppendorf, Hamburg
Pipette controller	Pipetus®	Hirschmann, Eberstadt
Plate reader	MultiscanGo	Thermo Scientific, Waltham, USA
Roller mixer	SRT6 Stuart	Stuart, Staffordshire, UK
Scanner	GT-9600	Epson, Meerbusch
Shaker	Rocky	Fröbel Labortechnik, Lindau
Spinning wheel	Rotator 2-1175	Neolab, Heidelberg
Thermocyclers	Mastercycler	Eppendorf, Hamburg
	Mastercycler, Gradient	Eppendorf, Hamburg
Transfer chamber	TE62 & TE22	Hoefer, Holliston, USA
UV transilluminator and imager	Darkroom Evo III	Raytest, Straubenhardt
Vacuum pump	PC 2004 VARIO	Vacuubrand, Wertheim
Vortex	Genie® 2	Scientific Industries, Bohemia, USA
Water bath	C 10	Water bath C 10 Schütt Labortechnik, Göttingen

Table 2.2: Consumables

Consumable	Company
Amicon Ultra Centrifugal filters 0.5 ml: Ultracel 10 K	Merck, Darmstadt
Coverslips	Glaswarenfabrik Karl Hecht, Sondheim
Cryovials	Nunc, Wiesbaden
Cuvetes	Plastibrand, Wertheim
Disposable material for cell culture	BD, Heidelberg; Sarstedt, Nümbrecht; Nunc, Wiesbaden
Disposable scraper	Sarstedt, Nümbrecht
Film cassettes	Rego, Augsburg
Gel electrophoresis combs	Hoefer, Holliston, USA
Gel glass plates	GE Healthcare, Munich
Immersion oil 518 C	Zeiss, Oberkochen
Lens paper MN 10 B	Zeiss, Oberkochen
Microslides (glass slides)	Glaswarenfabrik Karl Hecht
Pipette tips	Sarstedt, Nümbrecht; Eppendorf, Hamburg
PVDF	GE Healthcare, Munich
Reaction tubes	Sarstedt, Nümbrecht
Scalpels	Braun, Melsungen
Scintillation tubes	Perkin-Elmer, Waltham, USA

Sterile syringe filters	VWR, Darmstadt
Syringes	Braun, Melsungen
UV-cuvettes	Eppendorf, Hamburg
Whatmann papers	Whatman GmbH, Dassel
X-ray films	GE Healthcare, Munich

Table 2.3: Chemicals and reagents

Compound	Company
[^{35}S]-L-methionine (1 mCi/mmol)	GE Healthcare, Munich
1 kb DNA ladder	Invitrogen, Darmstadt
2,5-Diphenyloxazole (PPO)	Roth, Karlsruhe
4',6-Diamidino-2-phenylindole (DAPI)	Roth, Karlsruhe
6x Orange DNA Loading Dye	Fermentas, St. Leon-Rot
Acetic acid	Merck, Darmstadt
Acetone	Merck, Darmstadt
Acrylamide/Bisacrylamide	Roth, Karlsruhe
Agar	Roth, Karlsruhe
Agarose	AppliChem, Darmstadt
Ammonium chloride (NH_4Cl)	Sigma-Aldrich, Deisenhofen
Ammonium peroxodisulfate (APS)	Roth, Karlsruhe
Aqua-Poly/Mounting medium	Polysciences, Warrington, USA
Bovine serum albumin (BSA) powder	Serva, Heidelberg
BSA solution for Bradford (2 mg/ml)	Thermo Scientific, Waltham, USA
Calcium chloride ($CaCl_2$)	Merck, Darmstadt
Carbenicillin	Roth, Karlsruhe
Coomassie® Brilliant Blue G250 and R250	Serva, Heidelberg
Dimethylsulfoxide (DMSO)	Roth, Karlsruhe
di-Sodium hydrogen phosphate di-hydrate (Na_2PO_4 x $2H_2O$)	Merck, Darmstadt
Dithiothreitol (DTT)	Sigma-Aldrich, Deisenhofen
Ethanol	Merck, Darmstadt
Ethidium bromide	Sigma-Aldrich, Deisenhofen
Ethylenediaminetetraacetate (EDTA)	Roth, Karlsruhe
EZ-Link sulfo-NHS-SS-biotin	Thermo Scientific, Waltham, USA
GFP-Trap® A agarose beads	ChromoTek, Martinsried
Glucose	Sigma-Aldrich, Deisenhofen
Glycerol	Roth, Karlsruhe
Glycine	Roth, Karlsruhe
Hydrogen peroxide	Merck, Darmstadt
Kanamycin	Roth, Karlsruhe
Luminol	Roth, Karlsruhe
Magnesium chloride ($MgCl_2$)	Sigma-Aldrich, Deisenhofen
β-mercaptoethanol	Sigma-Aldrich, Deisenhofen
Methanol	Merck, Darmstadt

Milk powder non-fat dry	Roth, Karlsruhe
Mowiol®	Calbiochem, La Jolla, USA
NNN'N'-Tetramethylethylenediamine (TEMED)	Sigma-Aldrich, Deisenhofen
Nonidet P40 (NP40)	Roche Diagnostics, Mannheim
PageRuler™ Prestained Protein Ladder	Fermentas, St. Leon-Rot
Paraformaldehyde	Sigma-Aldrich, Deisenhofen
p-Cumaric acid	Sigma-Aldrich, Deisenhofen
Peptone/tryptone	Roth, Karlsruhe
Saponin	Sigma-Aldrich, Deisenhofen
Sodium chloride (NaCl)	Roth, Karlsruhe
Sodium deoxycholate	Merck, Darmstadt
Sodium dodecyl sulfate (SDS)	Sigma-Aldrich, Deisenhofen
Streptavidin Plus Ultra-Link Resin	Thermo Scientific, Waltham, USA
Sucrose	Sigma-Aldrich, Deisenhofen
Triton X-100	Sigma-Aldrich, Deisenhofen
Trizma base (Tris-Cl)	Sigma-Aldrich, Deisenhofen
Tween 20	Sigma-Aldrich, Deisenhofen
Ultrapure dNTP mix (10 mM each)	GE Healthcare Life Sciences, Munich
Yeast extract	Roth, Karlsruhe

2.1.2 Expression vectors, cDNAs and primers

The mammalian expression vectors and cDNA's used for cloning and expression are listed in Tables 2.4 and 2.5, respectively.

Table 2.4: Vectors

Vector	Size	Selection marker	Source
pcDNA™3.1D/V5 -His-TOPO®	5.4 kb	ampicillin/neomycin	Invitrogen, Darmstadt
pCR Blunt TOPO	3.5 kb	kanamycin	Invitrogen, Darmstadt
pCS2 mCherry	6.5 kb	ampicillin/neomycin	provided by Dr. C. Weber, UKE, Hamburg
pDisplay	5.3 kb	ampicillin/neomycin	Invitrogen, Darmstadt
pEGFP-N1	4.7 kb	kanamycin/neomycin	ClonTech, Palo Alto, USA
pFROG	5.0 kb	ampicillin/neomycin	provided by Dr. Schwake, University of Bielefeld, Bielefeld

Table 2.5 cDNAs

cDNA	GenBank™ accession no	Source
Furin	NM_002569	provided by Dr. Pohl, UKE, Hamburg
GlcNAc-1-phosphodiesterase	NM_016256.3	provided by Dr. Kornfeld, Washington University, St. Louis, USA
GNPTAB	NM_024312	provided by Dr. Storch, UKE, Hamburg
Sar1A	NM_001142648	imagENES, Berlin
SCRAB/LIMP-2 ER-Ret	NM_005506	provided by Dr. Schwake, University of Kiel, Kiel
β-Gal 3'-sulfotransferase GP3ST	AB040610	provided by Dr. Honke, Osaka University Medical School, Osaka, Japan

All oligonucleotides used for PCR, mutagenesis and sequencing were purchased from MWG Biotech Munich; (Tab. 2.6, 2.7 and 2.8).

Table 2.6: Sequences of primers used for site-directed mutagenesis

Construct	Sequences of oligonucleotides
PT α/β-Myc	F: 5'-CAC CAT GCT GTT CAA GCT CCT GCA G-3' R: 5'-CTA CAG ATC CTC TTC TGA GAT GAG TTT TTG TTC TAC TCT GAT TCG ATT GGG ACT-3'
PT α-Myc	F: 5'-CAC CAT GCT GTT CAA GCT CCT GCA G-3' R: 5'-CTA CAG ATC CTC TTC TGA GAT GAG TTT TTG TTC AAG TGC AAT TAA CTG CTC AGC-3'
HA-PT β	F: 5'-CCG CGG TGA TAC ATT TGC AGA TTC CCT C-3' R: 5'-GTC GAC CTA TAC TCT GAT TCG ATT GGG-3'
PT α/β-Myc $^{5}LL^{6}\rightarrow AA$	F: 5'-CGA TTC ACC ATG CTG TTC AAG GCC GCG CAG AGA CAG ACC TAT AC-3' R: 5'-GGT ATA GGT CTG TCT CTG CGC GGC CTT GAA CAG CAT GGT GAA TCG-3'
PT α/β-Myc $^{1236}KRK^{1238}\rightarrow AAA$	F: 5'-GCT GAG CAG TTA ATT GCA CTT GCG GCG GCG ATA TTT CCC AGA AGG AGG-3' R: 5'-CCT CCT TCT GGG AAA TAT CGC CGC CGC AAG TGC AAT TAA CTG CTC AGC-3'
PT α/β-Myc $^{1242}RRR^{1244}\rightarrow AAA$	F: 5'-G CGG AAG ATA TTT CCC GCA GCG GCG ATA CAC AAA GAA GCT AGT CCC-3' R: 5'-GGG ACT AGC TTC TTT GTG TAT CGC CGC TGC GGG AAA TAT CTT CCG C-3'
PT α/β-Myc $^{1253}RIR^{1255}\rightarrow AAA$	F: 5'-CAC AAA GAA GCT AGT CCC AAT GCA GCC GCA GTA GAA CAA AAA CTC ATC TCA G-3' R: 5'-C TGA GAT GAG TTT TTG TTC TAC TGC GGC TGC ATT GGG ACT AGC TTC TTT GTG-3'
PT α/β-Myc $K^{4}\rightarrow Q$	F: 5'-CGA TTC ACC ATG CTG TTC CAG CTC CTG CAG AGA CAG ACC-3' R: 5'-GGT CTG TCT CTG CAG GAG CTG GAA CAG CAT GGT GAA TCG-3'
PT α/β-Myc	F: 5'-CGA TTC ACC ATG CTG TTC GCG CTC CTG CAG AGA

$K^4 \rightarrow A$	CAG-3’ R: 5’-CTG TCT CTG CAG GAG CGC GAA CAG CAT GGT GAA TCG-3’
PT α/β-Myc	F: 5’-C ACC ATG CTG TTC AGG CTC CTG CAG AGA C-3’
$K^4 \rightarrow R$	R: 5’-G TCT CTG CAG GAG CCT GAA CAG CAT GGT G-3’
PT α/β-Myc	F: 5’-CAG AAT CGG CTT TCT CTG CCC ATG CCG-3’
$C^{70} \rightarrow S$	F: 5’-CGG CAT GGG CAG AGA AAG CCG ATT CTG-3’
PT α/β-Myc	F: 5’-ATC GAA GGG CTG TTC CAG AAG TTT ATT-3’
$S^{399} \rightarrow F$	R: 5’-AAT AAA CTT CTG GAA CAG CCC TTC GAT-3’
PT α/β-Myc	F: 5’-GCA AAA ATA CTG GGG CGC AAC TAA AAG AT-3’
$R^{925} \rightarrow A$	R: 5’-ATC TTT TAG TTG CGC CCC AGT ATT TTT GC-3’
PT α/β-Myc	F: 5’-CAG TTA ATT GCA CTT ATG CGG AAG ATA TTT CCC-3’
$K^{1236} \rightarrow M$	R: 5’-GGG AAA TAT CTT CCG CAT AAG TGC AAT TAA CTG-3’
PT α/β-Myc ER-Ret	F: 5’-AAA CTT ATT TCT GAA GAA GAT CTG AAG CAC ATC CTC TTC CGA CGG AGG-3’ R: 5’-GCG GCC GCG AAT TCA CTA GTG ATT CTA CTG CCT GAA GCC CCT TCT CCT-3’
PT α/β-Myc F	F: 5’-TAC TTC ACT GAT AGC AAA AAT AGA GCG AGG TAT AAA AGA GAT ACA-3’ R: 5’-GAG GGA ATC TGC AAG TGT ATC TCT TTT ATA CCT CGC TCT ATT TTT-3’

Table 2.7: Sequences of primers used for generation of mega primers

Construct	Sequences of oligonucleotides
PT α/β-Myc LD-LIMP-2	F: 5’-TTCCAG TTC GGA GAG GTG GGT CTG CGA GTC TTT CAG AAG GCG GTA-3’ R: 5’-AAT CAA TGT TGC TAG TAC AGA ATG AGT CGT GTT AAT CAC AGA CTT-3’
PT α/β-Myc TM1 LIMP-2	F: 5’-ACC TGC CTG TCC CAC AGG TAT GGG TGC TTC TAC ACG GCG GGG ACG-3’ R: 5’-ATG GTA TTG ATC TCG GCT CCA TTC AGC CAC TAG CAG CGT GAC GCT-3’
PT α/β-Myc TM2 LIMP-2	F: 5’-CGA GAC AAA TTG AAG TTT TGG ACC TTG GTT GTC ACC AAC ATA CCC-3’ R: 5’-CCT TCT GGG AAA TAT CTT CCG CTT ACA CGC CAG CCA CGT GAA AAC-3’
PT α/β-Myc NT→10A	F: 5’-GCC GCG GGA ATT CGA TTC ACC ATG GCT GCT GCA GCA GCA GCG GCT -3’ R: 5’-GAC GCC CAA GAA GCA CAC GTA GAG GGC GGC CGC AGC TGC TGC TGC-3’
PT α/β-Myc CT→10A	F: 5’-TTT GCT GAG CAG TTA ATT GCA CTT GCT GCT GCA GCA GCA GCG GCT-3’ R: 5’-CTC TTC TGA GAT GAG TTT TTG TTC TGC TGC TGC TGC CGC AGC TGC-3’
PT α/β-GFP	F: 5’-GCT AGT CCC AAT CGA ATC AGA GTA GTG AGC AAG GGC GAG GAG CTG-3’ R: 5’-TTC TGA GAT GAG TTT TTG TTC TTA CTT GTA CAG CTC GTC CAT G-3’

Table 2.8: Sequences of primers used for sequencing

Construct	Sequences of oligonucleotides
Seq 1	5'-ATT AAG GTG CCA ATG CTT GTC-3'
Seq 2	5'-ATT CAG AGG CCA GTG TAG CGC-3'
Seq 3	5'-TAC CTA AAT GAT GAT GTC ATG-3'
Seq 4	5'-GTT TGA TGC TGG CGA CTG TGG-3'
Seq 5	5'-TAA CAC TTC TTC CAG AGG CGG-3'
Seq 6	5'-TCA TGA CCA GGG TCA GAA TCC-3'
Seq 7	5'-TTG CAG ATT CCC TCA GAT ATG-3'
Seq 8	5'-TTC CTG CTG ATA TCA CGC AGC-3'
Seq 9	5'-GAA TGG AGG GCT TAT CGA GAC-3'

All primers are forward directed.

Knockdown of genes was performed using silencing RNAs (siRNAs) purchased from Dharmacon (Pittsburg, USA), Qiagen (Valencia, USA) and Invitrogen (Carlsbad, USA).

2.1.3 Kits, assays, enzymes, inhibitors and antibodies

Table 2.9: Kits and Assays

Product	Company
BCA Protein Assay	Roth, Karlsruhe
Bio-Rad Protein Assay	Bio-Rad, München
Fire Silver Staining Kit	Proteome Factory, Berlin
Gene Jet™ Gel Extraction Kit	Thermo Scientific, St. Leon-Rot
GeneJet™ Plasmid Miniprep Kit	Thermo Scientific, St. Leon-Rot
QIAplasmid® Midi Kit	QIAGEN, Hilden
QIAquick® Gel Extraction Kit (50)	QIAGEN, Hilden

Table 2.10: Enzymes

Enzyme	Company
Endoglycosidase H (Endo H); 0.005 U/µl	New England Biolabs, Frankfurt
Peptide-*N*-glycosidase F (PNGase F); 1 U/µl	Roche, Mannheim
Phusion™ High-Fidelity DNA polymerase; 2 U/µl	Thermo Fisher Scientific, Waltham, USA
Restriction enzymes; 1 FDU/µl	Thermo Fisher Scientific, Waltham, USA

Table 2.11: Inhibitors

Inhibitor	Company
Acetyl-Leu-Leu-Norleucinal (ALLN)	Sigma-Aldrich, Deisenhofen
Bafilomycin A1 (BafA1)	Sigma-Aldrich, Deisenhofen
Cycloheximide (CHX)	Sigma-Aldrich, Deisenhofen
Dynasore	Sigma-Aldrich, Deisenhofen
E-64	Sigma-Aldrich, Deisenhofen
Epoxomycin	Calbiochem, La Jolla, USA
Lactacystin	Sigma-Aldrich, Deisenhofen
Leupeptin	Sigma-Aldrich, Deisenhofen
MG132	Selleckchem, Munich
Pepstatin A	Sigma-Aldrich, Deisenhofen
Protease inhibitor cocktail	Sigma-Aldrich, Deisenhofen

Table 2.12: Primary antibodies

Epitope	Host species	Dilution	Source
Cathepsin D	goat, polyclonal	1:5,000 (IB)	Santa Cruz, Heidelberg
c-Myc	mouse, monoclonal	1:5,000 (IB)	Cell Signaling, Danvers, USA
c-Myc	rabbit, polyclonal	1:100 (IF)	Sigma-Aldrich, Deisenhofen
GFP	mouse, monoclonal	1:5,000 (IB)	Roche Diagnostics, Mannheim
GM130	mouse, monoclonal	1:5,000 (IB); 1:100 (IF)	BD Transduction Laboratories, Heidelberg
HA	rat, monoclonal	1:10,000 (IB); 1:100 (IF)	Roche Diagnostics, Mannheim
PDI	mouse, monoclonal	1:5,000 (IB); 1:500 (IF)	Enzo Life Science, Lausen, Belgium
PT α	monoclonal rat	1:25 (IB)	provided by Dr. Pohl and Prof. Dr. Nolte, UKE, Hamburg
RFP	rabbit, polyclonal	1:10,000 (IB)	provided by Dr. Kreienkamp, UKE, Hamburg
α-Tubulin	mouse, monoclonal	1:10,000 (IB)	Sigma-Aldrich, Deisenhofen

IF, immunofluorescence; IB, immunoblotting

Table 2.13: Secondary antibodies

Antibody	Dilution	Company
AF488-coupled anti-mouse IgG	1:1,000 (IF)	Invitrogen, Darmstadt
AF488-coupled anti-rabbit IgG	1:1,000 (IF)	Invitrogen, Darmstadt
AF546-coupled anti-mouse IgG	1:1,000 (IF)	Invitrogen, Darmstadt
AF546-coupled anti-rabbit IgG	1:1,000 (IF)	Invitrogen, Darmstadt
HRP-coupled anti-mouse IgG	1:3,000 (IB)	Dianova, Hamburg
HRP-coupled anti-rabbit IgG	1:5,000 (IB)	Dianova, Hamburg
HRP-coupled anti-rat IgG	1:3,000 (IB)	Dianova, Hamburg

IF, immunofluorescence; IB, immunoblotting

2.1.4 Mammalian cell lines and media

Table 2.14: Cell lines

Cell line	Source
CFBE: CFTR $F^{508}\Delta$ cystic fibrosis bronchial epithelial cells	provided by Prof. Dr. Balch, TSRI, San Diego, USA
COS-7: Kidney fibroblasts from african green monkey	ATCC, LGC Standards, Wesel
HEK293: Human embryonic kidney cells	ATCC, LGC Standards, Wesel
HeLa: Human cervical carcinoma cells	ATCC, LGC Standards, Wesel

Table 2.15: Media and solutions for cell culture

Solution or medium	Company
Dulbecco's Modified Eagle´s Medium (DMEM)	GIBCO/BRL, Eggenstein
Fetal bovine serum (FBS)	HyClone, South Logan, USA
Fetal calf serum (FCS)	PAA, Austria
GlutaMax™	GIBCO/BRL, Eggenstein
jetPEI Polyplus-transfection reagent	Polyplus-transfection SA, Illkirch, France
Lipofectamine RNAi	Invitrogen, Carlsbad, USA
Lipofectamin™2000	Invitrogen, Darmstadt
Minimum essential medium (MEM)	Invitrogen, Carlsbad, USA
Opti-MEM®-1 + GlutaMax™	GIBCO/BRL, Eggenstein
Penicillin/Streptomycin	GIBCO/BRL, Eggenstein
Penicillin/Streptomycin	Invitrogen, Carlsbad, USA
Phosphate Buffered Saline (PBS) (10X)	GIBCO/BRL, Eggenstein
Puromycin	InvivoGen, San Diego, USA
Sodium chloride (NaCl) solution (Jet PEI-transfection)	Polyplus-transfection SA, Illkirch, France
Trypsin/EDTA	GIBCO/BRL, Eggenstein

2.1.5 Software and online sources

Table 2.16: Software

Software	Company
Corel Draw v11.633	Corel, Unterschleißheim
CLC sequence viewer	CLC bio-QIAGEN, Aarhus, Denmark
Endnote X4.0.2	Thomson Reuters, New York, USA
FinchTV v1.4.0	Geospiza, Seattle, USA
ImageJ v1.44p	National Institutes of Health, Bethesda, USA
GraphPad PRISM	Graphpad Software Inc., San Diego, USA
Leica Confocal Software v2.61	Leica, Wetzlar
Microsoft Office 2010	Microsoft, Redmond, USA
Quantity One v4.6.7	Bio-Rad, Munich
Image Lab	Bio-Rad, Munich

Table 2.17: Online programs and databases

Database / Program	Website
NCBI BLAST	www.ncbi.nlm.nih.gov/blast
NCBI databases	www.ncbi.nlm.nih.gov/
Oligo Calc	www.basic.northwestern.edu/biotools/OligoCalc.html
UniProt	www.uniprot.org/
Mascot MS/MS Ion Search	www.matrixscience.com

2.1.6 Solutions, buffers and media

Unless otherwise specified, double distilled water (ddH_2O) was used for the preparation of all solutions, buffers and media. For dissolving nucleic acids and oligonucleotide primers ultra-pure, HPLC-purified H_2O (Roth, Karlsruhe) was used. Solutions, buffers and media were autoclaved if necessary.

2.2 Molecular biological methods

2.2.1 Transformation of competent *E. coli cells*

LB medium	10% (w/v) peptone/tryptone, 5% (w/v) yeast extract, 5% (w/v) NaCl; pH 7.5
LB-agar plates	15% (w/v) agar in LB medium
SOC medium	20 % peptone/tryptone, 5 % yeast extract, 10 mM NaCl, 2.5 mM KCl, 10 mM $MgCl_2$, 10 mM $MgSO_4$, 20 mM glucose, pH 7.5

For amplification, plasmids were transformed into chemically competent *Escherichia coli* TOP10 strain (*E. coli*, Invitrogen, Darmstadt). Competent cells were thawed on ice and 100 µl cell suspension were incubated with 20 µl of *Dpn* I-treated PCR product obtained from site-directed mutagenesis reactions. For retransformation 20 µl cell suspension was mixed with 1 µl (50 ng/µl) of plasmid-DNA. After careful mixing *E. coli* cells were incubated for 20 minutes on ice, heat shocked for two minutes at 42°C and incubated on ice for additional 20 minutes. Subsequently cells were mixed with 200 µl SOC or LB medium lacking antibiotics and incubated for one hour at 37 C on the horizontal shaker (200 rpm) to recover from the transformation. Afterwards cells were plated on LB agarose plates containing 100 µg/ml carbenicilin or 50 µg/ml kanamycin with a plastic spatula. Agarose plates were incubated for 16 h at 37 °C in an inverted position and stored at 4 °C.

2.2.2 Plasmid-DNA isolation

Three ml of LB medium containing carbenicilin (100 µg/ml) or kanamycin (50 µg/ml) were inoculated with single colonies from Agarose plates, cultivated for 16 to 20 hours at 37 °C and 200 rpm on a horizontal shaker. Two ml aliquots of these cultures were used to isolate plasmid in Mini scale or 100 µl were used to inoculate 50 mL LB medium for Midi scale plasmid preparation and cultivated for 16 to 20 hours at 37 °C and 200 rpm on the horizontal shaker. Plasmid preparation from small DNA amounts (up to 20 µg DNA) was performed using the GeneJET™ Plasmid Mini Kit and in Midi scale (up to 100 µg DNA) using Qiagen Plasmid Midiprep Kit according to the manufacturer's instructions. Isopropanol-precipitated DNA from the Midi plasmid preparation was dissolved in 100 µl pure water and diluted to 1 µg/µl if applicable. The yield of isolated plasmid DNA was up to 20 µg for Mini scale preparations or up to 100 µg for Midi scale preparations.

2.2.3 Photometric measurement of DNA concentrations

Concentration and purity of isolated DNA was determined by photometry. The concentration of double stranded DNA was measured using a photometer at 260 nm in a UV cuvette, in a 50 fold dilution in water. An $OD_{(260)}$ of 1 corresponds to a concentration of 50 µg DNA/ml. To determine the purity of the DNA sample the OD at 280 nm was measured. A ratio of 1.8 and 2.0 between $OD_{(260)}$ and $OD_{(280)}$ nm ($OD_{260/280}$) indicates pure DNA.

2.2.4 Site-directed mutagenesis

Missense mutations and specific substitutions were introduced by the Quick change site-directed mutagenesis method using the Phusion™ High-Fidelity DNA polymerase. Primers were designed according to the recommendations of the QuikChange® Site-Directed Mutagenesis Kit manual and crosschecked with the online programm Oligo Calc. Oligonucleotide primers contained the mismatched codon and 15 to 25 bp of the wild type sequence in the 5' part of the primer and 15 to 25 bp in the 3' part of the primer. The PCR reaction mixture and temperature profile are shown in Table 2.18 and 2.19. To remove methylated DNA, 20 µl of the PCR reaction was incubated with 2 µl of *Dpn* I for 1 hour at 37°C. The digested PCR product was used directly for bacterial transformation. *Dpn* I recognizes only the parental methylated plasmid DNA, thus digesting only the template plasmid, but not the mutant PCR product. Correct insertion of the sequences was verified by sequencing (SEQLAB, Göttingen). 600 ng of plasmid DNA was mixed with 20 pmol of primer in a final reaction volume of 7 µl.

Table 2.18: Standard PCR reaction mixture

Volume	Reagent
36.5 µl	ultra-pure water
1 µl	template plasmid (50 ng/µl)
1 µl	forward or reverse primer (concentration: 10 pmol/µL)
10 µl	Phusion HF buffer (5 ×)
1 µl	dNTP-mix (20 mM)
0.5 µl	Phusion™ High-Fidelity DNA polymerase (2 U/µl)
50 µl	total volume

Table 2.19: Temperature profile

Step	Temperature	Time	
1	98 °C	5 minutes	
2	98 °C	30 seconds	
3	45 °C	30 seconds	25 cycles
4	72 °C	1 minute/kb	
5	72 °C	5 minutes	
6	10 °C	∞	

2.2.5 Site-directed mutagenesis using megaprimers

A two-stage procedure was developed using megaprimers that are synthesized in a pre-PCR followed by a Quick change site-directed mutagenesis protocol (Wang & Malcolm, 1999). This method is used for insertions and deletion of larger fragments like the EGFP cDNA or sequences encoding whole luminal or transmembrane domains. For the amplification of megaprimers containing the insert sequence, short forward and reverse oligonucleotide primers were synthesized, which anneal both to the template sequence (e. g. PT 15 bp) and to the inserted sequence (for example EGFP or LIMP-2 LD, 21 bp). With these primers the first PCR reaction with 30 cycles resulted in amplification of the insert flanked by a short sequences annealing to defined positions in the acceptor DNA sequence. PCR products were separated by agarose gels, cutted and extracted from the gel using QIAquick Gel Extraction Kit. After photometric determination of DNA concentration, the Quick change mutagenesis PCR was performed using a second template DNA. The cycling conditions are described in Table 2.19 with the exception that 30 cycles were performed.

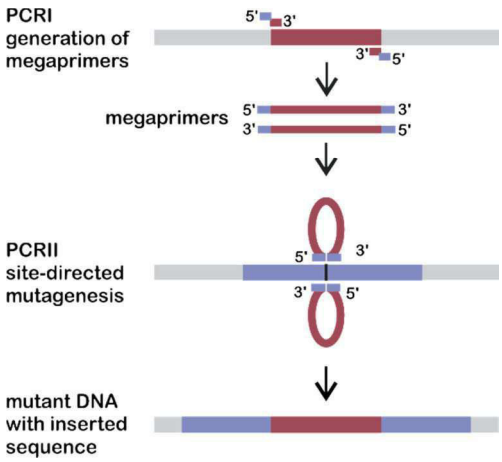

Figure 2.1: Site-directed mutagenesis using megaprimers. In the first PCR reaction megaprimers are generated using oligonucleotide primers, which anneal both to the first template (dark red) and the second template (purple). PCR products are separated by agarose gel electrophoresis, extracted from the gel and used as megaprimers in the second PCR reaction for site-directed mutagenesis PCR reaction resulting in the insertion of a larger fragment into the template sequence (purple).

2.2.6 Agarose gel electrophoresis

TAE buffer	40 mM Tris-HCl, pH 8.5, 20 mM acetic acid, 2 mM EDTA.

Agarose was dissolved in TAE buffer and heated in a microwave until completely dissolved. After cooling down to about 55 °C, ethidium bromide was added to a final concentration of 0.5 µg/ml and the solution was poured into a gel casting tray. After gelling the gel was transferred to an electrophoresis chamber and the chamber filled with TAE buffer. Samples were mixed with the loading dye and loaded onto the gel. Electrophoresis was performed at 3 to 4 V/cm. Ethidium bromide intercalates between the bases of double stranded DNA allowing visualization by UV illumination. Sizes of DNA fragments were estimated by comparison with DNA size markers, which were separated on the gel in parallel.

2.3 Cell Biology Methods

2.3.1 Cell culture

Standard growth medium	DMEM containing 10% (v/v) FCS, 1% (v/v) glutamax, 1% (v/v) penicilline/streptomycine (10000 Units/ml each)
Growth medium/CFBE cells	MEM 10% (v/v) FBS, 50 U/ml penicillin, 50 µg/ml streptomycin, 2 mM L-glutamine, 2 µg/ml puromycin

All mammalian cells were cultivated in 75 cm^2 polystyrene flasks and maintained in a 37 °C humidified CO_2 incubator. All media and solutions were prewarmed to 37 °C before use. Cells were cultivated in standard growth medium except for CFBE cells. Cells were passaged all two to three days. Growth medium was aspirated and cells were washed once with 5 ml of pre-warmed PBS (without Ca^{2+} and Mg^{2+}, sterile) and incubated up to 5 minutes with 1 ml trypsin-EDTA at 37°C in the incubator. Subsequently trypsin reaction was stopped by addition of 4 ml growth medium. Cells were suspended, diluted with growth medium to obtain the desired density and cultivated with 8 ml of medium or seeded onto 35 mm, 60 mm or 100 mm cell culture dishes (in 2, 4, or 8 ml medium), onto 24- or 96 well plates (in 500 or 100 µl medium) or onto 12 mm round glass cover slips in 24 well plates for experiments.

2.3.2 Cryopreservation of mammalian cells

Freezing medium DMEM, 10 % (v/v) FCS, 10 % (v/v) DMSO

For long-term preservation cells grown to confluence (75 cm^2 flasks) were trypsinized, suspended into 10 ml full medium and centrifuged at 800 ×g for 5 minutes Cell pellets were resuspended in 3 ml ice cold freezing medium. Cell suspension was divided into 3× 1 ml aliquots, transferred to cryovials and incubated at 80 °C overnight in a cryo freezing container filled with isopropanol, ensuring a constant reduction of temperature (1°C/minute). After 24 hours cells were transferred to a liquid nitrogen tank for long-term storage. For thawing of cryopreserved samples, cells were incubated for 2 minutes at 37 °C. Subsequently suspension was transferred to a 15 ml tube and diluted to a final volume of 10 ml with pre-warmed growth medium and centrifuged for 5 minutes at 800 ×g. DMSO containing supernatant was removed and cells were resuspended in 5 ml fresh pre-warmed growth medium, transferred to a culture flask and cultivated as described in paragraph 2.3.1.

2.3.3 Transient transfection of mammalian cells

For transient transfections cells were plated on dishes or cover slips and cultivated until they reached a confluency of 70 to 80%. Standard size of dishes for western blot analysis was 35 mm. Transfection of cells was performed using jetPEI® or Lipofectamine™2000 (LF2000), according to the manufacturer's instructions. Depending on the size of the culture dishes different amounts of plasmid-DNA and transfection reagent was used (Table 2.20 and 2.21). For the transfection with jetPEI®, plasmid-DNA and jetPEI®-reagents were diluted in equal volumes of NaCl-solution separately. After an incubation of 5 minutes at RT solutions were mixed on a vortex mixer, incubated for additional 25 minutes at RT and added on cells with fresh medium.

Table 2.20: jetPEI® transfection mixture

Plate/well	DNA [µg]	NaCl [µl]	jetPEI® [µl]	NaCl [µl]	total [µl]	medium [ml]
12 well	1.5	50	2	50	100	0.25
35 mm	3	100	5	100	200	1
60 mm	6	200	10	200	400	2
10 cm	12	400	20	400	800	4

The procedure of transfection with LF2000 was the same as for jetPEI®, using optimum instead of NaCl.

Table 2.21: LF2000 transfection mixture

Plate/well	DNA [µg]	Opti-MEM [µl]	LF2000 [µl]	Opti-MEM [µl]	total [µl]	medium [ml]
12 well	1.5	50	2	50	100	0.25
35 mm	3	100	5	100	200	1
60 mm	6	200	10	200	400	2
10 cm	12	400	20	400	800	4

For co-transfection experiments, PT α/β-Myc in combination with Sar1-mCherry and PT α/β-GFP in combination with PT γ-Myc, respectively, were transfected in a 4:1 ratio. The plasmid DNA amount for the single transfections was decreased in these experiments accordingly. At 5 hours after transfection medium was changed. Assays were performed after 24, 36 or 48 hours. For the identification of proteins secreted into the medium by SDS-PAGE and western blotting, media were concentrated using Millipore centrifugal concentrators.

2.3.4 Transfection of silencing RNAs (siRNA) into mammalian cells

To screen for proteins important factors for M6P-formation on lysosomal hydrolases, 200 genes coding for ER and Golgi localized as well as cytosolic proteins important for intracellular trafficking, protein folding and degradation, glycosylation and others were down regulated in CFBE or HeLa cells by transient transfection of siRNAs. SiRNA-mediated knockdown was performed in quadruplicates for each gene in 96 well plates allowing the analysis of 20 independent genes per plate. Medium, non-treated, scrambled control siRNA transfected cells, cells cultured in the presence of the weak base ammoniumchloride (NH_4Cl) or transfected with by *GNPTAB* siRNAs were used as negative and positive controls, respectively. A master transfection mix containing siRNAs and Lipofectamine RNAi max was prepared for five wells and partitioned into four wells of a 96 well plate as shown in Table 2.22 and Figure 2.2. The solutions were mixed on a vortex mixer transferred to the wells and incubated for 20 minutes at RT before cells were added.

Table 2.22: siRNA transfection mixture

Reagent	1 well	5 wells
Opti-MEM	78.9 µl	394.4 µl
siRNA (Stock: 10 µM; final concentration 50 nM/well)	0.80 µl	4.0 µl
Lipofectamine RNAi max	0.32 µl	1.6 µl

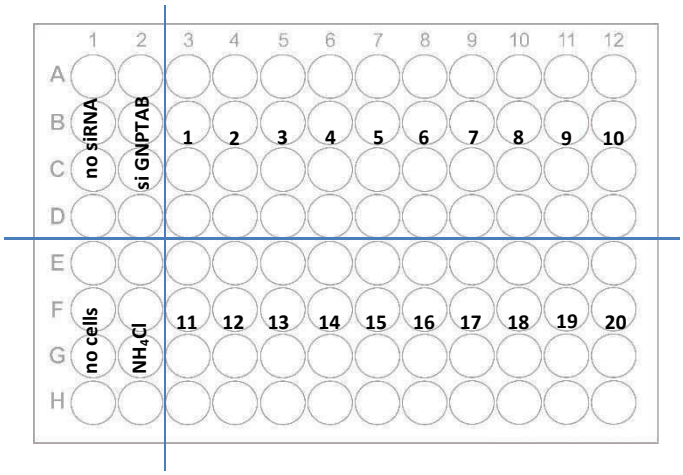

Figure 2.2: Loading scheme for siRNA knockdown on 96 well plates.

CFBE or HeLa cells treated with trypsin-EDTA were suspended in 10 ml growth medium and transferred to a 50 ml tube and centrifuged for 5 minutes at 800 ×g. The cell pellet was resuspended in 10 ml Opti-MEM containing 20% (v/v) FCS. Cell density was estimated using a haemocytometer and diluted with 10 ml Opti-MEM containing 20% (v/v) FCS respectively. 13200 cells in a volume of 80 µl were added to the transfection mixture to a final volume of 160 µl. After 48 hours of cultivation the medium was replaced by 100 µl Opti-MEM containing 0.1% (w/v) BSA and incubated for another 24 hours. The medium of positive control cells was supplemented with 10 mM NH_4Cl (final concentration, Fig. 2.2). Finally 80 µl of medium was transferred using a multichannel pipette on a new 96 well plate followed by the measurement of β-hexosaminidase activity in the media. Four 96 well plates were prepared at a time.

2.3.5 Cycloheximide-chase analyses

CHX-chase analyses are used to monitor protein degradation in eukaryotic cells, wherein the protein biosynthesis inhibitor CHX is added to the cells and the decrease in the steady state levels of a target protein is analyzed by immunoblotting after different chase periods. To analyze protein turnover of HeLa cells grown on 35 mm plates transiently expressing wild type and mutant PT α/β-Myc were either harvested or incubated in the presence of CHX (50 µg/ml) for different time periods (3, 6, 9, 12, and 15 h). Cells were harvested,

lysed and protein extracts processed by SDS-PAGE and Myc-immunoblotting. Densities of immunoreactive bands were quantified using the software.

2.3.6 Biotinylation of cell surface proteins

PBS	137 mM NaCl, 2.7 mM KCl, 10 mM Na_2HPO_4, 1.76 mM KH_2PO_4; pH 7.4

HeLa cells were plated onto 60 mm dishes and transfected with wild-type and mutant PT α/β-Myc constructs and cDNAs coding for the control proteins β-Gal-3'-sulfotransferase-Myc and Furin-Myc using jetPEI transfection reagent. 36 hours after the start of transfection, cells were placed on ice and washed three times with ice-cold PBS, supplemented with 0.5 mM $MgCl_2$ and 0.09 mM $CaCl_2$ (PBS**). Cells were incubated with 1.5 mg of membrane-impermeable, non-cleavable EZ-Link Sulfo-NHS-SS biotin in 2 ml PBS** per dish for 2 hours at 4°C with constant shaking. Subsequently cells were washed four times with 4 ml ice-cold PBS** containing 100 mM glycine to quench unbound biotin. After a final wash with 4 ml ice-cold PBS**, cells were scraped and centrifuged for 5 minutes at 800 ×g. Cell pellets were dissolved in 300 µl lysis buffer A (see chapter 2.4.1), incubated on ice for 30 minutes and centrifuged for 10 minutes at 16,000 ×g. Prior to streptavidin precipitation 10% of the cell homogenate was removed for quantification of cell surfaced-localized proteins. Supernatants were incubated with 100 µl Streptavidin Plus Ultra-Link Resin beads for 90 minutes on a spinning wheel at 4°C. Beads were washed 4 times with 1 ml of ice-cold lysis buffer. Biotinylated proteins bound to streptavidin-agarose beads were eluted in 2x Laemmli sample buffer supplemented with 50 mM DTT by heating for 5 minutes at 95 °C. Proteins were separated by SDS-polyacrylamide gel electrophoresis (SDS-PAGE) and analyzed by immunoblotting.

2.3.7 Metabolic labeling of proteins with [^{35}S]-methionine

Starvation medium	L-methionine and L-glutamine free DMEM, 1% (v/v) glutamax, 1% (v/v) penicilline/streptomycin (10000 Units/ml each)
Pulse medium	starvation medium, 100 µCi/ml [^{35}S]-methionine
Chase medium	standard growth medium, 25 mg/ml unlabeled methionine

HeLa cells grown on 35 mm dishes were transfected with PT α/β-GFP cDNA constructs using jetPEI. Fortyeight hours after transfection, cells were washed three times with PBS

and incubated in 1 ml starvation medium for 1 hour, following pulse with 800 µl pulse medium for 1 hour. Subsequently pulse medium was removed, cells were washed three times with PBS and either harvested or chased for 3, 6 or 12 hours in 1 ml chase medium. After the chase periods, medium was removed and cells were washed three times with PBS. Cells were harvested and centrifuged at 800 ×g at 4 °C and pellets processed by GFP-Trap® immunoprecipitation (see paragraph 2.4.4). Radioactivity of pulse media prior and after incubation of the cells was quantified in doublets by solving 2 µl sample in 2 ml scintillation solution using a scintillation counter.

2.3.8 Double-immunofluorescence confocal microscopy

For co-localization studies COS-7 were plated onto Ø 12 mm autoclaved round glass cover slips incubated with 95% ethanol for 10 minutes and washed 3 times with PBS prior to seeding of cells. 24 hours after the start of transfection with LF2000, cells were washed 3 times with cold PBS, fixed in 4% (w/v) paraformaldehyde in PBS for 15 minutes at RT, washed 3 times with 50 mM NH_4Cl and incubated for 5 minutes with 50 mM NH_4Cl to mask free aldehyde groups. When indicated cells were incubated with cycloheximide (100 µg/ml) for 2 hours prior to fixation. Subsequently cells were permeabilized with PBS containing 0.1% (w/v) saponin (PBS/sap) for 10 minutes. Non-specific antibody binding was blocked by incubation of cells for 30 minutes with PBS/sap containing 3% (w/v) BSA (PBS/sap/BSA). Antibodies were diluted in PBS/sap/BSA. Cells were incubated with primary antibodies for 1 hour at RT or overnight at 4°C, followed by three times washing with PBS/sap for 5 minutes and incubation with fluorochrome conjugated secondary antibodies for 1 hour. Subsequently cells were washed for another 3 times with PBS/sap, incubated for 5 minutes with 100 ng/ml DAPI in PBS and sealed in mounting medium. Cells were analyzed on a confocal laser scanning microscope (63-fold magnification) and images were merged using Adobe Photoshop 7.0.

2.4 Biochemistry Methods

2.4.1 Protein extraction

Lysis buffer A	50 mM Tris-HCl, pH 7.4, 1 mM EDTA, 1 % (v/v) Triton X-100, protease inhibitor cocktail
Lysis buffer B	10 mM Tris-HCl, pH 7.5, 150 mM NaCl, 5 mM EDTA, 0.1% (w/v) SDS, 1% (v/v) Triton X-100, 1% (w/v) sodium deoxycholate, protease inhibitor cocktail

Cells were placed on ice, washed once with 1 ml ice-cold PBS, harvested in 800 µl PBS, centrifuged for 5 minutes at 800 ×g and lysed either with ice-cold lysis buffer A or B. After 30 minutes incubation on ice; samples were centrifuged for 10 minutes at 4°C, 20,000×g, and the supernatant was transferred into a new tube.

2.4.2 Determination of protein concentration

Protein concentration was measured either using Bradford or bicinchoninic acid (BCA) Protein Assay. Both methods are colorimetric protein assays based on an absorbance shift upon binding of the dye to proteins. All measurements were performed in duplicates. Two µl of cell extract was combined with 798 µl ddH_2O and 200 µl Bradford reagent and mixed on a vortex mixer. After 10 minutes incubation at RT, the $OD_{(595)}$ was measured in cuvettes using a photometer. The BCA assay was performed in 96 well plates. Two µl sample was added to 48 µl ddH_2O. BCA working solution was prepared by mixing solution A and B in a ratio of 50:1 according to the manufacturer's instructions. 50 µl working solution was added to the samples and incubated for 30 minutes at 37°C. Absorbance was measured at 562 nm in a plate reader. For both methods comparison with BSA standards (concentrations of 0, 2.5, 5, 10, 15 and 20 µg/ml) allowed the determination of protein concentration using Microsoft Excel for quantifications.

2.4.3 Enzymatic deglycosylation of proteins

Enzymatic deglycosylation of proteins with endoglycosidase H (endo H, EC 3.2.1.96, glycopeptide-D-mannosyl-N^4-(N-acetyl-D-glucosaminyl)-2-asparagine 1,4-N-acetyl-β-glucos-aminohydrolase) and peptide-*N*-glycosidase F (PNGase F, EC 3.5.1.52, Peptide-*N*-glycosidase F Peptide-N4-(acetyl-β-glucosaminyl)-asparagine amidase) provides

information about the presence of *N*-linked oligosaccharides and the localization of protein in the Golgi apparatus. PNGase F hydrolyzes all *N*-linked oligosaccharides and endo H only high mannose-type oligosaccharides.

All steps were performed on ice. 50 µg protein in lysis buffer A was diluted to a final volume of 36 µl for incubation with endo H or PNGase F. First proteins were denatured adding 4 µl of 10 fold concentrated denaturation buffer (NEB endo H kit: 5% SDS, 10% β-mercaptoethanol, pH 5.5) or 4 µl of 2.5% (w/v) SDS and 3 µl of ddH_2O, respectively. Samples were incubated at 95 °C for 10 minutes and cooled on ice. For endo H treatment, samples were supplemented with 5 µl of 10 fold concentrated G5 Buffer (NEB endo H kit: 50 mM sodium citrate pH 5.5), 2 µl endo H (500 U/µl) and 3 µl ddH_2O. For incubation with PNGase F samples were mixed with 5 µl 10% (w/v) NP-40 and 2 µl PNGase F (1 U/µl, Roche). Digestion was performed at 37 °C for 2 hours in a final volume of 50 µl for both reactions. Non-treated samples were mixed with ddH_2O to a final volume of 50 µl. Subsequently all samples were supplemented with Laemmli sample buffer (see chapter 2.4.5), boiled at 95 °C for 5 minutes and analyzed by SDS-PAGE and western blotting.

2.4.4 Immunoprecipitation using GFP-Trap® agarose beads

Lysis buffer	10 mM Tris-HCl pH 7.5, 150 mM NaCl, 0.5 mM EDTA, 0.1% (w/v) NP-40, protease inhibitor cocktail
Dilution buffer	10 mM Tris-HCl pH 7.5, 150 mM NaCl, 0.5 mM EDTA, protease inhibitor cocktail

GFP-Trap® immunoprecipitation of extracts from HeLa or HEK293 cells expressing PT α/β-GFP fusion proteins was performed for identification of proteins interacting with PT α/β-GFP or for precipitation of [^{35}S]-labelled GFP-fusion proteins.

For identification of interacting proteins, HEK293 cells grown on two 10 cm plates transiently expressing GFP or PT α/β-GFP were harvested, centrifuged for 5 min at 1,000×g and pellets were resuspended in 100 µl ice-cold GFP-Trap® lysis buffer. Cell extracts were incubated for 30 minutes on ice, followed by centrifugation at 4 °C and 20,000×g for 10 minutes. Supernatants were transferred to a fresh tube and mixed with 150 µl dilution buffer. 80 µl GFP-Trap® beads previously equilibrated with dilution buffer were mixed with cell extracts and incubated for 2 hours at 4 °C on a spinning wheel. The suspension was centrifuged at 2,000×g at 4 °C for 2 minutes to spin down the beads.

Supernatant was transferred to a new tube. The beads were washed 4 times with 1 ml dilution buffer without protease inhibitor cocktail. Precipitated proteins were eluted in Laemmli buffer by boiling the samples at 95 °C for 5 minutes. Aliquots were taken from input, supernatant, wash and bound fractions, separated by SDS-PAGE and analyzed by silver staining and GFP-immunoblotting, respectively.

[^{35}S]-methionine-labeled HeLa cells grown on 35 mm plates (see paragraph 2.3.6) were harvested, centrifuged and pellets were resuspended in 100 µl ice-cold GFP-Trap® lysis buffer. Cell extracts were incubated for 30 minutes on ice, followed by centrifugation at 20,000 ×g for 10 minutes at 4°C. Supernatants were transferred to a fresh tube and mixed with ice-cold 150 µl dilution buffer. GFP-Trap®agarose beads were pre-incubated with extracts from non-pulsed cells to block unspecific interactions with radiolabeled proteins for 2 hours at 4 °C on a spinning wheel. Then 10 µl of GFP-Trap®agarose beads were added to each cell extract and incubated for 2 hours at 4 °C on a spinning wheel. The suspension was centrifuged at 2,000 ×g at 4 °C for 2 minutes to spin down the beads. Supernatants were transferred to a new tube. The beads were washed 4 times with 1 ml dilution buffer. Precipitated proteins were eluted in Laemmli buffer by boiling the samples at 95 °C for 5 minutes. Proteins were separated by SDS-PAGE and analyzed by fluorography.

2.4.5 SDS-polyacrylamide-gel electrophoresis (SDS-PAGE)

Anode buffer	25 mM Tris-HCl, pH 8.6, 192 mM glycine.
Cathode buffer	25 mM Tris-HCl, pH 8.6, 192 mM glycine, 0.1 % (w/v) SDS
Transfer buffer	25 mM Tris-HCl, pH 7.4, 192 mM glycine, 20 % (v/v) methanol.
Laemmli sample buffer	125 mM Tris-HCl, pH 6.8, 1% (w/v) SDS, 10% (v/v) glycerol, Coomassie® Blue G

Proteins were separated by one dimensional discontinuous SDS-polyacrylamide-gel electrophoresis (SDS-PAGE, using vertical slab gel electrophoresis units with glass plates measuring 18 x 16 x 1.8 cm and 15 to 21 well combs. For some applications mini gels were used (10 x 10 x 0.8 cm). Depending on the molecular masses of the analyzed proteins variable acrylamide concentrations ranging from 8%-15% were used (10% acrylamide was standard, otherwise specified Tab. 2.23). First the running gel was prepared and poured between two glass plates. Isopropanol was layered on top of the solution. Once the gel was polymerized the isopropanol was removed and the stacking gel poured on top of the

running gel and a comb was inserted immediately. Samples were prepared and denatured in Laemmli sample buffer for 5 minutes at 95° C. To solubilize proteins under reducing conditions, sample buffer was supplemented with DTT (final concentration: 10 mM) and β-mercaptoethanol (final concentration: 0.1 mM). Up to 100 µl sample were loaded per well. Electrophoresis was performed for 3 hours at 20 to 50 mA per gel. Gels were either processed by fluorography (chapter 2.4.6), western blotting (chapter 2.4.7), or silver staining (chapter 2.4.8).

Table 2.23: Running gel solution

Reagents	8%	10%	15%
H_2O	14.10 ml	12.2 ml	7.3 ml
1.5 M Tris-HCl, pH 8.8	7.50 ml	7.5 ml	7.5 ml
10% (w/v) SDS	0.30 ml	0.3 ml	0.3 ml
(30%/0.8% w/v) Acrylamide/Bis-Acrylamide	7.80 ml	9.8 ml	14.7 ml
10% (w/v) APS	0.25 ml	0.25 ml	0.25 ml
TEMED	0.025 ml	0.025 ml	0.025 ml

Table 2.24: Stacking gel solution

Reagents	4%
H_2O	6.0 ml
1.5 M Tris-HCl, pH 6.8	2.5 ml
10% (w/v) SDS	0.1 ml
Acrylamide/Bis-acrylamide (30%/0.8% w/v)	1.3 ml
10% (w/v) APS	0.1 ml
TEMED	0.01 ml

2.4.6 Fluorography

[^{35}S]-methionine-labeled GFP-fusion proteins were precipitated using GFP-Trap® agarose beads, bound proteins separated by SDS-PAGE and detected by fluorography, which allows high sensitivity detection of [^{35}S]-methionine-labeled proteins. After SDS-PAGE the gel was incubated 3 times in DMSO for 20 minutes with constant shaking to remove water. Subsequently the gel was incubated with DMSO supplemented with 20 % (w/v) 2.5-diphenyloxazole (PPO) overnight. PPO is a fluorophore that is excised by the particles that are emitted by [^{35}S]-methionine. Upon excitation, PPO emits visible light, which can be detected by a photographic film (Bonner & Laskey, 1974). Gels were washed three times

with ddH_2O for 10 minutes and dried for 3 h in a gel dryer. The dried gel was placed between two photographic films in a cassette and stored for 2 weeks at -80 °C. The film was digitalized by scanning and band intensities were quantified using ImageJ software.

2.4.7 Western-Blotting

Wash buffer	50 mM Tris-HCl, pH 7.4, 150 mM NaCl, 0.5% (v/v) Tween 20
Blocking buffer	50 mM Tris-HCl, pH 7.4, 150 mM NaCl, 0.5% (v/v) Tween 20; 5% (w/v) milk powder
ECL solution A	100 mM Tris-HCl, pH 8.5, 2.7 mM luminol, 0.44 mM p-cumaric acid
ECL solution B	100 mM Tris-HCl, pH 8.5, 0.02% H_2O_2

To transfer proteins separated by SDS-PAGE onto a PVDF membrane, a sandwich was assembled (fiber pad, 2 sheets of paper, activated PVDF membrane, running gel, 2 sheets of paper, fiber pad), kept together by a plastic cassette, in transfer buffer. The cassette was inserted in a transfer buffer tank containing ice-cold transfer buffer and the transfer was performed at 900 mA for 2 hours or at 120 mA for 14 hours. Afterwards the membrane was blocked with blocking buffer for 1 hour, followed by incubation with primary antibody in blocking buffer for 1 hour at RT or overnight at 4 °C. After 3 times washing for 10 minutes with wash buffer, the membrane was incubated with HRP-coupled secondary antibodies in blocking buffer for 1 hour at RT and washed again for 3 times 10 minutes and another 30 minutes. Immunoreactive bands were detected using ECL reaction solution prepared by mixing of equal volumes of ECL solutions A and B. The mixed solutions were directly applied to the membranes and incubated for 1 minute. Blot membranes were imaged on a Molecular Imager. Densitometric analysis was performed using Image lab software. Statistical significance was evaluated with a two-tailed, unpaired t-test using Graph Pad Prism software. Molecular masses were estimated by comparison with electrophoretic mobilities of molecular mass marker proteins.

2.4.8 Mass-spectrometric identification of proteins

For identification of interaction partners of the PT α/β-subunits, HEK293 cells were transiently transfected with PT α/β-GFP cDNA. Cells were harvested 24 hours after the start of transfection and PT α/β-GFP and PT β-GFP was immunoprecipitated using GFP-Trap® agarose beads (see paragraph 2.4.4). Precipitated proteins were separated by SDS-

PAGE and stained with silver using Fire Silver Staining Kit according to the manufacturer's instructions. Silver stained lanes were excised from the gel were sliced into 11 peace and proteins were digested with trypsin. Mass spectrometric analysis of the samples was performed by the Core Facility Massenspektrometrische Proteomanalytik, Institute for Clinical Chemistry, University Hospital Hamburg-Eppendorf. Characterization of the peptide masses and identification of proteins was performed using Mascot MS/MS Ion Search and data base searches.

2.4.9 Measurement of β-hexosaminidase enzyme activity

Reaction mixture	10 mM 4-nitrophenyl-N-acetyl-β-D-glucosaminide, 0.1% (v/v) Triton X-100, 0.4% (w/v) BSA, 0.2 M sodium citrate; pH 4.6

To measure the β-hexosaminidase enzyme activity in media of cells transfected with siRNAs, 20 µl of media were transferred onto a 384 well plate and supplemented with 20 µl reaction mixture using an electronic multichannel pipette. Mixtures were incubated for 22 hours at 37 °C. The absorbance was measured at 405 nm after 12 hours using a plate reader. Data was evaluated by calculating the average and standard deviation (SD) of quadruplicates. Values were normalized to non-transfected controls from the same 96 well plate.

3 RESULTS

3.1 Structural requirements for the transport of the PT α/β subunit precursor protein from the ER to the Golgi.

The S1P-mediated cleavage of the PT α/β-subunit precursor protein in the Golgi apparatus is essential for the catalytic activity of the PT complex towards lysosomal enzymes (Marschner et al, 2011). Thus efficient ER export and anterograde transport of the newly synthesized PT complex to the Golgi apparatus is prerequisite for its proteolytic activation. The first aim of my studies was to identify structural requirements for the efficient ER export of the PT α/β-subunit precursor protein and the identification of ER export motifs.

3.1.1 The PT α/β-subunit precursor protein is cleaved after transport to the Golgi apparatus

To analyze the transport of the PT α/β-subunit precursor, cDNA constructs with a C-terminal Myc-epitope tag (PT α/β-Myc) alone or fused to an ER retention motif of the human α_{2C}-adrenergic receptor (KHILFRRRRRGFRQ, Zerangue et al, 2000; PT α/β-Myc ER-Ret) were cloned. In addition, a non-cleavable PT α/β-Myc $R^{925}A$ mutant with alanine substitution of a critical arginine residue in the S1P-cleavage site (Marschner et al, 2011) alone (PT α/β-Myc $R^{925}A$) or fused to the ER-retention motif (PT α/β-Myc $R^{925}A$ ER-Ret) was generated (Fig. 3.1A). Constructs were overexpressed in COS-7 or HeLa cells. Acquisitions of complex-type *N*-linked oligosaccharides and S1P-mediated cleavage were analyzed by anti-Myc western blotting. To test the presence of high mannose- and complex-type *N*-linked oligosaccharides, cell lysates were treated with PNGase F and endo H, respectively (Fig 3.1B). PNGase F removes all *N*-linked oligosaccharides from proteins, whereas endo H only removes high mannose-type, but not complex-type *N*-glycans. Additionally, intracellular localization was analyzed by double immunofluorescence microscopy (Fig. 3.1C). When indicated, protein biosynthesis was inhibited with cycloheximide (CHX) prior to harvesting to prevent intracellular mislocalization of PT α/β due to saturation of the ER export machinery. In western blots of cells expressing wild type PT α/β-Myc immunoreactive bands with apparent molecular masses of 180 kDa and 45 kDa representing the uncleaved PT α/β-subunit precursor protein and the cleaved mature PT β-subunit, respectively, were detected, which were not observed in extracts of pEGFP transfected control cells (Fig. 3.1B, lanes 1 and 2).

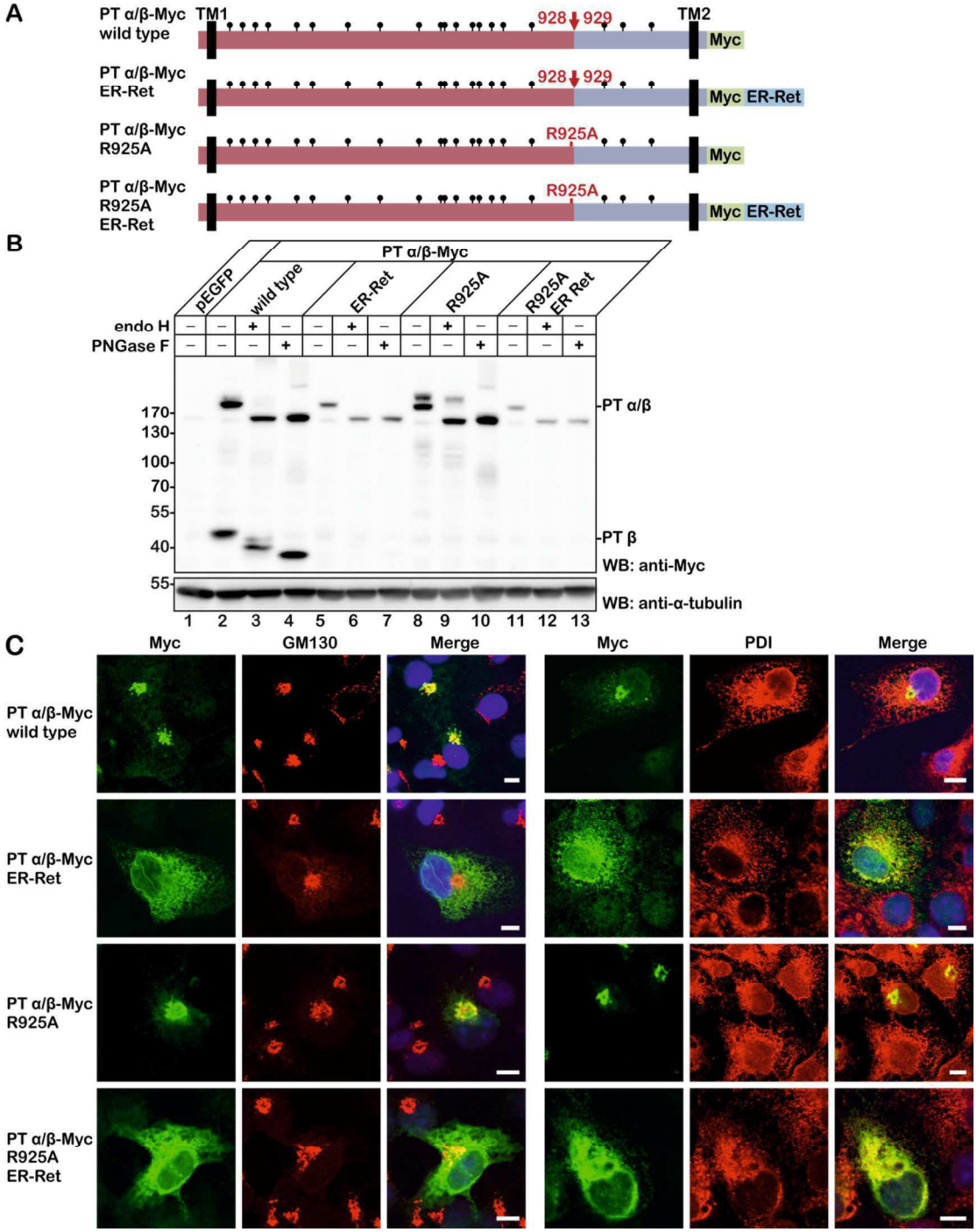

Figure 3.1: S1P-mediated cleavage of the PT α/β-subunit precursor protein occurs after ER export to the Golgi apparatus. (A) Schematic representation of PT α/β-cDNA constructs used for expression analysis. The positions of the Myc-epitope (green), C-terminal ER retention motif (ER-Ret, blue), transmembrane domains (TM), potential *N*-glycosylation sites (🍒), S1P cleavage-site (arrow) and alanine substituted R^{925} are indicated. (B) HeLa cells were transfected with pEGFP as negative control, PT α/β-Myc wild type, ER-Ret, R^{925}A and R^{925}A ER-Ret subunit precursor cDNA constructs and harvested 36 hours after transfection. Cell extracts were incubated in the absence (-) or presence (+) of endo H or PNGase F, separated by SDS-PAGE (8 % acrylamide) and analyzed by anti-Myc western blotting. Equal loading of the gel was verified by anti-α-tubulin immunoblotting. Positions of molecular mass marker proteins, the PT α/β-subunit precursor protein and the cleaved PT β-subunit are indicated. (C) COS-7 cells were transfected with PT α/β-Myc, PT α/β-Myc ER-Ret, PT α/β-Myc R^{925}A and PT α/β-Myc R^{925}A ER-Ret subunit precursor cDNA constructs. After 24 hours cells were treated with 100 µg/ml CHX for 2 hours, fixed and incubated with antibodies against the Myc epitope (green), the *cis*-Golgi marker protein GM130 (red), or the ER marker protein PDI (red). Nuclei were visualized by DAPI staining (blue). In merged images yellow indicates co-localization. Scale bars 10 µm.

Treatment of cell lysates with endo H and PNGase F resulted in a shift of the molecular mass from 180 kDa to 150 kDa, indicating the presence of endo H-sensitive, *N*-linked high mannose-type oligosaccharides. The molecular mass of the mature PT β-subunit in contrast shifted to a doublet of 42/40 kDa after treatment with endo H and to 38 kDa after treatment with PNGase F, indicating the presence of endo H-resistant, complex-type *N*-glycans (Fig. 3.1B, lanes 2, 3 and 4). In western blots of cells expressing the PT α/β-Myc ER-Ret only the 180 kDa subunit precursor protein containing endo H-sensitive, *N*-linked glycans could be detected, but not the cleaved mature PT β-subunit (Fig. 3.1B, lanes 5, 6 and 7). In western blots of cells transfected with the S1P cleavage-resistant mutant PT α/β-Myc $R^{925}A$ 200 kDa and 180 kDa immunoreactive proteins representing complex-type, endo H-resistant and high mannose-type and endo H-sensitive *N*-glycosylated forms were detected (Fig. 3.1B, lanes 8, 9 and 10). The fusion of the ER retention motif of the α_{2C}-adrenergic receptor to the PT α/β-Myc $R^{925}A$ mutant resulted in the same band pattern as PT α/β-Myc ER-Ret with endo H-sensitive *N*-glycans only (Fig. 3.1B, lanes 11, 12 and 13). To verify the intracellular localization of wild type and mutant PT α/β-Myc subunit precursor protein double immunofluorescence microscopy was performed with COS-7 cells using antibodies against marker proteins of the ER and the *cis*-Golgi apparatus. Wild type PT α/β-Myc subunit precursor protein and the cleaved PT β-Myc subunit co-localized mainly with the *cis*-Golgi marker protein GM130, but not with the ER marker PDI (Fig. 3.1C). In contrast, no co-localization of the PT α/β-Myc ER-Ret protein with the *cis*-Golgi marker protein was observed, but complete overlapping localization with the ER marker protein. The S1P cleavage-resistant PT α/β-Myc $R^{925}A$ co-localized mainly with the *cis*-Golgi marker protein GM130, whereas no co-localization was detectable with the ER-resident PDI. Localization of PT α/β-Myc $R^{925}A$ ER-Ret overlapped mainly with PDI, but not with GM130, as shown for PT α/β-Myc ER-Ret (Fig. 3.1C). Golgi localization of the cleavage-resistant PT α/β-Myc subunit precursor protein and absent cleavage of the ER-retained mutant PT α/β-Myc ER-Ret protein indicate, that the uncleaved PT α/β-Myc subunit precursor protein is exported form the ER and is cleaved in the Golgi apparatus. In subsequent experiments proteolytic cleavage, acquisition of complex-type *N*-glycans of mature PT α- and β-subunits and co-localization with *cis*-Golgi marker protein GM130 were used as criteria to quantify transport from the ER to the Golgi apparatus.

3.1.2 The PT α/β-subunit precursor protein is gradually cleaved in the Golgi apparatus

To analyze the kinetics of ER to Golgi transport of the PT α/β-Myc subunit precursor protein, pulse chase experiments were performed with metabolically labeled HeLa cells. Cells were transfected with PT α/β-subunit precursor cDNA fused to GFP at the C terminus (PT α/β-GFP, Fig 3.2A), pulse labeled for 1 hour with [^{35}S]-methionine and either harvested (0 hours chase) or chased for different time periods (3 to 12 hours chase). After lysis of cells PT α/β-GFP was immunoprecipitated from cell extracts using GFP-Trap® beads and precipated proteins analyzed by SDS-PAGE and fluorography (Fig. 3.2).

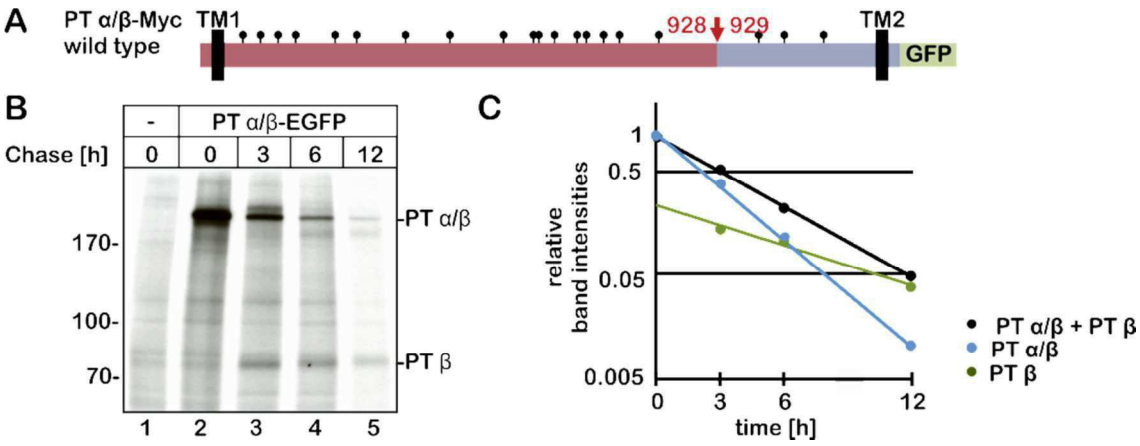

Figure 3.2: Kinetics of ER to Golgi transport of the PT α/β-subunit precursor protein. (A) Schematic representation of used PT α/β-GFP cDNA-construct. Positions of the GFP-epitope (green), transmembrane domains (TM), potential *N*-glycosylation sites and S1P cleavage-site (arrow) are indicated. (B) Forty eight hours after transfection with wild type PT α/β-GFP subunit precursor cDNA, HeLa cells (35 mm plates) were metabolically labeled for 1 h with 100 µCi [^{35}S]-methionine and either harvested (0 hours, pulse) or chased for different periods (3, 6, and 12 h). Non-transfected cells were used as controls. After cell lysis, immunoprecipitation of PT α/β-GFP was performed using GFP-Trap®-Agarose beads. Immunoprecipitated PT α/β-GFP was separated by SDS-PAGE and detected by fluorography. Positions of molecular mass marker proteins, the PT α/β-GFP subunit precursor protein and the PT β-GFP subunit are indicated. (C) Intensities of radioactive bands were quantified by densitometry. Relative amounts of total uncleaved and cleaved PT α/β-GFP (black), non-cleaved PT α/β-GFP-subunit precursor protein alone (blue) and cleaved PT β-GFP subunit were plotted against the chase times in a diagram with half logarithmic scale. Relative amount of non-cleaved PT α/β-GFP at time point 0 hours was arbitrarily set as 1.

After 1 hour pulse period, a 210 kDa band corresponding to the PT α/β-GFP subunit precursor protein was immunoprecipitated, which was absent in non-transfected cells (Fig. 3.2B, lane 2). After a 3 hours chase period, a doublet of 215/210 kDa and a 75 kDa band were detected, which represent differentially *N*-glycosylated PT α/β-GFP subunit precursor proteins and the mature PT β-GFP subunit, respectively (Fig. 3.2B, lane 3). During the 12 hours chase period the amounts of the PT α/β-GFP subunit precursor protein decreased, accompanied by increased levels of PT β-GFP, indicating transport of

PT α/β-GFP to the Golgi and S1P-mediated cleavage (Fig. 3.2B, lane 5). Densitometric evaluation of the band intensities revealed a relative rate of 2 hours for ER to Golgi transport and subsequent cleavage of wild type PT α/β-subunit (Fig. 3.2C). The data indicate, that both uncleaved and cleaved PT α/β-subunit precursor proteins exist in the Golgi apparatus and that the PT α/β-subunit precursor protein is gradually cleaved to the mature PT α- and β-subunits.

3.1.3 PT α/β is transported as subunit precursor protein from the ER to the Golgi apparatus

Acquisition of endo H-resistance of the S1P cleavage-resistant PT α/β-R^{925}A mutant indicated that the non-cleaved PT α/β-subunit precursor protein is efficiently exported from the ER. To examine whether separated PT α- and β-subunits are transported to the Golgi apparatus, isolated PT α-Myc and HA-PT β-subunits were expressed separately or in combination in COS-7 cells (Fig. 3.3A). ER export was quantified by examination of endo H-resistance and co-localization with the *cis*-Golgi marker protein (Fig. 3.3). In western blots of cells expressing PT α-Myc, a polypeptide with an apparent molecular mass of 140 kDa was detected. After endo H and PNGase F treatment the molecular mass of the PT α-subunit shifted to 110 kDa indicating the modification with high mannose-type *N*-linked oligosaccharides only (Fig. 3.3B, lanes 4, 5 and 6). In western blots of cells expressing the HA-PT β-subunit, a 45 kDa immunoreactive polypeptide was observed. In contrast to the PT β-subunit derived by cleavage of the PT α/β-subunit precursor protein, the separately expressed HA-PT β was completely endo H-sensitive, indicating its retention in the ER (Fig. 3.3B, lanes 7, 8 and 9). To exclude that ER retention of isolated subunits is due to lack of the partner subunit, individual subunits were expressed together. The co-expression of PT α-Myc and HA-PT β-cDNA constructs did not result in the endo H-resistance of *N*-glycans on single PT α- and β-subunits, indicating their retention in the ER (Fig. 3.3B, lanes 10, 11 and 12). Double immunofluorescence microscopy confirmed by complete co-localization with the ER marker protein PDI the ER localization of isolated PT α- and β-subunits (Fig. 3.3C). The data demonstrate that only the uncleaved PT α/β-subunit precursor protein can be exported from the ER.

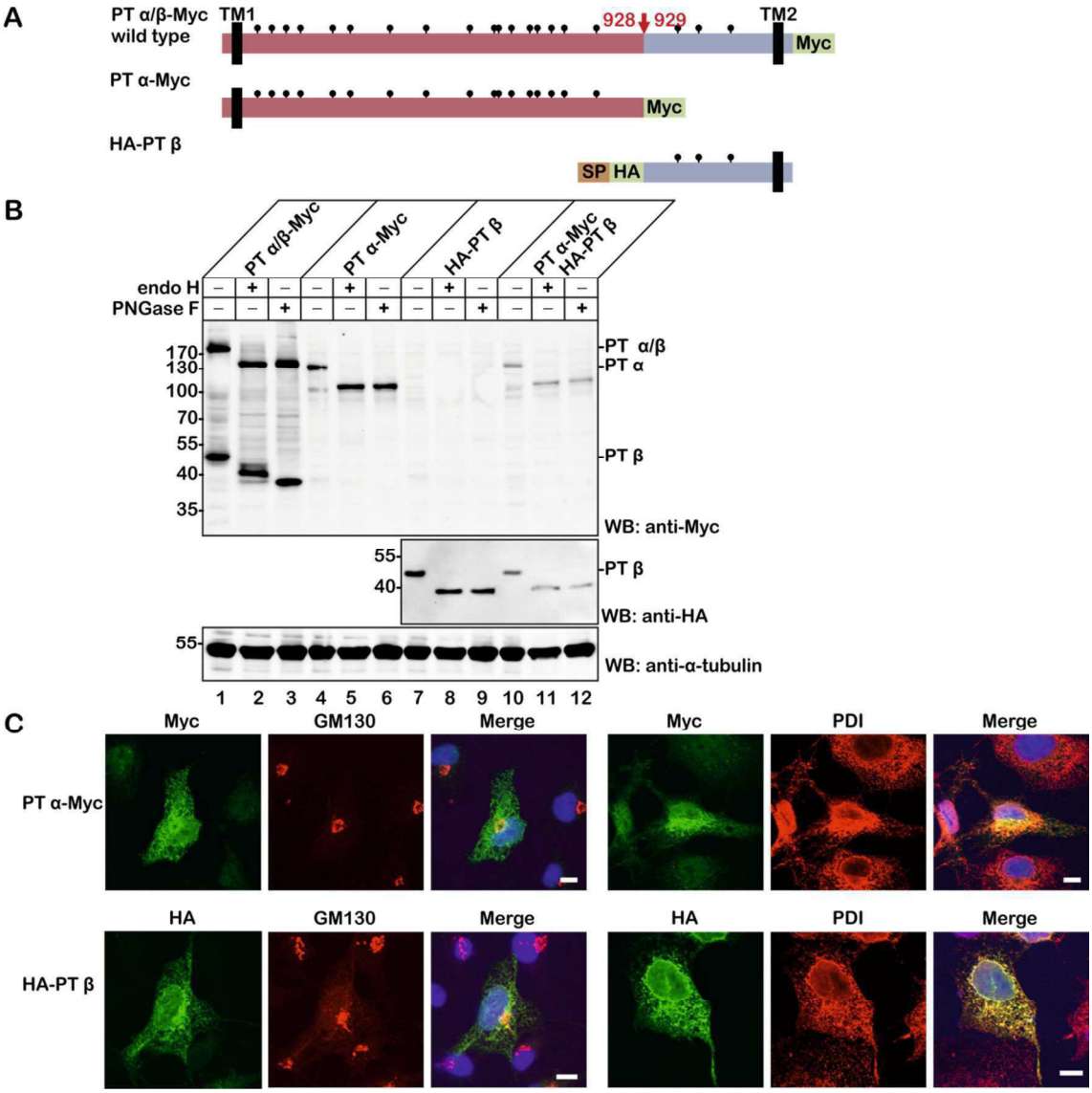

Figure 3.3: The isolated PT α- and β-subunits are retained in the ER. (A) Schematic representation of PT α/β-constructs used for expression analysis. Positions of the Myc- and HA-epitope (green) are indicated. SP: signal peptide. (B) COS-7 cells were transfected with wild type PT α/β-Myc subunit precursor, PT α-Myc subunit, HA-PT β-subunit or co-transfected with PT α-Myc and HA-PT β-cDNA constructs. Twenty four hours after transfection cells were treated for 4 hours with 100 µg/ml CHX. Cell extracts were treated with endo H or PNGase F, separated by SDS-PAGE and analyzed by anti-Myc- and anti-HA-western blotting. Equal loading of the gel was verified by anti-α-tubulin immunoblotting. Positions of molecular mass marker proteins, PT α/β-subunit precursor protein and the individual PT α- and β-subunits are indicated. (C) COS-7 cells were transfected with PT α-Myc and HA-PT β cDNA constructs. After 24 hours cells were treated with 100 µg/ml CHX for 2 hours, fixed and incubated with antibodies against the Myc-epitope (green), the *cis*-Golgi marker protein GM130 (red), or the ER marker protein PDI (red). Nuclei were visualized by DAPI staining (blue). In merged images yellow indicates co-localization. Scale bars 10 µm.

3.1.4 The triple arginine motif in the C-terminal cytosolic domain of the PT β-subunit is not a functional ER retention motif

For a number of multisubunit-type I proteins triple arginine-based ER localization motifs have been identified in the C-terminal cytoplasmic domain, which conform to the

consensus sequence ψ/φ/R-R-X-R, where ψ/φ are bulky hydrophobic or aromatic amino acids and X is any amino acid (Michelsen et al, 2005). The cytoplasmic domain of the PT β-subunit also contains a highly conserved triple arginine motif (^{1242}RRR^{1244}, Fig 3.4A). To examine whether it represents a functional ER retention motif, the triple arginine residues were substituted by alanines (HA-PT β-^{1242}RRR^{1244}→AAA). To exclude additional retention motifs, complete cytoplasmic tail of the PT β-subunit (21 amino acids) was deleted (HA-PT β-ΔCT, Fig. 3.4.A). To analyze the arrival of the constructs in the Golgi apparatus, extracts of cells expressing HA-PT β, HA-PT β-^{1242}RRR^{1244}→AAA and HA-PT β-ΔCT were incubated in the absence or presence of endo H and PNGase F and analyzed by western blotting.

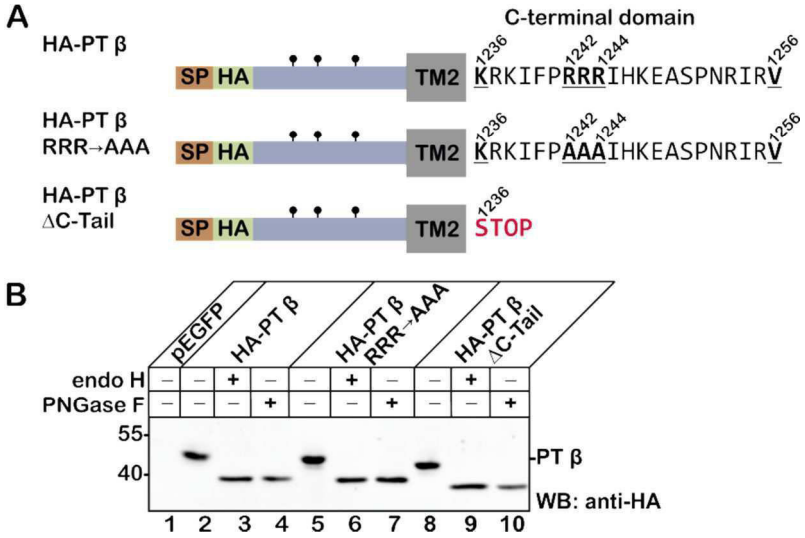

Figure 3.4: The C-terminal domain of the isolated PT β-subunit does not contain an ER retention motif. (A) Schematic representation of PT β-cDNA constructs used for transfection. (B) COS-7 cells were transfected with pEGFP control or isolated wild type and mutant HA-PT β-subunit cDNA, with alanine substitution of the potential ER retention motif (HA-PT β-^{1242}RRR^{1244}→AAA) or deletion of the entire C-terminal tail (HA-PT β-ΔCT). After 24 hours cells were treated for 4 hours with 100 µg/ml CHX. Cell extracts were incubated in the absence (-) or presence (+) of endo H and PNGase F and analyzed by anti-HA western blotting. Positions of molecular mass marker proteins and PT β-subunit are indicated.

In western blots of cells expressing HA-PT β-ΔCT an immunoreactive band with slightly higher electrophoretic mobility compared to wild type or mutant HA-PT β-^{1242}RRR^{1244}→AAA was detected, which is due to the deletion of C-terminal domain (K^{1236} to V^{1256}, Fig. 3.4B, lanes 2, 5 and 8). Both wild type and mutant PT β-forms contained endo H-sensitive *N*-glycans only, indicating their retention in the ER (Fig. 3.4B). The data suggest that the C-terminal cytosolic domain of isolated PT β-subunit does not contain any functional ER retention motifs.

3.1.5 Dimerization of the PT α/β-subunit precursor protein is required for efficient ER export

The bovine PT-complex is proposed to be a heterohexameric complex composed of two α-, two β- and two γ-subunits, where the α- and γ-subunits are linked by disulfide bridges to homodimers (Bao et al, 1996). Truncated human PT α-subunit protein has been shown to exist as homodimer, covalently linked by a disulfide bridge between cysteine residues in position 70 (Marschner, 2011). The mutation C70S was introduced into the PT α/β-Myc full-length cDNA (PT α/β-Myc $C^{70}S$). The mutant was expressed in COS-7 cells, and cell lysates were separated by non-reducing SDS-PAGE and analyzed by western blotting (Fig. 3.5B).

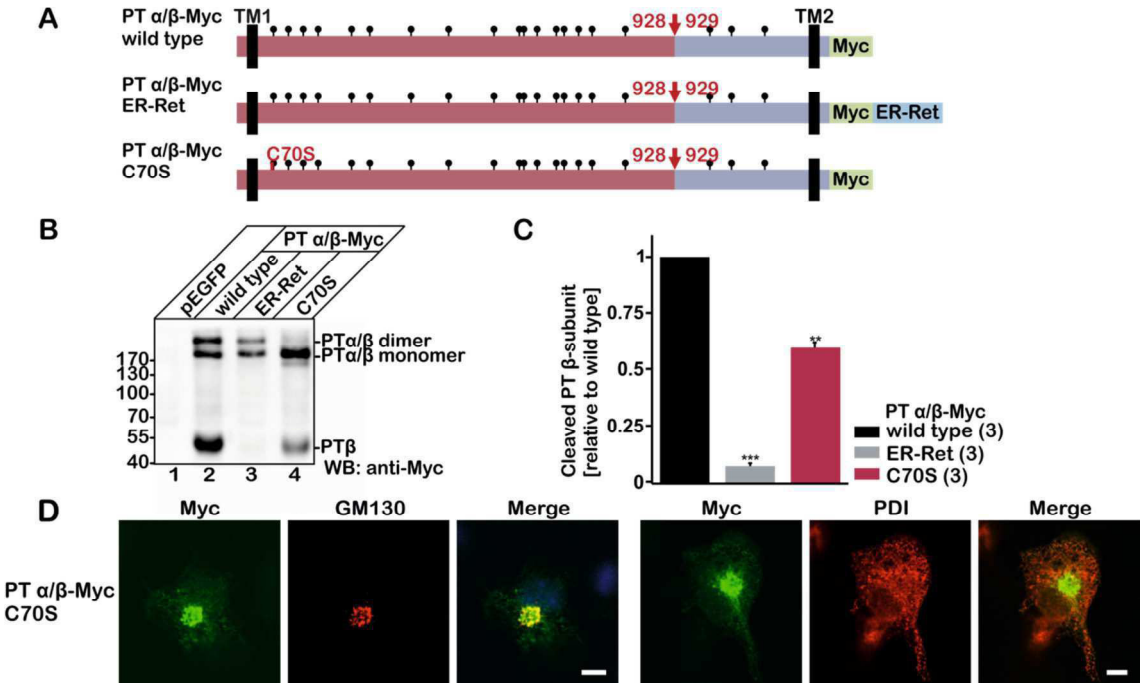

Figure 3.5: Dimerization of the PT α/β-subunit precursor protein by disulfide bridges at position 70 is required for efficient ER exit. (A) Schematic representation of PT α/β-cDNA constructs used for expression analysis. The position of C70 substituted by serine is indicated. (B) COS-7 cells were transfected with pEGFP as negative control, wild type and mutant PT α/β-Myc ER-Ret and C70S subunit precursor cDNA constructs. After 24 hours cells were treated for 4 hours with 100 µg/ml CHX. Cell extracts were separated by non-reducing SDS-PAGE and analyzed by anti-Myc western blotting. Positions of molecular mass marker proteins, the monomeric and dimeric PT α/β-subunit precursor protein and the cleaved PT β-subunit are indicated. (C) Intensities of immunoreactive bands were quantified by densitometry. Amounts of cleaved PT β-subunit related to total amount of cleaved and uncleaved PT α/β-forms (β-subunit / [α/β-subunit precursor + β-subunit]) are shown as average ± SD in a bar diagram. The amount of cleaved PT β-subunit in extracts of wild type expressing cells was arbitrarily set as 1. Number of independent transfections used for statistical evaluation is indicated in brackets. Statistically significant differences to wild type values are marked (***, $p < 0.0001$; **, $p < 0.01$). (D) COS-7 cells were transfected with PT α/β-Myc C70S subunit precursor cDNA. After 24 hours cells were treated with 100 µg/ml CHX for 2 hours, fixed and incubated with antibodies against the Myc-epitope (green), the *cis*-Golgi marker protein GM130 (red), or the ER marker protein PDI (red). Nuclei were visualized by DAPI staining (blue). In merged images yellow indicates co-localization. Scale bars 10 µm.

Additionally to the cleaved mature 45 kDa PT β-subunit and the monomeric 180 kDa PT α/β-subunit precursor protein, the homodimeric form of the wild type PT α/β-Myc subunit precursor protein was detected with a molecular mass of 360 kDa under non-reducing conditions, (Fig. 3.5B, lane 2). Retention of the precursor in the ER impaired proteolytic cleavage, but the homodimeric form however could be detected, indicating that the dimerization occurs in the ER (Fig. 3.5B, lane 3). In contrast, in western blots of cells expressing the mutant PT α/β-Myc $C^{70}S$, the 360 kDa dimeric precursor protein did not appear, accompanied by increased levels of monomeric 180 kDa form (Fig. 35B, lane 4). Furthermore, the amount of cleaved PT β-subunit was decreased by 40% (Fig. 3.5B). Double immunofluorescence microscopy of cells expressing PT α/β-$C^{70}S$ mutant revealed co-localization with the *cis*-Golgi marker protein GM130, but also minor co-localization with the ER marker protein PDI (Fig. 3.5C). The data suggest that impairment of stable dimerization of the PT α/β-subunit precursor protein leads to reduced ER export and proteolytic activation in the Golgi apparatus.

3.1.6 Luminal domains of the PT α/β-subunit precursor protein are required for efficient ER export

To define whether the highly glycosylated LD of the PT α/β-subunit precursor protein is required for efficient ER export, the 1165 aa LD of the PT α/β-subunit precursor protein was replaced by the 406 aa LD of the lysosomal integral membrane protein 2 (LIMP-2), generating PT α/β-Myc LD-LIMP-2 (Fig. 3.6A). LIMP-2 is a type III membrane protein containing two TMDs, thus bearing the identical membrane topology as the PT α/β-subunit precursor protein (Fujita et al, 1992). ER export of LIMP-2 can be monitored by the acquisition of complex-type *N*-linked oligosaccharides (Blanz et al, 2010). Wild type LIMP-2-Myc and mutant LIMP-2 fused to a C-terminal ER retention motif (LIMP-2-Myc ER-Ret) were used as positive and negative controls for ER export, respectively (Fig. 3.6A). In western blots of cells expressing wild type LIMP-2-Myc a 85 kDa immunoreactive band was detected (Fig. 3.6B, lane 4). Treatment with endo H resulted in the shift of the molecular masses to 70 kDa and 55 kDa, which represent the major endo H-resistant and the minor endo H-sensitive ER forms of LIMP-2 (Fig. 3.6B, lane 5). PNGase F treatment resulted in a molecular mass shift to the non *N*-glycosylated 55 kDa LIMP-2 form (Fig. 3.6B, lane 6). The acquisition of complex-type *N*-linked oligosaccharides confirmed that wild type LIMP-2 protein is exported from the ER. In western blots of cells expressing PT

α/β-Myc LD-LIMP-2 and LIMP-2-Myc ER-Ret immunoreactive bands with apparent molecular masses of 72 kDa were detected (Fig. 3.6B, lanes 1 and 7). Treatment with endo H and PNGase F resulted in a shift to the 55 kDa form indicating that PT α/β-Myc LD-LIMP-2 and LIMP-2-Myc ER-Ret contain only endo H-sensitive *N*-glycans, thus are retained in the ER (Fig. 3.6B, lanes 2, 3, 8, and 9). The LD of the PT α/β-subunit precursor protein is critically required for efficient ER export.

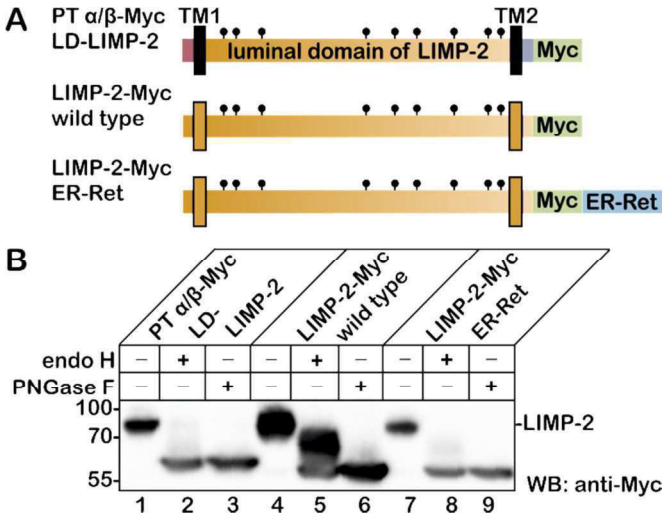

Figure 3.6: The luminal domain of PT α/β-subunit precursor protein is essential for ER export. (A) Schematic representation of PT α/β-subunit precursor/LIMP-2 chimera and LIMP2 cDNA constructs used for expression analysis. The positions of the Myc-epitope (green), C-terminal ER retention motif (ER-Ret, blue), transmembrane domains (TM) and *N*-glycosylation sites (🍍) are indicated. (B) HeLa cells were transfected with PT α/β-Myc LD-LIMP-2, LIMP-2-Myc and LIMP-2-Myc ER-Ret cDNA constructs. After 36 hours cells were harvested and extracts were separated by SDS-PAGE and analyzed by anti-Myc western blotting. Positions of molecular mass marker proteins and wild type LIMP-2 are indicated.

3.1.7 Substitution of transmembrane domain 1 reduces ER export of the PT α/β-subunit precursor protein

The TMDs of integral type II membrane proteins have been shown to be involved in intracellular localization and transport in the secretory and endocytic pathways, mainly by their physical properties, such as the length and hydrophobicity of the TMDs (Cosson et al, 2013). To study the role of the TMDs of the PT α/β-Myc subunit precursor protein for ER export, both TMDs where individually exchanged against the TMD of LIMP-2, which have the same length of 23 aa as those of the PT α/β-subunit precursor protein (PT α/β-Myc TM 1-LIMP-2 and PT α/β-Myc TM 2-LIMP-2, Fig. 3.7A). The chimeric cDNA constructs where expressed in HeLa cells, extracts incubated in the absence or presence of endo H and PNGase F and analyzed by western blotting.

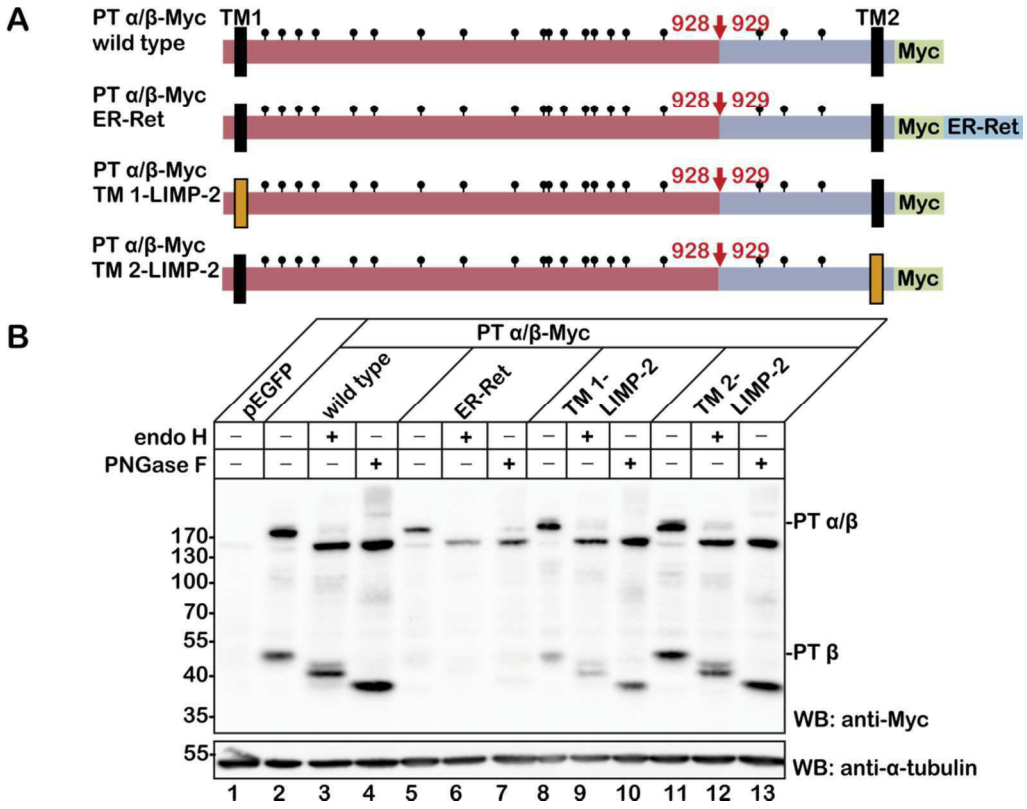

Figure 3.7: Substitution of transmembrane domain 1 impairs moderately the ER export of PT α/β-subunit precursor protein. (A) Schematic representation of PT α/β-cDNA constructs used for expression analysis. Transmembrane domains of LIMP-2 are marked in yellow. (B) HeLa cells were transfected with pEGFP as negative control, wild type and mutant PT α/β-Myc ER-Ret, TM 1-LIMP-2 and PT α/β-Myc TM 2-LIMP-2 cDNA constructs. Cell extracts were separated by SDS-PAGE and analyzed by anti-Myc western blotting. Equal loading of the gel was verified by anti-α-tubulin immunoblotting. Positions of molecular mass marker proteins, the PT α/β-subunit precursor protein and the cleaved PT β-subunit are indicated.

In extracts of cells expressing wild type PT α/β-Myc, PT α/β-Myc TM 1-LIMP-2 and PT α/β-Myc TM 2-LIMP-2 both the 180 kDa PT α/β-subunit precursor protein and the cleaved mature 45 kDa PT β-subunit were detected (Fig. 3.7B, lanes 2, 8 and 11), indicating that chimeric proteins were properly folded and expressed at levels comparable to the wild type. Endo H and PNGase F treatment of both mutants resulted in the same band pattern as observed for the wild type protein (Fig 3.7B, lanes 2 to 4 and 8 to 13). In western blots of cells transfected with the PT α/β-Myc ER-Ret cDNA only the 180 kDa band representing the uncleaved PT α/β-subunit precursor protein was observed confirming complete ER retention (Fig. 3.7B, lane 5). Chimeric PT α/β-Myc TM 2-LIMP-2 amounts of PT β were equal to wild type PT α/β-Myc, indicating unaltered ER export of the chimeric protein (Fig. 3.7B). Substitution of TMD 1 led to slightly decreased levels of mature PT β-subunit, which might indicate an impaired ER export.

3.1.8 Both cytosolic domains of the PT α/β-subunit precursor protein contain ER export motifs

ER export of transmembrane protein cargo is mediated by short sorting motifs in their cytosolic domains (Bonifacino & Glick, 2004). To check the presence of sorting motifs in cytosolic domains of the PT α/β-Myc subunit precursor protein, complete N- and C-terminal cytosolic domains were substituted by 10 alanine residues (PT α/β-Myc NT-10xA and PT α/β-Myc CT-10xA, respectively, Fig. 3.8A).

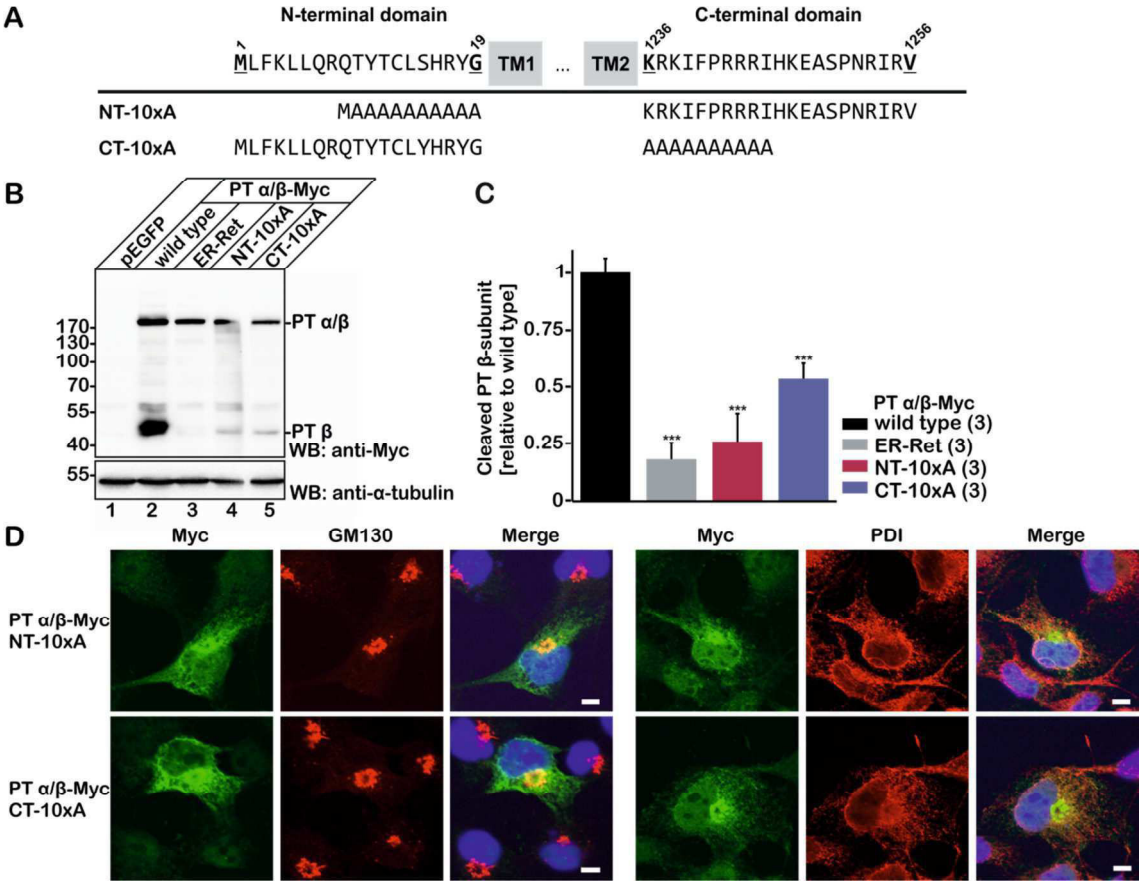

Figure 3.8: N- and C-terminal cytosolic domains of the PT α/β-subunit precursor are both important for ER export. (A) Amino acid sequences of wild type and alanine substituted N- and C-terminal cytosolic domains of the PT α/β-subunit precursor constructs, used for expression analysis. (B) COS-7 cells were transfected with pEGFP as negative control, wild type and mutant PT α/β-Myc ER-Ret, NT-10xA and CT-10xA subunit precursor cDNA constructs. After 24 hours of transfection cells were treated with 100 µg/ml CHX for 4 hours and cell extracts were separated by SDS-PAGE and analyzed by anti-Myc western blotting. Equal loading of the gel was verified by anti-α-tubulin immunoblotting. Positions of molecular mass marker proteins, PT α/β-subunit precursor and the cleaved PT β-subunit are indicated. (C) Relative intensities of immunoreactive bands were quantified by densitometry. Amounts of cleaved PT β-subunit related to total amount of cleaved and uncleaved PT α/β-forms (β-subunit / [α/β-subunit precursor + β-subunit]) are shown as average ± SD. The amount of cleaved PT β-subunit in extracts of wild type expressing cells was arbitrarily set as 1. Number of independent transfections used for statistical evaluation is indicated in brackets. Statistically significant differences to wild type values are marked (***, $p < 0.0001$). (D) COS-7 cells were transfected with PT α/β-Myc NT-10xA and PT α/β-Myc CT-10xA subunit precursor cDNA. After 24 hours cells were treated with 100 µg/ml CHX for 2 hours, fixed and incubated with antibodies against the Myc epitope (green), the *cis*-Golgi marker protein GM130 (red), or the ER marker protein PDI (red). Nuclei were visualized by DAPI staining (blue). In merged images yellow indicates co-localization. Scale bars 10 µm.

Constructs were expressed in COS-7 cells and cell lysates analyzed by western blotting. Presence of cleaved PT β-subunit was used as an indicator for ER exit (Fig. 3.8B). In western blots of cells expressing PT α/β-Myc wild type, PT α/β-Myc NT-10xA and PT α/β-Myc CT-10xA both, the 180 kDa PT α/β-subunit precursor and the 45 kDa cleaved mature PT β-subunit were detected (Fig. 3.8B). The amounts of cleaved PT β-subunit in extracts of PT α/β-Myc NT-10xA and PT α/β-Myc CT-10xA expressing cells were strongly reduced (to 26% and 50%, respectively) compared to the wild type protein, indicating impaired ER export of mutants (Fig. 3.8B, lanes 4 and 5, C). In western blots of cells expressing the control PT α/β-Myc ER-Ret construct no cleavage was observed at all (Fig. 3.8B and C). Double immunofluorescence microscopy of PT α/β-Myc NT-10xA and PT α/β-Myc CT-10xA revealed partial co-localization with the *cis*-Golgi marker protein GM130 or the ER marker protein PDI (Fig. 3.8D). N- and C-terminal cytosolic domains are both important for the ER export of the PT α/β-subunit precursor. But both, PT α/β-Myc NT-10xA and PT α/β-Myc CT-10xA show still residual transport to the Golgi apparatus.

3.1.8.1 The PT α/β-subunit precursor protein contains highly conserved cytosolic domains

To identify sorting motifs for ER export within the cytosolic domains of the PT α/β-subunit precursor, sequences of the N- and C-terminal cytosolic domains were compared with consensus sequences of known ER export motifs (Bonifacino & Glick, 2004). Four potential highly conserved ER export motifs were found in the cytoplasmic domains of the PT α/β-subunit precursor: a dileucine motif (^{5}LL^{6}) in the N-terminal domain and three dibasic [RK]X[RK]-based motifs (^{1236}KRK^{1238} , ^{1242}RRR^{1244}, and ^{1253}RIR^{1255}) in the C-terminal domain (Kollmann et al, 2010). The C-terminal domain contains clusters of positively charged basic arginine and lysine residues which account for 40% of total residues. Comparison of the N- and C-terminal cytosolic tails of the PT α/β-subunit precursor protein of different species *(Homo sapiens, Pan troglodytes, Macaca mulatta, Mus musculus, Rattus norvegicus, Bos taurus, Gallus gallus, Danio rerio,* and *Canis lupus*) showed that identified potential sorting motifs were highly conserved, except for the homologous PT α/β-subunit precursor protein from dog, which lacked the N-terminal dileucine motif due to its shorter N-terminal domain (Fig. 3.9). In the homologue from zebrafish the C-terminal K^{1238} of the KRK motif and the IR of ^{1253}RIR^{1255} motif are not conserved. The analyses showed high

sequence conservation between different species suggesting an important function of both cytosolic tails (Fig. 3.9)

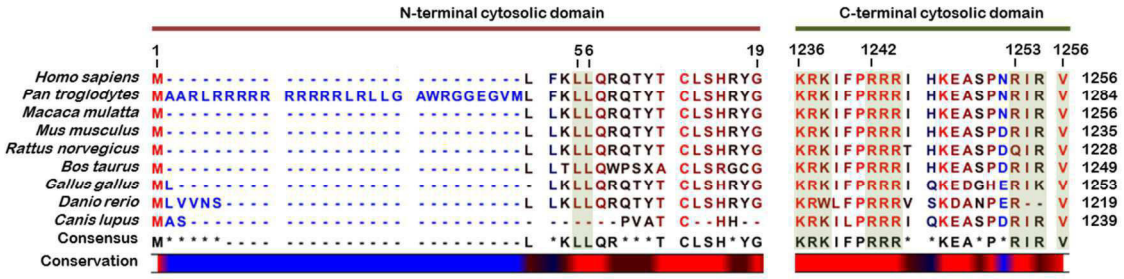

Figure 3.9: N- and C-terminal cytosolic domains of the PT α/β-subunit precursor protein are highly conserved. Homology analysis by multiple alignments of amino acid sequences of cytosolic N- and C-terminal domains of the PT α/β-subunit precursor proteins of indicated species was performed with CLC-sequence viewer software. Terminal aa are numbered on the right. Upper numbers mark the amino acid positions of the human protein. The conservation of aa is depicted by the coloring of letters and in a bar below, where blue indicates lack of conservation and red shows high conservation. The consensus sequence represents a match of at least 80 % of annealed sequences.

3.1.8.2 ER export of the PT α/β-subunit precursor protein is mediated by a combinatorial sorting motif

To analyze which of the potential ER export motifs are functional, alanine substitutions of of the N-terminal dileucine motif (^{5}LL^{6}) and the C-terminal dibasic [RK]X[RK]-based motifs (^{1236}KRK^{1238}, ^{1242}RRR^{1244}, and ^{1253}RIR^{1255}) alone or in combination were introduced into the PT α/β-subunit precursor cDNA. Wild type and mutant PT α/β-subunit precursor proteins were expressed in COS-7 cells and extracts were analyzed by western blotting. The presence of the cleaved PT β-subunit was used as an indicator for ER exit. The densities of the 180 kDa PT α/β-subunit precursor protein and 45 kDa PT β-subunit immunoreactive bands were quantified by densitometry.

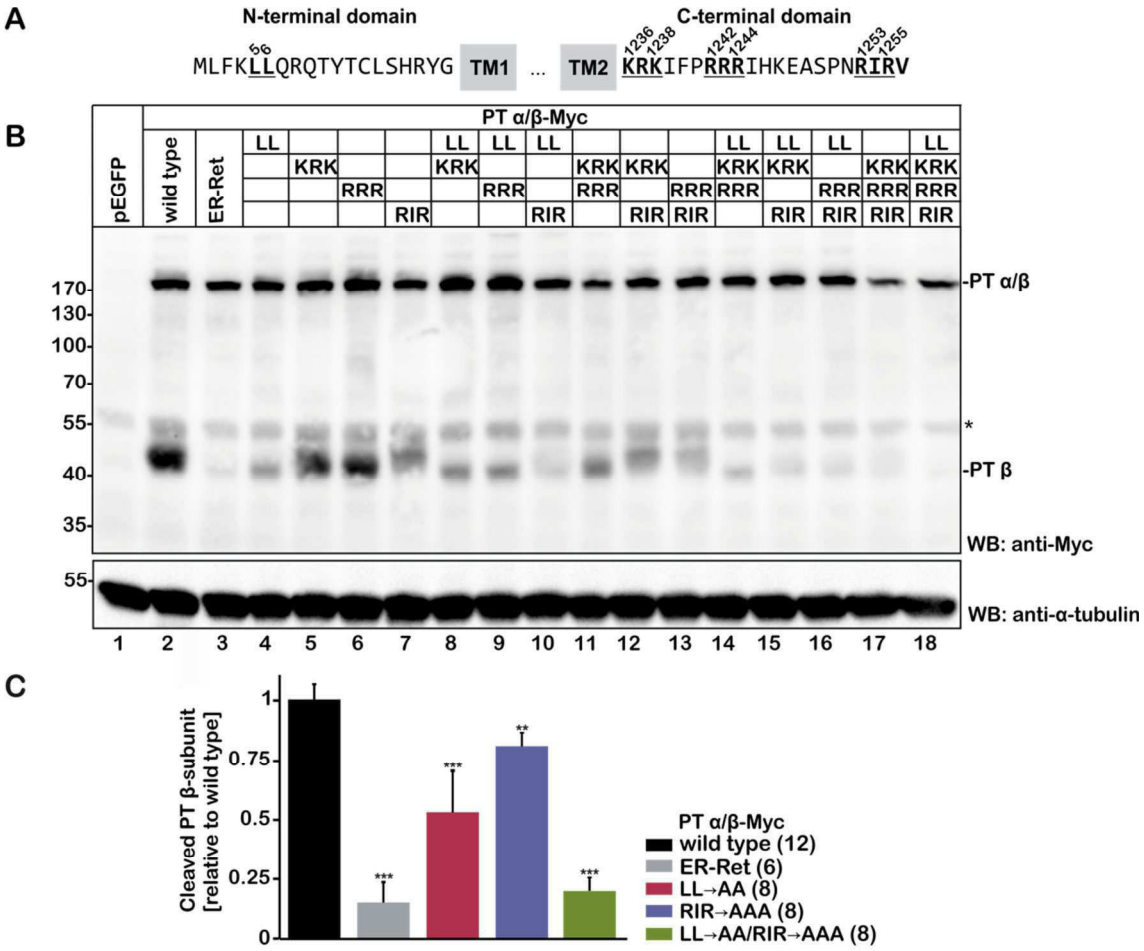

Figure 3.10: Sorting motif-mediated ER export of the PT α/β-subunit precursor protein. (A) Amino acid sequences of the N- and C-terminal cytosolic domains of the PT α/β-subunit precursor protein. Potential ER export motifs (bold, underlined) and amino acid numbers are indicated. (B) Wild type and mutant PT α/β-subunit precursor proteins with alanine substitutions of potential ER export motifs were expressed for 24 hours in COS-7 cells. Prior to harvesting, cells were incubated with CHX (100 µg/ml) for 4 hours and cell lysates were analyzed by anti-Myc western blotting. pEGFP and PT α/β-Myc ER-Ret expressing cells were used as controls. Positions of molecular mass marker proteins, the PT α/β-subunit precursor protein and the cleaved PT β-subunit are indicated. Equal loading of the gel was verified by anti-α-tubulin immunoblotting. The asterisk indicates cross-reactivity of the antibody with a non-specific polypeptide. (C) Relative intensities of immunoreactive bands were quantified by densitometry. Fractions of the cleaved PT β-subunit related to total amount of cleaved and uncleaved PT α/β-forms (β-subunit / [α/β-subunit precursor + β-subunit]) are shown as average ± SD. The amount of cleaved PT β-subunit in extracts of wild type expressing cells was arbitrarily set as 1. Number of independent transfections used for statistical evaluation is indicated in brackets. Statistically significant differences to wild type values are marked (***, $p < 0.0001$; **, $p < 0.01$).

Substitution of the N-terminal dileucine motif ^{5}LL^{6} with alanine residues resulted in the reduction of the intensity of the 45 kDa immunoreactive band (Fig. 3.10B, lanes 2 and 4). Densitometric evaluation revealed a highly significant reduction of cleavage efficiency by 46 ± 18% (Fig. 3.10C). Alanine substitution of individual C-terminal ^{1236}KRK^{1238}, ^{1242}RRR^{1244} and ^{1253}RIR^{1255} motifs showed that the relative amounts of cleaved PT β-subunits were similar to wild type (Fig. 3.10B, lanes 5, 6 and 7). Densitometric quantification revealed a reduction of 20 ± 17% for the ^{1253}RIR^{1255} (Fig. 3.10C). When the N-terminal

dileucine motif was substituted by alanine residues in combination with one of the C-terminal [RK]X[RK]-based motifs, cosubstitution of ^{1253}RIR^{1255} resulted in the strongest reduction of the intensity of the 45 kDa immunoreactive band (Fig. 3.10B, lane 10). Densitometric evaluation revealed a highly significant reduction of cleavage efficiency by 80 ± 9% comparable with the PT α/β-Myc ER-Ret construct (Fig. 3.10B, lane 3). Combined alanine-substitution of two C-terminal dibasic motifs ^{1236}KRK^{1238}/^{1242}RRR^{1244} and ^{1236}KRK^{1238}/^{1253}RIR^{1255} (Fig. 3.10B, lanes 11 and 12) resulted in a minor decrease in the amount of cleaved PT β-subunit, 13% and 34% respectively, whereas in case of ^{1242}RRR^{1244}/^{1253}RIR^{1255} (Fig. 3.10B, lane 13) the amount of PT β-subunit dropped down to 52 %. Of note, expression of double motif mutants ^{1236}KRK^{1238}/^{1253}RIR^{1255} and ^{1242}RRR^{1244}/^{1253}RIR^{1255} resulted in cleaved PT β-subunits exhibiting slightly increased molecular masses (Fig. 3.10B, lanes 12 and 13). The reason for the altered electropohoretic mobilities is unclear. Combined alanine substitution of three or all four of the motifs leads to the decrease in cleaved PT β-subunit comparable to PT α/β-Myc ER-Ret or ^{5}LL^{6}/^{1253}RIR^{1255} mutants (Fig. 3.10B, lanes 3, 10 and 14 to 18).

Double immunofluorescence microscopy analyses revealed that dileucine motif mutant (LL→AA) or the dibasic motif mutants (KRK→AAA, RRR→AAA, RIR→AAA) mainly co-localized with the *cis*-Golgi marker protein GM130. Only small fractions of LL→AA were also codistributed with the ER marker protein PDI. Combined alanine substitution of the ^{5}LL^{6} and ^{1253}RIR^{1255} motifs (LL→AA/RIR→AAA) led to overlapping distribution with PDI. A minor fraction still co-localized with the *cis*-Golgi marker protein GM130, indicating ER retention (Fig. 3.11). Taken together, both cytosolic motifs, the ^{5}LL^{6} at the N-terminal domain and the ^{1253}RIR^{1255} at the C-terminal domain are required for efficient ER export of the PT α/β-subunit precursor.

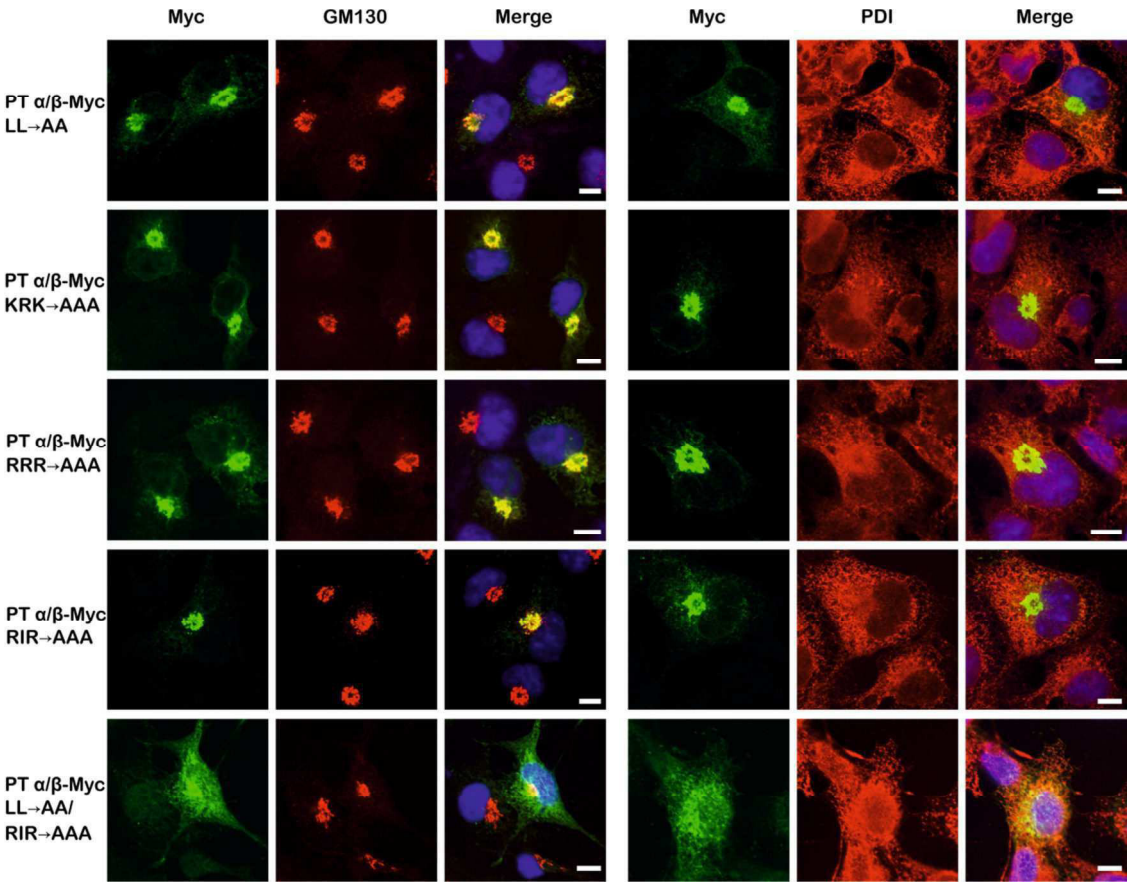

Figure 3.11: PT α/β-Myc LL→AA/RIR→AAA mutant is retained in the ER. COS-7 cells were transfected with the indicated PT α/β-Myc cDNA constructs. After 24 hours cells were treated with 100 µg/ml CHX for 2 hours, fixed and incubated with antibodies against the Myc-epitope (green), the *cis*-Golgi marker protein GM130 (red), or the ER marker protein PDI (red). Nuclei were visualized by DAPI staining (blue). In merged images yellow indicates co-localization. Scale bars 10 µm.

3.1.8.3 ER export depends on two distinct sorting motifs with defined positions

To examine whether the positions of the sorting motifs are interchangeable, the N-terminal dileucine motif (^{5}LL^{6}) and the C-terminal dibasic-based (^{1253}RIR^{1255}) motif were substituted by di- and triple- alanine, dibasic or dileucine residues (Fig. 3.12A). Replacement of the N-terminal dileucine motif ^{5}LL^{6} by dibasic RIR or RR residues (RIR/RIR or RR/RIR) led to a PT α/β-subunit precursor with two basic sorting motifs in the N- and C-terminal domains. These mutations inhibited the cleavage of the PT α/β-subunit precursor comparable with alanine substitution of the ^{5}LL^{6} motif (AA/RIR, Fig. 3.12B, lanes 4, 7 and 8). Furthermore, substitution of the N-terminal ^{5}LL^{6} motif by dibasic-based motifs RIR or RR in combination with alanine substitution of the C-terminal ^{1253}RIR^{1255} motif (RIR/AAA or RR/AAA) prevented cleavage (Fig. 3.12B, lanes 10 and 11). Two dileucine sorting motifs in the N- and C-terminal domain of the PT α/β-subunit precursor (LL/LL) dramatically

reduced the proteolytic processing to the mature PT β-subunit (Fig. 3.12B, lane 9). Also the transfer of the dileucine motif to the C-terminal domain replacing the dibasic-based motif ^{1253}RIR^{1255} in combination with the substitution of the N-terminal dileucine motif (AA/LL), blocked the ER exit and the subsequent proteolytic cleavage to mature PT β-subunit (Fig. 3.12B, lane 12). The data show that the exchange of the sorting motifs at the N- and C-terminal domains leads to an ER export defect. Thus, the export motifs need to be positioned at their proper place and cannot be interchanged.

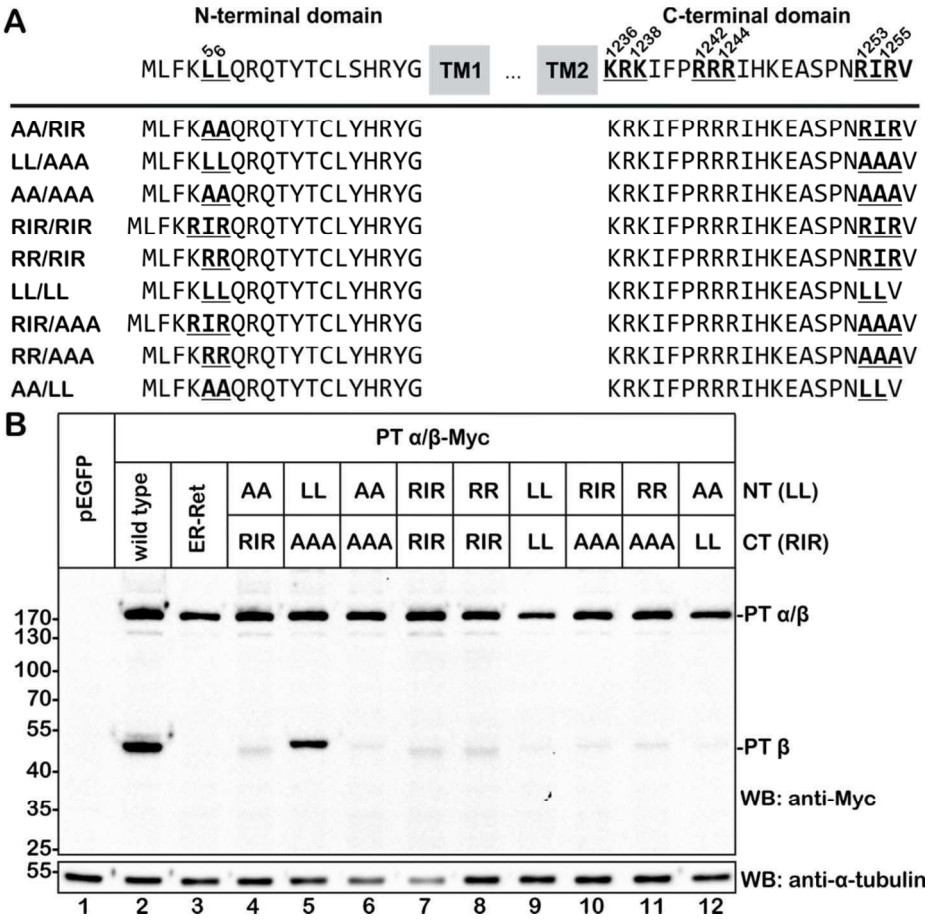

Figure 3.12: ER export of the PT α/β-subunit precursor protein requires the presence of two distinct sorting motifs at defined positions in the N- and C-terminal domains. (A) Amino acid sequences of the N-terminal and C-terminal cytosolic domains of the PT α/β-subunit precursor constructs used for expression analysis. N-terminal dileucine sorting motif (^{5}LL^{6}, red) and the C-terminal dibasic (R/K)X(R/K)-based (^{1253}RIR^{1255}, green) motif were substituted by di- and triple- alanine, dibasic or dileucine residues (bold, underlined) as indicated. (B) Wild type and mutant PT α/β-subunit precursor proteins were expressed in HeLa cells and analyzed 36 hours after transfection by anti-Myc western blotting. pEGFP and PT α/β-Myc ER-Ret expressing cells were used as controls. Positions of molecular mass marker proteins, the PT α/β-subunit precursor and the cleaved PT β-subunit are indicated. Equal loading of the gel was verified by anti-α-tubulin immunoblotting.

3.1.9 MLIII alpha/beta patient mutation K^4Q impairs the ER export of the PT α/β-subunit precursor protein

Two MLII/III alpha/beta missense mutations K^4Q and $K^{1236}M$ which alter the sequence of the cytosolic domains were identified (Kudo et al, 2006; Tiede et al, 2005a). To analyze whether these missense mutations affect ER export and proteolytic cleavage of the PT α/β-subunit precursor, they were introduced into the PT α/β-Myc cDNA.

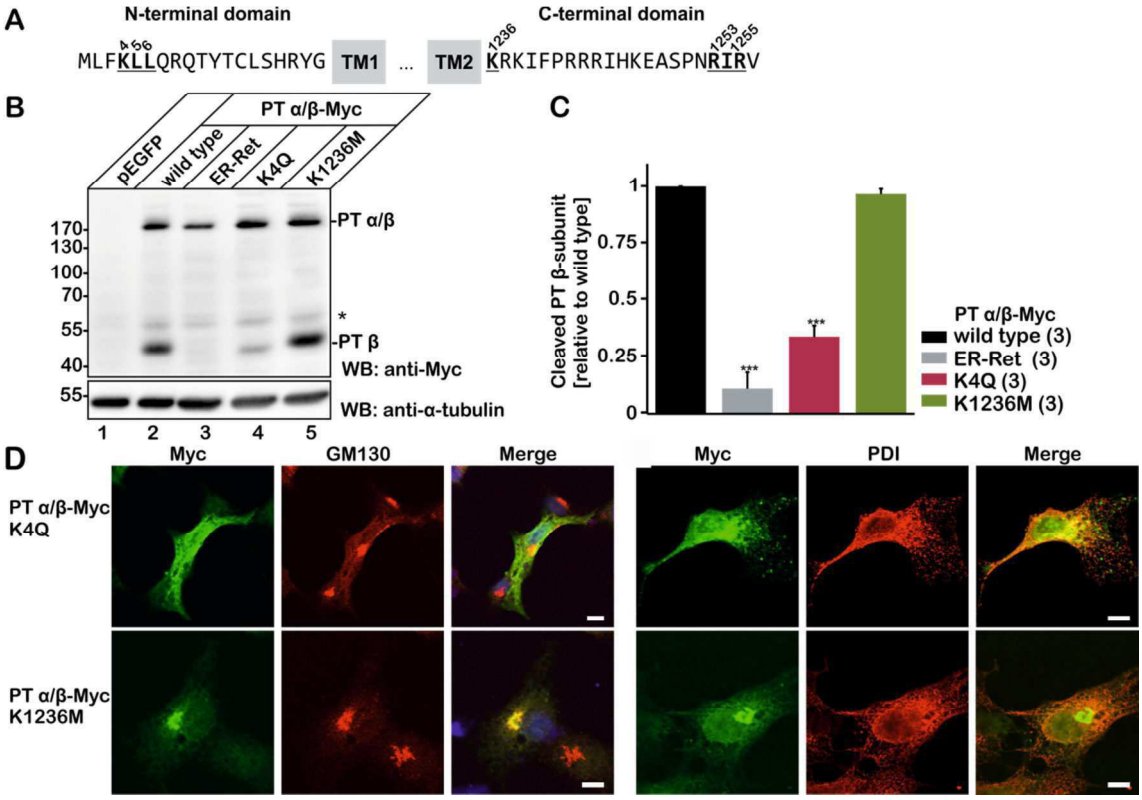

Figure 3.13: Pathogenic mutation K^4Q impairs the ER export of the PT α/β-subunit precursor protein. (A) Amino acid sequences of the N-terminal and C-terminal domains of the PT α/β-subunit precursor. The positions of MLIII patient mutations K^4Q and $K^{1236}M$ (bold, underlined) are marked. (B) COS-7 cells were transfected with pEGFP as negative control, wild type and mutant PT α/β-Myc ER-Ret, K^4Q and $K^{1236}M$ subunit precursor cDNA constructs. 4 hours prior to harvesting cells were treated with 100 µg/ml CHX. Cell extracts were separated by SDS-PAGE and analyzed by anti-Myc western blotting. Equal loading of the gel was verified by anti-α-tubulin immunoblotting. Positions of reference proteins, the PT α/β-subunit precursor and the cleaved PT β-subunit are indicated. (C) Relative intensities of immunoreactive bands were quantified by densitometry. Amounts of cleaved PT β-subunit related to total amount of cleaved and uncleaved PT α/β-forms (β-subunit / [α/β-subunit precursor + β-subunit]) are shown as average ± SD. The amount of cleaved PT β-subunit in extracts of wild type expressing cells was arbitrarily set as 1. Number of independent transfections used for statistical evaluation is indicated in brackets. Statistically significant differences to wild type values are marked (***, $p < 0.0001$). (D) COS-7 cells were transfected with PT α/β-Myc K^4Q and PT α/β-Myc $K^{1236}M$ subunit precursor cDNA. After 24 hours cells were treated with 100 µg/ml CHX for 2 hours, fixed and incubated with antibodies against the Myc-epitope (green), the *cis*-Golgi marker protein GM130 (red), or the ER marker protein PDI (red). Nuclei were visualized by DAPI staining (blue). In merged images yellow indicates co-localization. Scale bars 10 µm.

In western blots of cells expressing the mutant PT α/β-Myc K^4Q, levels of the 45-kDa PT β-subunit were reduced by 70% compared to wild type, whereas the cleavage pattern of PT α/β-Myc $K^{1236}M$ was unchanged (Fig. 3.13B and C). Double immunofluorescence analyses of COS-7 cells transfected with PT α/β-Myc showed that the K^4Q mutant co-localized mainly with the ER marker PDI, but also to a minor extent with the *cis*-Golgi marker protein GM130. In contrast mutant PT α/β-Myc $K^{1236}M$ co-localized mainly with the *cis*-Golgi marker protein GM130 (Fig. 3.13D). The results indicate that mutation K^4Q impairs ER export of the mutant PT α/β-subunit precursor protein.

In HeLa cells expressing the PT α/β-Myc K^4Q and PT α/β-Myc $K^{1236}M$, analysis of *N*-linked oligosaccharides revealed the presence of endo H-sensitive, high mannose-type *N*-glycosylated PT α/β-subunit precursor and endo H-resistant, complex-type *N*-glycosylated PT β-subunit for both mutants (data not shown). The data demonstrate that MLII/III alpha/beta associated mutation K^4Q, positioned proximal to the dileucine sorting motif at the N-terminal cytosolic domain disturbs ER export of the PT α/β-subunit precursor.

3.1.9.1 Identity of the lysine residue at position 4 is important for efficient ER export

The MLIII disease associated K^4Q leads to the loss of positive charge in the N-terminal cytosolic tail and reduced ER export. To analyze whether the presence of the positive charge or the identity of the basic amino acid is critical for efficient ER exit, lysine residue in position 4 was substituted by the neutral amino acid alanine or the positively charged amino acid arginine (PT α/β-Myc K^4A and PT α/β-Myc K^4R, Fig. 3.14A). In all mutant PT α/β-subunit precursor proteins the amount of cleaved PT β-subunit was decreased compared to the wild type construct (Fig. 3.14B) indicating impaired ER export. Thus, the identity of the basic residue in position 4 and not the presence of a positively charged amino acid is important for efficient ER exit.

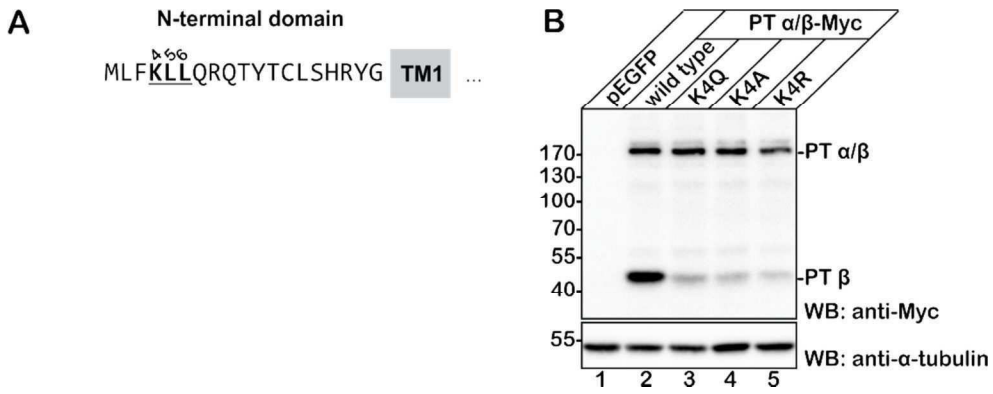

Figure 3.14: The identity of the N-terminal lysine at position 4 is required for efficient ER export. HeLa cells were transfected with pEGFP, wild type and mutant PT α/β-Myc K^4Q, K^4A and -K^4R subunit precursor cDNA constructs. Cell extracts were separated by SDS-PAGE and analyzed by anti-Myc western blotting. Equal loading of the gel was verified by anti-α-tubulin immunoblotting. Positions of molecular mass marker proteins, the PT α/β-subunit precursor protein and the cleaved PT β-subunit are indicated.

3.1.10 Sar1-dependent ER export of the PT α/β-subunit precursor protein

For most type I, type II and type III membrane proteins sorting into COPII coated vesicles for transport to the Golgi apparatus is dependent on the small GTPase Sar1 (Sato & Nakano, 2007). To test a potential role of Sar1 for the transport of the PT α/β-subunit precursor protein from the ER to the Golgi apparatus, wild type PT α/β-Myc was co-expressed with wild type Sar1-mCherry or a GTP-restricted, dominant-negative Sar1-mCherry $H^{79}G$ mutant in COS-7 cells.

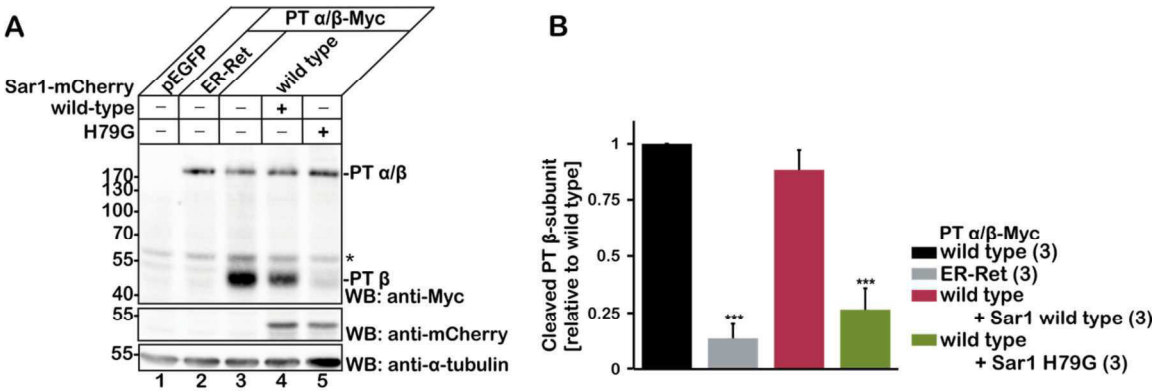

Figure 3.15: Sar1-mediated transport of the PT α/β-subunit precursor protein. (A) COS-7 cells were transfected with pEGFP, PT α/β-Myc ER-Ret, PT α/β-Myc or co-transfected with PT α/β-Myc and wild type or dominant-negative mutant Sar1-H79G mCherry. After 24 hours cells were harvested and extracts were separated by SDS-PAGE and analyzed by anti-Myc and anti-mCherry western blotting. Equal loading of the gel was verified by anti-α-tubulin immunoblotting. Positions of the PT α/β-subunit precursor protein and the cleaved PT β-subunit are indicated. The asterisk indicates the reactivity with a non-specific polypeptide. (C) Relative intensities of immunoreactive bands were quantified by densitometry. Amounts of cleaved PT β-subunit related to total amount of cleaved and uncleaved PT α/β-forms (β-subunit / [α/β-subunit precursor + β-subunit]) are shown as average ± SD. The amount of cleaved PT β-subunit in extracts of wild type expressing cells was arbitrarily set as 1. Number of independent transfections used for statistical evaluation is indicated in brackets. Statistically significant differences to wild type values are marked (***, $p < 0.0001$).

Western blot analysis of cells expressing PT α/β-Myc alone or PT α/β-Myc and wild type Sar1-mCherry in combination, the 180 kDa PT α/β-subunit precursor and the cleaved 45 kDa PT β-subunit were detected in equal ratios (Fig. 3.15A, lane 3 and 4). In cells co-expressing PT α/β-Myc and dominant-negative Sar1 $H^{79}G$, the 180 kDa PT α/β-subunit precursor and a faint band at 45 kDa corresponding to the PT β-subunit were detected (Fig. 3.1.16). Densitometric evaluation of intensities of immunoreactive bands revealed that dominant-negative mutant Sar1 $H^{79}G$ decreased ER export of the PT α/β-subunit precursor by 75% (Fig. 3.15 B), demonstrating the dependence of ER export on Sar1. The data show that the PT α/β-subunit precursor is exported in COPII coated vesicles from the ER.

3.1.11 The PT α/β-subunit precursor protein interacts with multiple proteins of the COPI- and COPII-trafficking machinery

To identify soluble and membrane associated interacting proteins, wild type PT α/β-subunit precursor protein fused to GFP (PT α/β-GFP) at its C terminus was expressed in HEK293 cells (Fig. 3.16B). Preliminary work showed that the fusion of a C-terminal GFP-tag to the wild type PT α/β-subunit precursor protein did not impair its localization in the Golgi apparatus. To test whether the C-terminal fusion of GFP interferes with PT complex formation, PT α/β-GFP was co-expressed with PT γ-Myc followed by co-precipitation (Fig. 3.16A).

In co-transfected HEK293 cells both the 210 kDa PT α/β-GFP, the 75 kDa PT β-GFP and the 38 kDa PT γ-Myc proteins were precipitated by GFP-Trap® indicating formation of the PT complex composed of all three subunits and correct S1P-mediated cleavage (Fig. 3.16A, lane 4). The co-precipitation of the co-expressed PT γ-Myc subunit proved, that interaction partners of the PT α/β-GFP can be co-precipitated with GFP-Trap® beads.

For the identification of interaction partners PT α/β-GFP or GFP alone were expressed in HEK293 and precipitated by GFP-Trap® beads. Aliquots of input, supernatant wash fractions and total of bound proteins were separated by SDS-PAGE and stained with silver (Fig. 3.16B). Further processing of the silver stained gel for the mass spectrometric analysis was done by the Core Facility for Mass Spectrometric Proteomics (UKE, Hamburg).

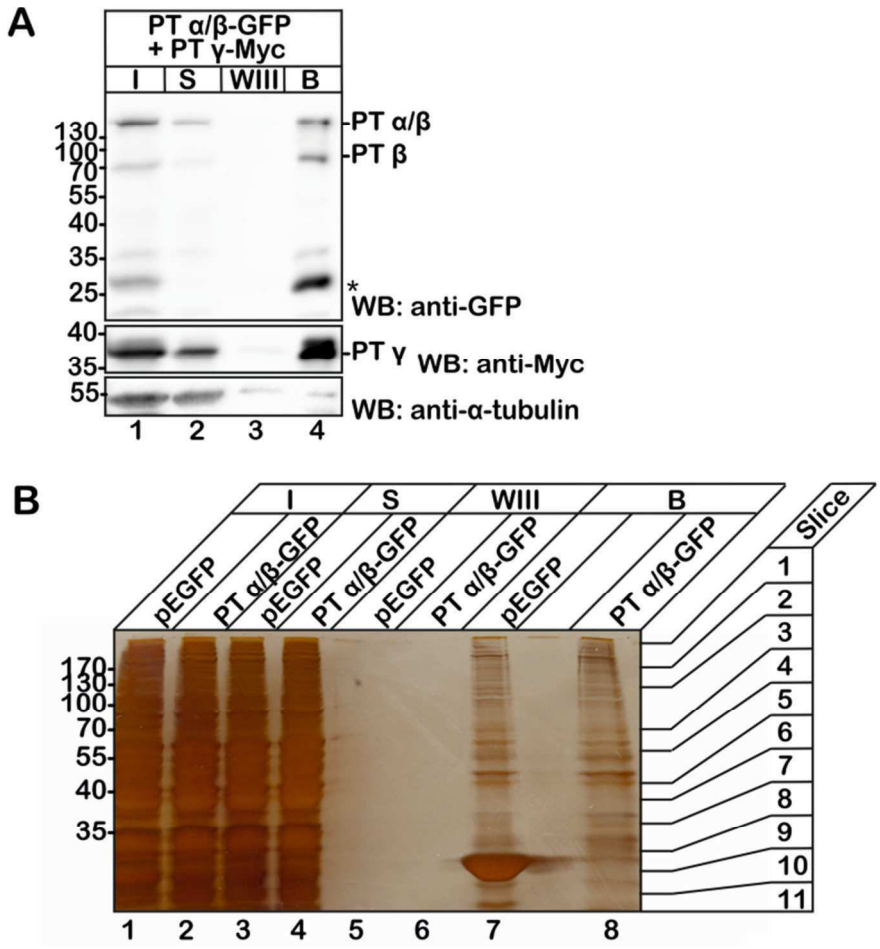

Figure 3.16: Analysis of proteins interacting with the PT α/β-GFP subunit precursor protein. (A) HEK293 cells were co-transfected with PT α/β-GFP and PT γ-Myc cDNA constructs, harvested and PT α/β-GFP was precipitated using GFP-Trap®-Agarose beads. Aliquots of input (I), supernatant (S), third wash fraction (WIII) and complete bound (B) fraction were separated by SDS-PAGE (15% acryl amide) and analyzed by anti-GFP and anti-Myc western blotting. Purity of wash and bound fractions was verified by anti-α-tubulin immunoblotting. Positions of the molecular mass marker proteins, PT γ-subunit, PT α/β-GFP subunit precursor and the cleaved PT β-GFP subunit are indicated. (B) HEK293 cells were transfected with PT α/β-GFP cDNA construct, harvested and PT α/β-GFP was precipitated from cell extracts using GFP-Trap®-Agarose beads. Aliquots of input (I), supernatant (S), third wash fraction (WIII) and complete bound fraction were separated by SDS-PAGE (10 % acryl amide, minigel). After silver staining, interacting proteins of GFP and PT α/β-GFP expressing cells were excised from the gel (11 pieces per lane), digested by trypsin and the resulting peptides analyzed by mass spectrometry.

A total number of 277 proteins was identified in the bound fraction isolated from cell lysates expressing the PT α/β-GFP subunit precursor. As expected, the peptide sequences derived from tryptic digestion of the bait protein PT α/β-GFP were detected with highest abundance, whereas PT γ-Myc has not been identified. Proteins interacting non-specifically with the GFP-Trap® matrix or with GFP alone as well as keratins, ribosomal proteins, proteins of the cytoskeleton, transcription and translation factors, DNA binding proteins, heat shock proteins, stress related proteins and mitochondrial proteins were removed from the list. The positions of the proteins in the gel, according to the gel-slices they were identified in, have been crosschecked with their molecular masses. The remaining 32

proteins, specifically interacting with PT α/β-GFP, PT α and PT β-GFP are listed in Table 3.1. The list contains predominantly cytosolic proteins involved in vesicular transport like COPI components (α- and γ-COP), COPII-components (Sar1A, Sec23A), clathrin coat components (AP-1), Golgi-resident (Rab 1A, Rab 6A, and Rab 33B) and other Rab proteins (Rab 7A, Rab 10, and Rab 15, Table 3.1). Interesting is that also the cation-independent 300 kDa M6P-receptor was found.

Table 3.1: Proteins interacting with PT α/β-GFP identified by mass spectrometry

Name	Protein Name	Location
ACLY	ATP-citrate synthase	cytosol
AP1B1	AP-1 complex subunit beta-1	cytosol, TGN, endosomes
BAG6	Large proline-rich protein BAG6	cytosol, nucleus
BEX5	Protein BEX5	cytosol
CALX	Calnexin	Integral ER-membrane protein
COPA	Coatomer subunit alpha	cytosol, Golgi apparatus
COPG1	Coatomer subunit gamma-1	cytosol, Golgi apparatus
F125A	Multivesicular body subunit 12A	cytoskeleton, cytosol, nucleus, endosomes
KI13A	Kinesin-like protein KIF13A	cytoskeleton, cytosol, endosome, Golgi apparatus
KIF3C	Kinesin-like protein KIF3C	cytoskeleton, cytosol
KT3K	Ketosamine-3-kinase	
MARCS	Myristoylated alanine-rich C-kinase substrate	cytoskeleton, cytosol, membrane
MPRI	Cation-independent mannose-6-phosphate receptor	membrane protein, TGN, endosomes, cell surface
MTAP	S-methyl-5'-thioadenosine phosphorylase	cytosol, nucleus
PFD2	Prefoldin subunit 2	nucleus, cytosol, mitochondrion
PPIA	Peptidyl-prolyl cis-trans isomerase A	cytosol
PPIB	Peptidyl-prolyl cis-trans isomerase B	ER lumen, melanosome
PYR1	CAD protein	cytosol
RAB10	Ras-related protein Rab-10	cell membrane, cytosol
RAB15	Ras-related protein Rab-15	cell membrane, cytosol
RAB1A	Ras-related protein Rab-1A	ER, Golgi apparatus, cytosol
RAB6A	Ras-related protein Rab-6A	Golgi apparatus, cytosol
RAB7A	Ras-related protein Rab-7a	late endosome, lysosome, phagosome, cytosol
RAB33B	Ras-related protein Rab-33B	Golgi apparatus, cytosol
SAHH	Adenosylhomo-cysteinase	cytosol, melanosome
SAR1A	GTP-binding protein SAR1a	ER, cytosol
SEC23A	Protein transport protein Sec23A	ER, cytosol
TRIPB	Thyroid receptor-interacting protein 11	cytoskeleton, cytosol, *cis*-Golgi
TRPM3	Transient receptor potential cation channel subfamily M member 3	multi-pass membrane protein
1433E	14-3-3 protein epsilon	cytosol, melanosome
1433Z	14-3-3 protein zeta/delta	cytosol, melanosome
4F2	4F2 cell-surface antigen heavy chain	apical cell membrane

Interaction partners of PT α/β-GFP identified by mass spectrometry are listed in alphabetical order. Interacting proteins important for intracellular trafficking are marked in green.

3.2 Turnover of wild type and mutant PT α/β-subunit precursor proteins

In the second part of my thesis I analyzed the half-life time of wild type and mutant PT α/β-subunit precursor proteins and mechanisms contributing to their turnover by using drugs inhibiting proteasomes and lysosomes. For this the wild type PT α/β-subunit precursor protein and several mutant control constructs were used, including PT α/β-Myc ER-Ret, $C^{70}S$, $R^{925}A$ as well as MLII/III alpha/beta related mutants $K^{4}Q$ and $K^{1236}M$ (Fig 3.17). An additional MLII alpha/beta related mutation $S^{399}F$, located in the luminal part of the PT α/β-subunit precursor, was included (Bargal et al, 2006; Cury et al, 2013; Encarnacao et al, 2009). This mutation leads to an ER export deficiency of a PT α/β-subunit precursor protein, where amino acids 431 to 848 in the luminal domain are deleted (De Pace, unpublished data, Marschner et al, 2011). Furthermore two TGN located, single pass type I membrane proteins were used as controls: the GlcNAc-1-PD C-terminally tagged with an HA-epitope and the endopeptidase Furin C-terminally tagged with a Myc-epitope (Rohrer & Kornfeld, 2001; Thomas, 2002). Finally also a single pass type II membrane β-Gal-3'-sulfotransferase C-terminally tagged with a Myc-epitope (GP3ST-Myc) protein located in the *trans*-Golgi cisternae was included (Honke et al, 2001). For all experiments of this part HeLa cells were used as expression systems.

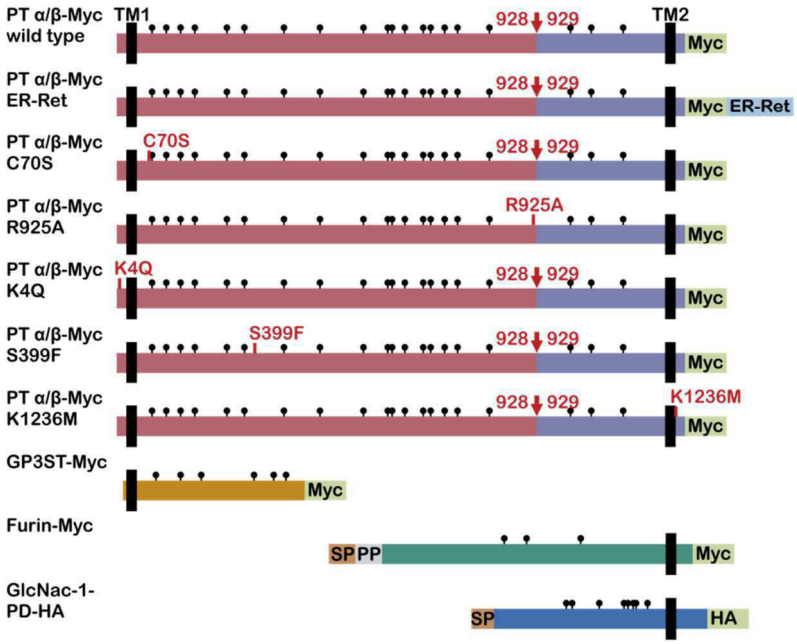

Figure 3.17: Schematic representation of wild type and mutant PT α/β-Myc subunit precursor protein, GlcNAc-1-PD-HA, Furin-Myc and GP3ST-Myc cDNA constructs used for expression analysis. The positions of the Myc-epitope (green), C-terminal ER-retention motif (ER-Ret, blue), transmembrane domains (TM), potential *N*-glycosylation sites, S1P-cleavage site (arrow) and substituted amino residues are indicated. SP: signal peptide; PP: propeptide.

3.2.1 Kinetics of the Golgi-resident membrane protein turnover

The half-life time of the wild type PT α/β-subunit precursor protein was determined by CHX-chase analyses. CHX-chase analyses are used to monitor protein degradation in eukaryotic cells, wherein the protein biosynthesis inhibitor CHX is added to the cells and the decrease in the steady state levels of a target protein is analyzed by immunoblotting after different chase periods. To determine the half-life time of the PT α/β-subunit precursor protein and control proteins GP3ST-Myc, Furin-Myc, and GlcNAc-1-PD, protein synthesis was blocked with CHX (50 µg/ml) 36 hours after the start of transfection. Protein degradation was followed over a time of 15 hours by western blot analysis of cells harvested at different chase times (Fig 3.18).

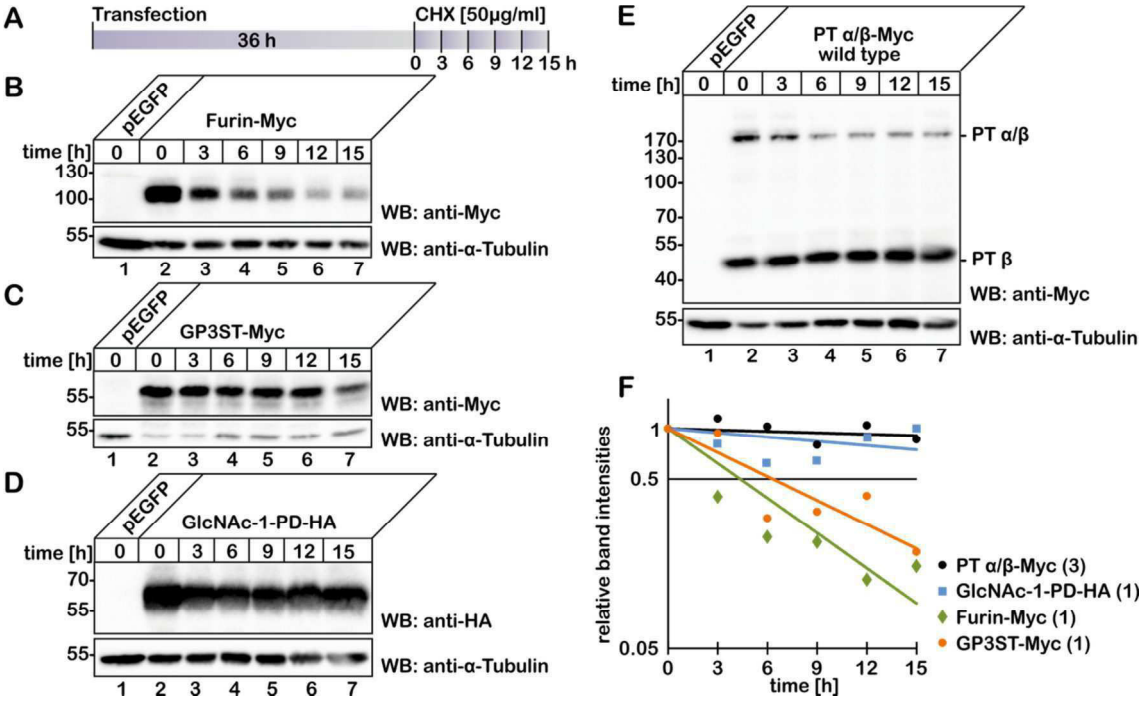

Figure 3.18: CHX-chase analyses of Furin-Myc, GP3ST-Myc, GlcNAc-1-PD and PT α/β-subunit precursor protein stability in HeLa cells. (A) Experimental setup of CHX-chase analyses showing used CHX concentration and chase periods. (B-E) HeLa cells expressing EGFP, Furin-Myc, GP3ST-Myc, GlcNAc-1-PD-HA and PT α/β-Myc subunit precursor protein were either harvested or incubated in the presence of CHX (50 µg/ml) for 3, 6, 9, 12 and 15 hours. Cell lysates were separated by SDS-PAGE and analyzed by anti-Myc or anti-HA western blotting. Equal loading of the gel was verified by α-tubulin immunoblotting. CHX incubation times [h] and the positions of PT α/β-subunit precursor protein, the PT β-subunit and molecular marker proteins are indicated. (F) Intensities of immunoreactive bands were quantified by densitometry. Relative protein amounts normalized to the amount of α-tubulin were plotted against the chase times in a diagram with half logarithmic scale. The relative amount of protein prior to the chase was arbitrarily set as 1. Numbers of independent transfections used for quantification are indicated in brackets.

In western blots of cells expressing Furin-Myc, GP3ST-Myc and GlcNAc-1-PD-HA immunoreactive bands with apparent molecular masses of 100 kDa (Fig. 3.18B), 60 kDa

(Fig. 3.18C) and 65 kDa (Fig. 3.18D), respectively, were detected. The calculated molecular mass of the non-glycosylated GP3ST-Myc is 47,000. During the 15 hour CHX-chase period amounts of Furin-Myc and GP3ST-Myc decreased, whereas the levels of GlcNAc-1-PD-HA remained largely unaltered (Fig. 3.18B-D). Densitometric analyses revealed an approximate half-life time for Furin-Myc of 5 hours, for GP3ST-Myc of 6 hours and for GlcNAc-1-PD-HA > 15 hours in HeLa cells (Fig. 3.18F). In contrast, levels of the PT α/β-subunit precursor protein and the PT β-subunit are most likely determined by both, proteolytic cleavage in the Golgi apparatus and degradation. The amounts of 180 kDa PT α/β-subunit precursor protein decreased constantly indicating proteolytic cleavage to the mature PT α- and β-subunits (Fig. 3.18E). However, after a chase period of 15 hours, the PT α/β-subunit precursor protein could still be detected, indicating stability of the precursor protein and the gradual cleavage into the mature PT α- and β-subunits in the Golgi apparatus. The amount of mature 45 kDa PT β-subunit was stable over 15 hours. In summary the data indicate high stability of PT α/β-subunit precursor protein and GlcNAc-1-PD with half-life times longer than 15 hours, compared to Furin-Myc and GP3ST-Myc.

3.2.1.1 Mutant PT α/β-subunit precursor proteins are rapidly degraded

CHX-chase analyses of mutant PT α/β-Myc proteins revealed decreased stability in comparison to wild type protein (Fig 3.19). The most striking phenotype was observed in extracts from cells expressing PT α/β-Myc $K^{4}Q$ (Fig. 3.19A, lanes 7 to 12). The mutant PT α/β-subunit precursor protein was relatively stable with t ½ > 15 hours (Fig. 3.19C), whereas the small amount of cleaved mature PT β-subunit was rapidly degraded with t ½ = 3 hours (Fig. 3.19D). Dimerization deficient in mutant PT α/β-Myc $C^{70}S$, however, led to decreased stability of the PT β-subunit and α/β-precursor protein with t ½ = 9 and 4 hours respectively (Fig. 3.19A, lanes 13 to 18, C and D). The decrease in PT α/β-subunit precursor protein immunoreactivity is a process composed by loss due to cleavage and reduced stability of the mutant precursor protein. The cleavage deficient PT α/β-Myc $R^{925}A$ mutant was also rapidly degraded (t ½ = 6 hours, Fig. 3.19A, lanes 19 to 24, B). Mutant PT α/β-Myc $K^{1236}M$ subunit precursor protein and the cleaved PT β-subunit showed comparable stability as the wild type protein (Fig. 3.19C and D).

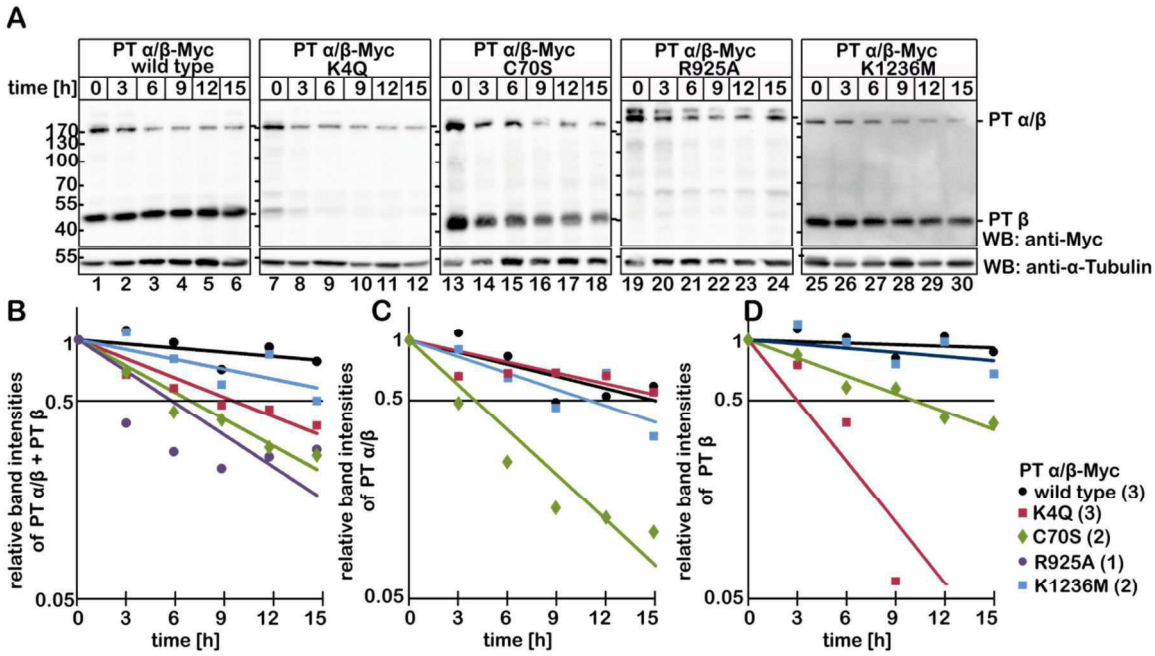

Figure 3.19: Kinetics of the mutant PT α/β-Myc K^4Q, $C^{70}S$, $R^{925}A$ and $K^{1236}M$ turnover. (A) Cells were transfected with pEGFP as negative control, wild type and mutant PT α/β-Myc K^4Q, $C^{70}S$, $R^{925}A$ and $K^{1236}M$ cDNA constructs and either harvested or incubated in the presence of CHX (50 µg/ml) for 3, 6, 9, 12 and 15 hours. Cell extracts were analyzed by SDS-PAGE and anti-Myc western blotting. Equal loading of the gels was verified by α-tubulin immunoblotting. Positions of molecular mass marker proteins, the PT α/β-subunit precursor and the cleaved PT β-subunit are indicated. Intensities of immunoreactive bands of both uncleaved and cleaved PT α/β-forms (B), the PT α/β-subunit precursor (C) and the PT β-subunit (D) were quantified by densitometry, normalized to amounts of α-tubulin and plotted against the chase times in a diagram with half-logarithmic scale. Numbers of independent transfections used for quantification are indicated in brackets. Amounts of uncleaved and cleaved PT α/β-forms prior to the CHX-chase were arbitrarily set as 1.

The ER-retained precursor protein was relatively stable with t ½ >15 hours compared to wild type (Fig. 3.20A, lanes 1 to 6, B), indicating that the decreased amount of PT precursor in wild type PT α/β-Myc expressing cells is mainly due to proteolytic cleavage into the mature PT α- and β-subunits. In western blots of cells expressing the mutant, MLIII alpha/beta associated PT α/β-Myc $S^{399}F$, both the 180 kDa precursor protein and minor amounts (less than 10 % compared to wild type) of the cleaved 45 kDa β-subunit were detected (Fig. 3.20A, lanes 7 to 12). The ER localized mutant precursor protein was rapidly degraded with a half-life time of 4 hours (Fig. 3.20B). The predominant ER localization of mutant PT α/β-Myc $S^{399}F$ suggests that ER export is strongly impaired and that the reduction of precursor protein over the time is not due to proteolytic cleavage but most likely caused by ERAD. The data demonstrate that missense mutations in cytosolic and luminal domains can affect ER export and subsequently lead to reduced half-life times of the mutant non-cleaved precursor protein. Moreover they can lead to the rapid degradation of the PT α/β-subunit precursor protein as well as mature subunits which reach the Golgi apparatus.

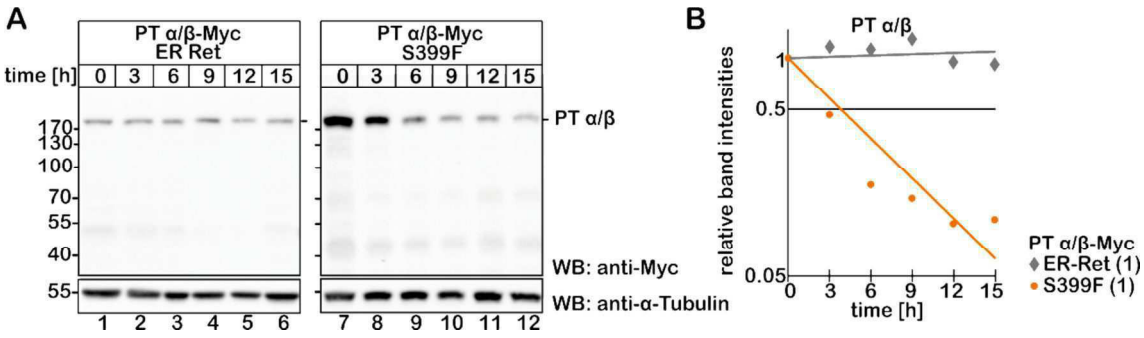

Figure 3.20: CHX-chase analysis of PT α/β-Myc S399F stability. (A) 36 hours after the start of transfection with wild type and PT α/β-Myc S399F subunit precursor cDNA constructs, cells were either harvested or incubated in the presence of CHX (50 µg/ml) for 3, 6, 9, 12 and 15 hours. Cell extracts were analyzed by SDS-PAGE and anti-Myc western blotting. Equal loading of the gels was verified by α-tubulin immunoblotting. Positions of molecular mass marker proteins, the PT α/β-subunit precursor and the cleaved PT β-subunit are indicated. (B) Intensities of immunoreactive bands of PT α/β-subunit precursor protein were quantified by densitometry, normalized to amounts of α-tubulin and plotted against the chase times in a diagram with half-logarithmic scale. Numbers of independent transfections used for quantification are indicated in brackets. Amounts of uncleaved and cleaved PT α/β-forms prior to the CHX-chase were arbitrarily set as 1.

3.2.2 Analyses with inhibitors of proteasomes and lysosomes to identify compartment mediating turnover of PT α- and β-subunits

To identify the compartment involved in the degradation of wild type and mutant PT α/β-subunit precursor protein, cells were incubated in the absence and presence of different drugs listed in Table 3.2, which inhibit degradation in proteasomes and lysosomes.

Table 3.2: List of drugs inhibiting the proteasome, lysosomal proteases and lysosomal acidification used for identification of compartments involved in the degradation of Golgi-resident membrane proteins.

Protease Inhibitor	Target	Working concentration
Lactacystin	irreversible inhibitor of proteasomes	2 µM
MG132	competitive inhibitor of proteasomes	10 mM
Epoxomycin	irreversible inhibitor of proteasomes	2 µM
ALLN	competitive inhibitor of neutral cysteine proteases and proteasomes	2 µM
Leupeptin	competitive inhibitor of serine , cysteine and trypsin-like proteases	100 µM
Pepstatin A	competitive inhibitor of aspartyl proteases, cathepsin D, pepsin and renin	100 µM
E64	irreversible inhibitor of cysteine proteases	30 µM
NH_4Cl	Weak base, which neutralizes acidic compartments	50 mM
BafA1	Potent inhibitor of vacuolar-type H^+-ATPases	100 nM

Used drugs inhibiting the proteasome (green) and lysosomal proteases/lysosomal acidification (red). Working concentrations used for cultured cells are indicated.

3.2.2.1 ERAD contributes to the increased turnover of mutant PT α/β-subunit K^4Q and $S^{399}F$-subunit precursor proteins

Since ER export and thus proteolytic cleavage of mutant PT α/β-subunit K^4Q and $S^{399}F$ precursor proteins are impaired, proteasomal inhibitors lactacystin, MG132, epoxomycin and ALLN were applied to analyse possible turnover of the mutant proteins by ERAD and the proteasome. Cells expressing the ER-retained mutants PT α/β-Myc ER-Ret, K^4Q and $S^{399}F$ were incubated for 6 or 12 hours in the absence or presence of lactacystin, MG132, epoxomycin or ALLN and cell extracts were analyzed by western blotting (Fig. 3.21).

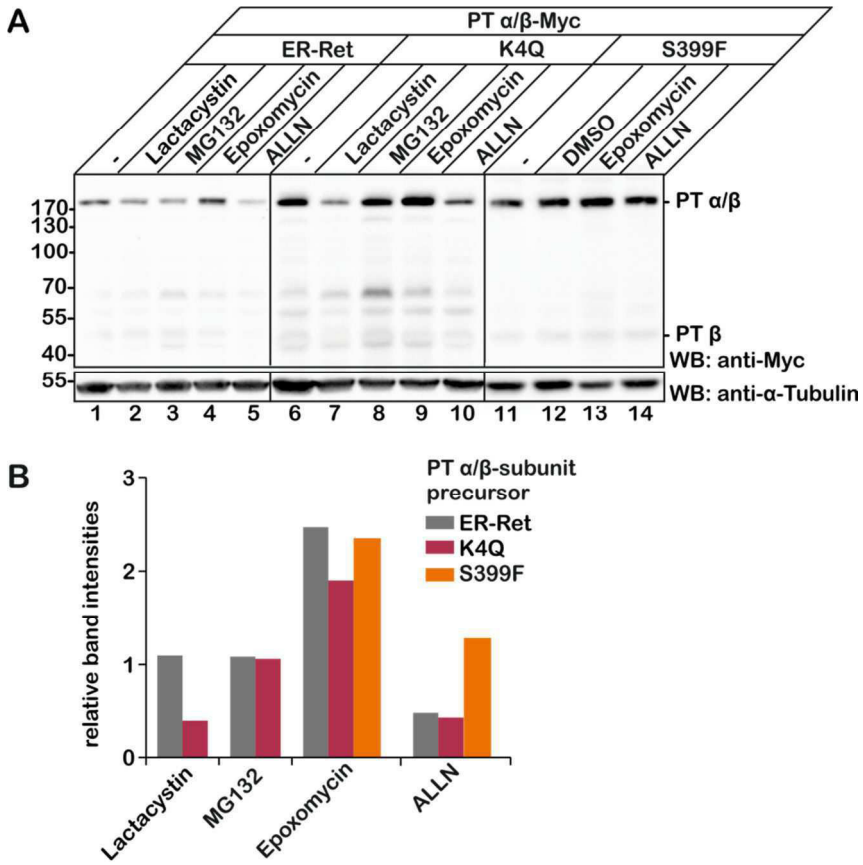

Fig. 3.21: Effect of proteasome inhibition on the degradation of PT α/β-Myc K^4Q and $S^{399}F$ subunit precursor protein. (A) Cells were transfected with PT α/β-Myc ER-Ret, K^4Q and $S^{399}F$ subunit precursor cDNA constructs. After 36 hours cells were incubated in the absence (-) or presence of the indicated proteasomal inhibitors for 6 ($S^{399}F$) or 12 hours (ER-Ret, K^4Q). Cell lysates were separated by SDS-PAGE and analyzed by anti-Myc western blotting. Equal loading of the gel was verified by anti-α-tubulin immunoblotting. Positions of molecular mass marker proteins, the PT α/β-subunit precursor and PT β-subunit are indicated. (B) Intensities of immunoreactive bands of the PT α/β-subunit precursor were quantified by densitometry, normalized to the amount of α-tubulin and shown in a bar diagram. Amounts of the PT α/β-subunit precursor protein in samples of non-treated cells were arbitrarily set as 1.

Quantification of the immunoreactive band intensities revealed a 2 fold increase in the amounts of the 180 kDa subunit precursor protein in extracts of epoxomycin treated cells expressing PT α/β-Myc ER-Ret, K^4Q and $S^{399}F$ (Fig. 3.21A, lanes 4, 9 and 13, B). In

contrast, proteasomal inhibitors lactacystin and ALLN resulted in decreased levels of PT α/β-Myc ER-Ret and K^4Q subunit precursor proteins (Fig. 2.21A, lanes 5, 7 and 10, B), probably due to the toxicity of the compounds. The data demonstrate that ER-retained mutant PT α/β-Myc K^4Q and $S^{399}F$ subunit precursor proteins are degraded by ERAD. Thus impaired ER export and ERAD contribute to decreased amounts of mature, catalytically active PT α- and β-subunits in the Golgi apparatus of these MLII/III patients.

3.2.2.2 Detection of the mature PT α-subunit and PT α-fragment

In the previous experiments half-life times and stability of the cleaved wild type and mutant PT β-subunits were analyzed. However, depending on the position of the mutation (K^4Q in PT α; $K^{1236}M$ in PT β) different stabilities of the PT α- and β-subunits cannot be ruled out. To analyze stability of wild type and mutant PT α-subunits, a monoclonal rat anti-PT α-subunit antibody generated by Dr. Pohl and coworkers, was used. In western blots of cells expressing the wild type PT α/β-Myc the 180 kDa PT α/β-subunit precursor protein and a 120 kDa immunoreactive band were detected by anti-PT α immunoblotting (Fig. 3.22A, lane 2). Treatment of extracts with PNGase F resulted in a shift of the glycosylated 180 kDa precursor protein to the 150 kDa deglycosylated precursor protein and deglycosylated 130 kDa α-subunit. The calculated molecular weights of the deglycosylated precursor protein and the deglycosylated α-subunit are 144 kDa and 105 kDa, respectively (Fig. 3.22A, lane 4). The 120 kDa band shifted to 100 kDa and 80 kDa after endo H- and PNGase F-treatment, respectively (Fig. 3.22A, lanes 3 and 4) indicating the presence of endo H-resistant *N*-glycans. No immunoreactive band representing the 130 kDa PT α-subunit was detected in extracts of cells expressing the S1P-cleavage deficient PT α/β-Myc $R^{925}A$ mutant (Fig. 3.22A, lane 7). To verify specificity of the anti-PT α antibody, extracts of cells expressing the isolated, ER-retained PT α-Myc were analyzed. The 140 kDa PT α-Myc was detected, which shifted to a molecular mass of 110 kDa after endo H and PNGase F treatment (Fig. 3.22B, lanes 5-7). The 20 kDa molecular mass difference between the 140 kDa PT α-Myc and the 120 kDa immunoreactive protein is unclear (Fig. 3.22B, lane 2). The apparent molecular mass of 80 kDa for the deglycosylated PT α-fragment suggests a length of the polypeptide of approximately 700 amino acids. In cells expressing a PT α/β-subunit precursor protein, which lacks amino acid residues 431 to 848, no shorter PT α-fragments were detected (data not shown), suggesting a possible cleavage between residues 700 and 850. Taken together the presence of the PT α-fragments

both in wild type and S1P-cleavage deficient PT α/β-subunit precursor proteins suggest that the precursor protein is cleaved in the LD generating a 120 kDa PT α-fragment, which is independent of prior cleavage by S1P.

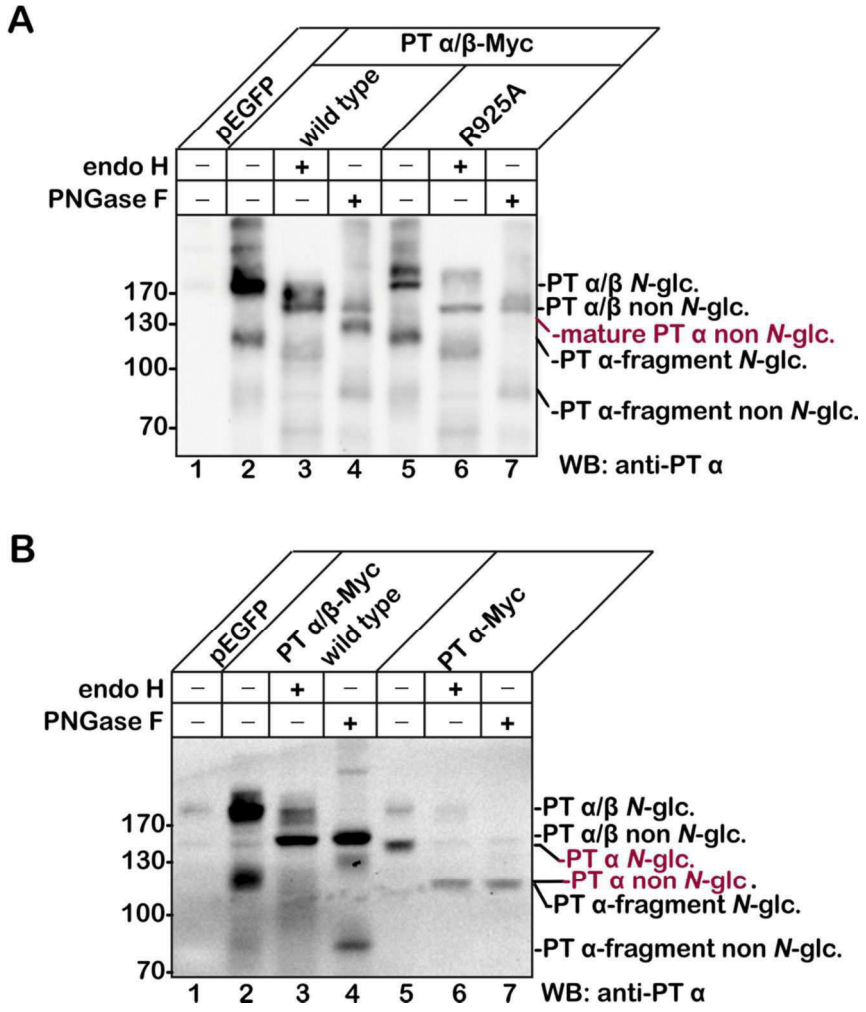

Figure 3.22: S1P-independent cleavage of the PT α/β-Myc subunit precursor protein by an unknown protease. (A and B) HeLa cells were transfected with wild type PT α/β-Myc and S1P-cleavage deficient mutant PT α/β-Myc $R^{925}A$ and isolated PT α-Myc subunit cDNA constructs. pEGFP transfected cells served as controls. Cell extracts were incubated in the absence (-) or presence (+) of endo H and PNGase F, separated by SDS-PAGE (8% acrylamide) and analyzed by anti-PT α western blotting. Equal loading of the gel was verified by anti-α-tubulin immunoblotting. The positions of the molecular mass marker proteins, the PT α/β-subunit precursor and the individual PT α- and β-subunits are indicated. (*N*-glc.: *N*-glycosylated)

3.2.2.3 Degradation of PT α-fragment and PT β-subunit can be inhibited by BafA1

To analyze whether the PT β-subunit and PT α-fragment are degraded in proteasomes or lysosomes cells expressing wild type PT α/β-Myc were incubated for 6 hours with the solvent control DMSO, the proteasomal inhibitors epoxomycin and ALLN or lysosomal protease inhibitors (leupeptin, pepstatin A, E64), endosome-lysosome acidification inhibitors (BafA1, NH_4Cl).

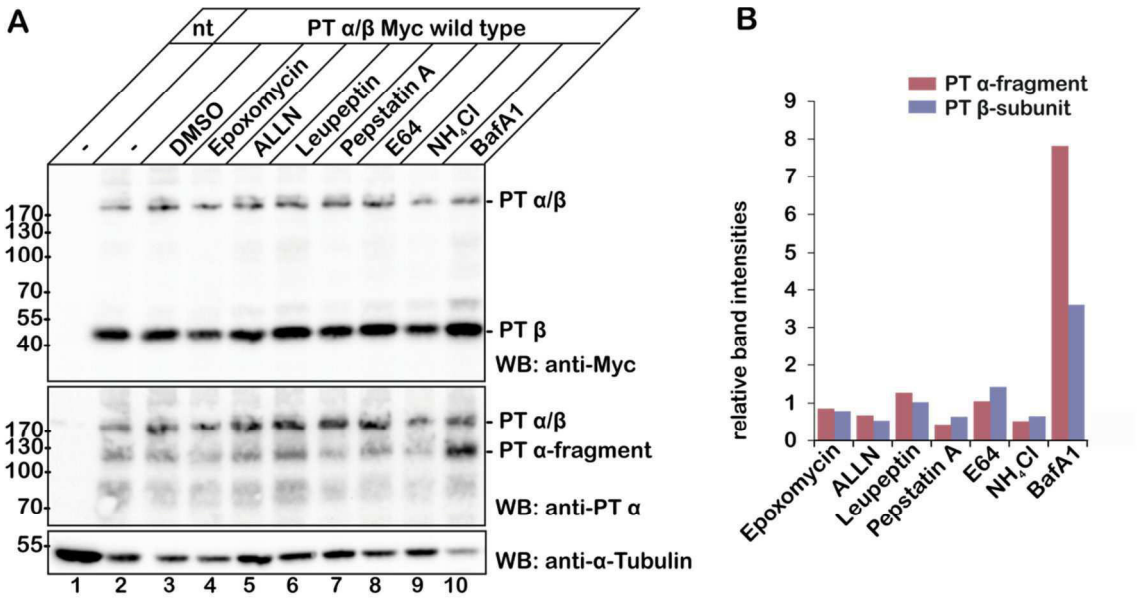

Figure 3.23: Effect of proteasome and lysosome inhibition on the degradation of PT α/β-subunit precursor and mature α- and β-subunits. (A/B) Cells were transfected with wild type PT α/β-Myc subunit precursor cDNA construct. After 36 hours cells were incubated in the absence (-) or presence of solvent control (DMSO) or the indicated protease inhibitors for 6 hours. Non-transfected (nt) cells served as controls. Cell lysates were analyzed by SDS-PAGE and anti-Myc and anti-PT α-western blotting. Equal loading of the gel was verified by anti-α-tubulin immunoblotting. Positions of molecular mass marker proteins, PT α/β-subunit precursor, PT β-subunit and PT α-fragment are indicated. (B) Intensities of immunoreactive bands of the PT α-fragments and the PT β-subunits were quantified by densitometry. Relative amounts of α-fragments and β-subunits were normalized to the levels of α-tubulin and represented as mean in a bar diagram. Amounts of α-fragments and β-subunits in samples of DMSO treated cells were arbitrarily set as 1.

Western blotting of extracts from cells treated with the vacuolar H^+-ATPase inhibitor BafA1 revealed 8- and 3-fold increase in amounts of the 120 kDa PT α-fragment and the 45 kDa β-subunit, respectively, compared to DMSO-treated cells (Fig. 3.23, lane 10). The Inhibitors had no effect on the PT α/β-subunit precursor. Interestingly inhibition of lysosomal proteases and lysosomal acidification did not lead to increased levels of the α-fragment and the β-subunit (Fig. 3.23, lane 2 to 9). In addition, treatment of cells with proteasomal inhibitors did not alter the amounts of α-fragment and β-subunit (Fig. 3.23, lane 4 and 5. The results indicate that the 120 kDa PT α-fragment and the β-subunit are degraded in lysosomes.

3.2.2.4 PT α-fragment and mature PT β-subunit are degraded in lysosomes

Since most striking effects on the turnover of wild type PT α- and β-subunits were observed in cells treated with BafA1, the drug was also applied to cells expressing mutant PT α/β-Myc K^4Q, $K^{1236}M$, $C^{70}S$ and $R^{925}A$. Golgi-resident membrane proteins Furin-Myc, GP3ST-Myc as well as ER-retained PT α/β-Myc ER-Ret and $S^{399}F$ were used as controls (Fig. 3.24).

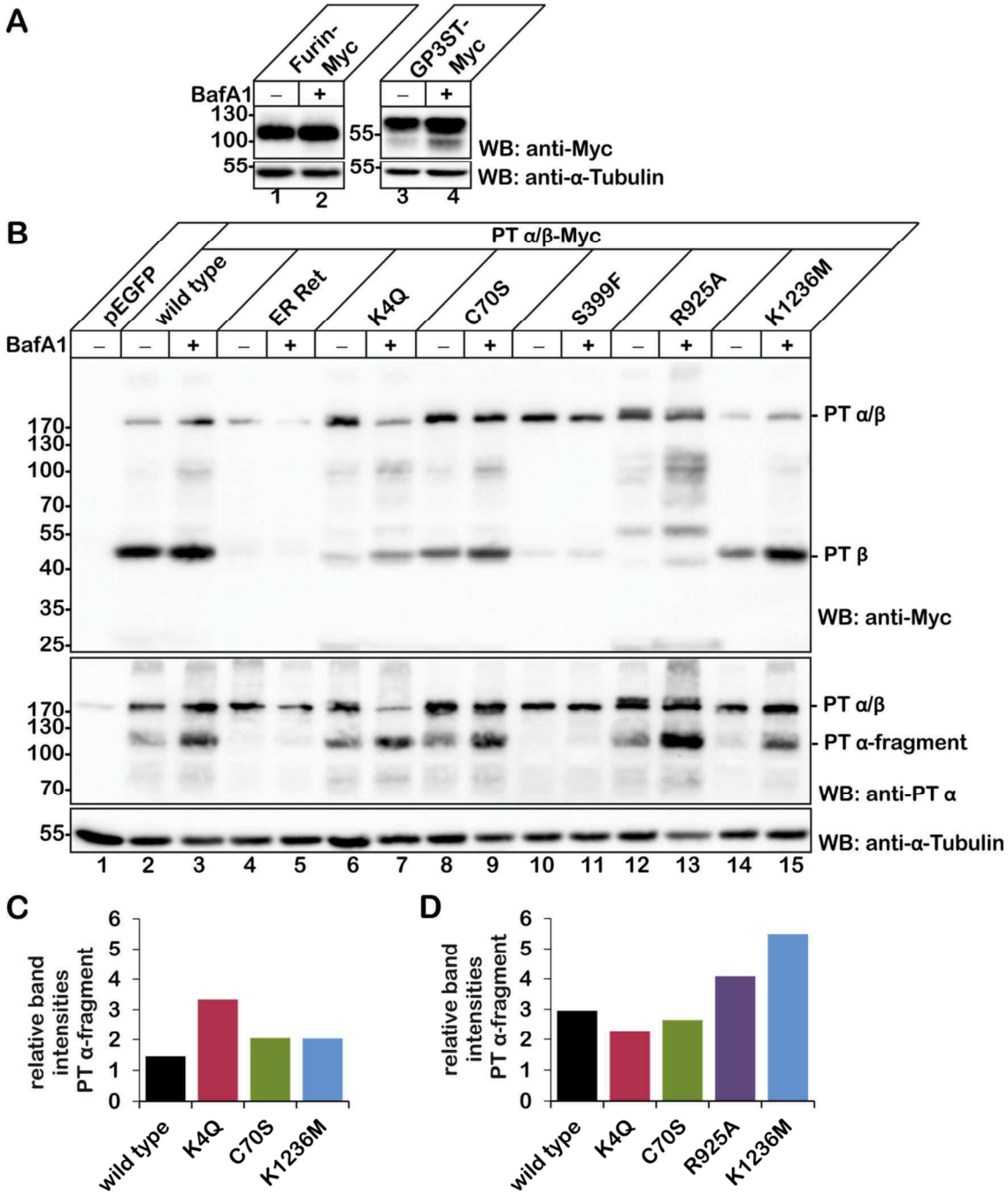

Figure 3.24: Decreased turnover of wild type and mutant PT α/β-Myc by inhibition of vacuolar-type H⁺-ATPases. (A/B) Cells were transfected with pEGFP as control, wild type and mutant PT α/β-Myc ER-Ret, K^4Q, $C^{70}S$, $S^{399}F$, $R^{925}A$, $K^{1236}M$, Furin-Myc and GP3ST-Myc. After 36 hours cells were incubated with the solvent control DMSO or BafA1. Cell extracts were analyzed by SDS-PAGE and anti-Myc and anti-PT α-western blotting. Equal loading of the gel was verified by anti-α-tubulin immunoblotting. Positions of molecular mass marker proteins, PT α/β-subunit precursor, PT β-subunit and PT α-fragment are indicated. Intensities of PT β-subunit (C) and PT α-fragment (D) immunoreactive bands were quantified by densitometry and relative amounts of cleaved PT β-subunit and α-fragment normalized to the amount of α-tubulin shown in a bar diagram. Amounts of PT β-subunits and PT α-fragments in DMSO treated cells were arbitrarily set as 1.

Treatment of the cells expressing wild type and mutant PT α/β-Myc K^4Q, $C^{70}S$, $R^{925}A$ and $K^{1236}M$ with BafA1 did not lead to increased amounts of the 180 kDa PT α/β-Myc subunit precursor protein, suggesting that the precursor protein is not degraded in lysosomes (Fig.

3.24, lanes 2, 3, 6-9 and 12-15). As expected, amounts of the ER-retained PT-ER-Ret and $S^{399}F$ precursor proteins did not increase in the presence of BafA1 (Fig. 3.24, lanes 4, 5, 10 and 11). BafA1 treatment resulted in higher amounts of the cleaved 45 kDa PT β-subunit in cells expressing wild type and mutant PT α/β-Myc K^4Q, $C^{70}S$, $R^{925}A$ and $K^{1236}M$ (Fig. 3.24B). Densitometric quantification revealed a 1.5- (wild type), 3- (K^4Q), and 2-fold ($C^{70}S$, $K^{1236}M$) increase of the β-subunits compared to DMSO-treated controls (Fig. 3.24C). The 120 kDa PT α-fragments were detected in extracts of cells expressing wild type and mutant PT α/β-Myc, but not in the ER-retained PT and mutant $S^{399}F$ (Fig. 3.24B, lanes 4, 5 and 10, 11). Densitometric quantification revealed a 3- (wild type), 2- (K^4Q), 2.5- ($C^{70}S$), and 5-fold ($K^{1236}M$) increase in the amounts of the PT α-fragments compared to DMSO-treated control cells (Fig. 3.24D). Inhibition of the vacuolar H^+-ATPases by BafA1 had only minor or no effect on the turnover of control proteins GP3ST-Myc and Furin-Myc (Fig. 3.24A). The data suggest that both wild type and mutant PT complexes containing mature, cleaved α- and β-subunits are degraded in lysosomal compartments. The absence of the cleaved 120 kDa PT α-fragments in cells expressing ER-retained precursor proteins indicates that S1P-independent cleavage of the precursor proteins occurs in post-ER compartments. Decreased turnover of the PT α-fragments in BafA1-treated cells demonstrates that the generated fragments are further degraded in lysosomes.

3.2.2.5 The mature PT α-subunit is cleaved prior to degradation in lysosomes

To analyze whether the mature PT α-subunit is degraded in lysosomes, cells were transfected with wild type and cleavage-deficient mutant PT α/β-Myc $R^{925}A$. After 36 hours cells were cultured in the presence of BafA1 for 6 hours. Cell extracts were treated with PNGase F and analyzed by western blotting (Fig. 3.25). In extracts of cells treated with BafA1 amounts of the 180 kDa precursor proteins were unchanged compared to DMSO-treated control cells, whereas the levels of the 120 kDa PT α-fragment were strongly increased (Fig. 3.25, lanes 2-5). Levels of the deglycosylated mature 130 kDa PT α-subunit were not altered in extracts of cells treated with BafA1 compared to control cells (Fig. 3.25, lanes 6-7) indicating second cleavage occurs before the PT α-subunit reaches the lysosomes. In contrast, amounts of the deglycosylated 80 kDa PT α-fragment were increased in homogenates of BafA1 treated cells (Fig. 3.25, lanes 7 and 9). The data show that BafA1 has only an effect on the degradation of the PT α-fragment, which appears as a

relatively weak band without BafA1 treatment, but not on the mature PT α-subunit, suggesting the PT α-fragment might be a degradation intermediate.

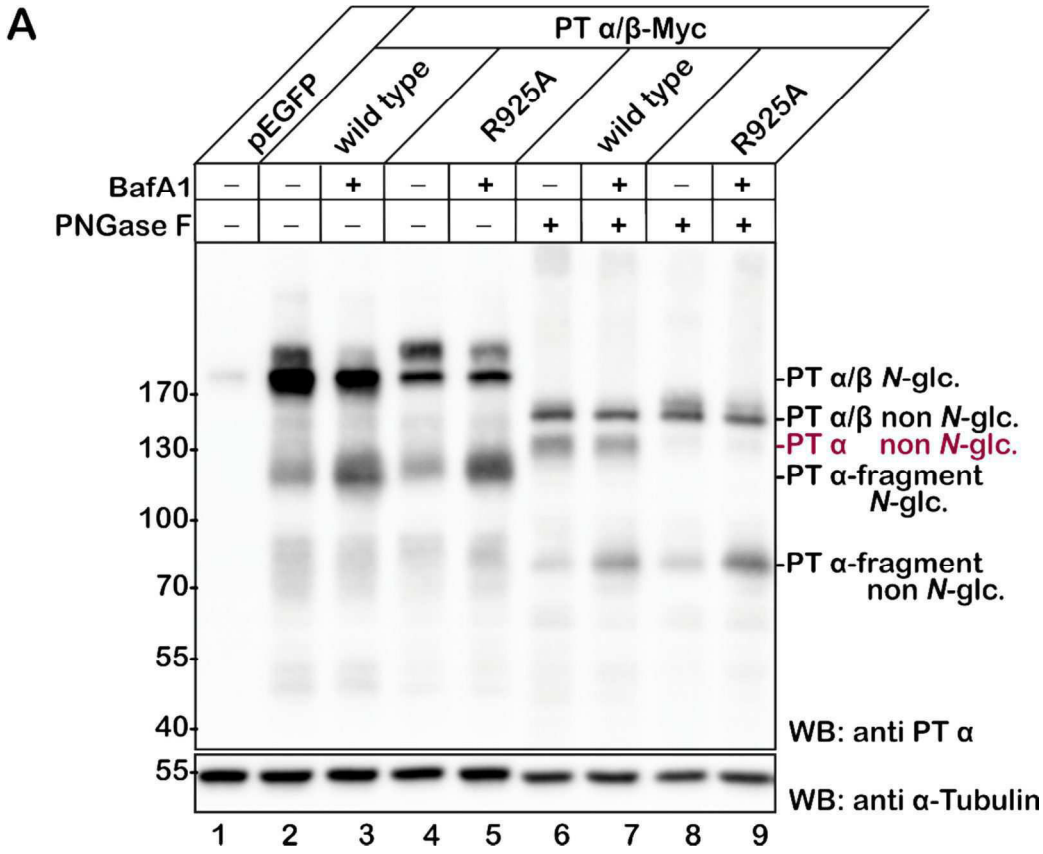

Figure 3.25: Degradation of PT α-fragment in lysosomes. Cells were transfected with pEGFP as control, wild type PT α/β-Myc and PT α/β-Myc $R^{925}A$ cDNAs. After 36 hours cells were incubated with the solvent control DMSO or BafA1 for 6 hours. Cell extracts were treated in the absence (-, lanes 1-5) or presence of PNGase F (+, lanes 6-9) and analyzed by SDS-PAGE (8% acrylamide) and anti-PT α western blotting. Equal loading of the gel was verified by anti-α-tubulin immunoblotting. Positions of molecular mass marker proteins, glycosylated and deglycosylated PT α/β-subunit precursor, PT α-subunit and PT α-fragment are indicated. (*N*-glc.: *N*-glycosylated)

3.2.3 The PT α/β-subunit precursor protein and the mature β-subunit are not localized at the cell surface at steady state

Lysosomal degradation of cell surface receptors (for example EGF-receptors), internalized ligands (e. g. LDL), damaged organelles and cytosolic components is well characterized (Saftig & Klumperman, 2009), but the degradative pathways of Golgi-resident membrane proteins are poorly understood. Since lysosomal degradation contributes to the turnover of wild type and mutant PT α- and β-subunits (Fig. 3.24), a direct pathway from the TGN to endosomes and lysosomes or an indirect pathway via the cell surface with subsequent internalization and final delivery to lysosomes as described for the biosynthetic pathway for lysosomal membrane proteins is possible (Braulke & Bonifacino, 2009). To study the indirect pathway, cell surface biotinylation experiments were performed with HeLa cells

transfected with wild type and mutant PT α/β-Myc $K^{4}Q$, $C^{70}S$ and $K^{1236}M$. The ER-retained PT α/β-Myc ER-Ret and $S^{399}F$, Golgi-localized GP3ST as well as Furin-Myc and endogenous transferrin receptor (TfR) were used as negative and positive control proteins for cell surface localization, respectively. The dynamin inhibitor dynasore was applied to inhibit clathrin mediated endocytosis (Fig. 3.26B, Macia et al, 2006). Thirty-six hours after the start of transfection, cells were incubated in the absence or presence of dynasore for 3 hours, followed by incubation with a membrane-impermeable biotin at 4°C to avoid internalization. Biotinylated proteins were precipitated with streptavidin beads and aliquots of the input and total precipitated proteins by anti-Myc and anti-TfR immunoblotting (Fig. 3.26). In cells expressing the negative control GP3ST-Myc a 60 kDa immunoreactive protein was detected in the input fraction, but not at the cell surface (Fig. 3.26A, lanes 3-4, 9-10). In cells transfected with the positive control Furin-Myc an immunoreactive protein with an apparent molecular mass of 100 kDa was detected both in the input fraction and at the cell surface (Fig. 3.26A, lanes 5-6, 11-12). Densitometric quantification revealed that 6% of total Furin-Myc was present at the cell surface in HeLa cells. The endogenous 110 kDa TfR was detected both in the input and at the cell surface (Fig. 3.26A and B). 8% of total TfR was located at the cell surface. Incubation of cells in the presence of the endocytosis inhibitor dynasore did not result in the expected increased cell surface expression of the TfR. The absence of GP3ST and the presence of Furin-Myc and TfR at the plasma membrane showed that cell surface biotinylation was sensitive to detect specific expression of membrane proteins at the cell surface. In cells transfected with the ER-retained negative control PT α/β-Myc ER-Ret and $S^{399}F$ only the 180 kDa precursor protein was found in the input fractions indicating ER retention and absent S1P-mediated proteolytic cleavage (Fig. 3.26B, lanes 3-4, 9-10). As expected, no biotinylated PT α/β proteins were detected at the cell surface. In cells expressing wild type and mutant PT α/β-Myc $K^{4}Q$, $C^{70}S$ and $K^{1236}M$ both the 180 kDa precursor protein and the mature 45 kDa β-subunit were detected in the input fraction indicating ER export and proteolytic cleavage (Fig. 3.26B, lanes 5-8, 11-12). Small amounts of the 180 kDa precursor protein and the mature 45 kDa β-subunit were detected at the cell surface. Quantification revealed that less than 0.1 % of total PT α/β-precursor and β-subunit proteins were biotinylated at steady state indicating that wild type and mutant PT α- and β-subunits were not located at the cell surface.

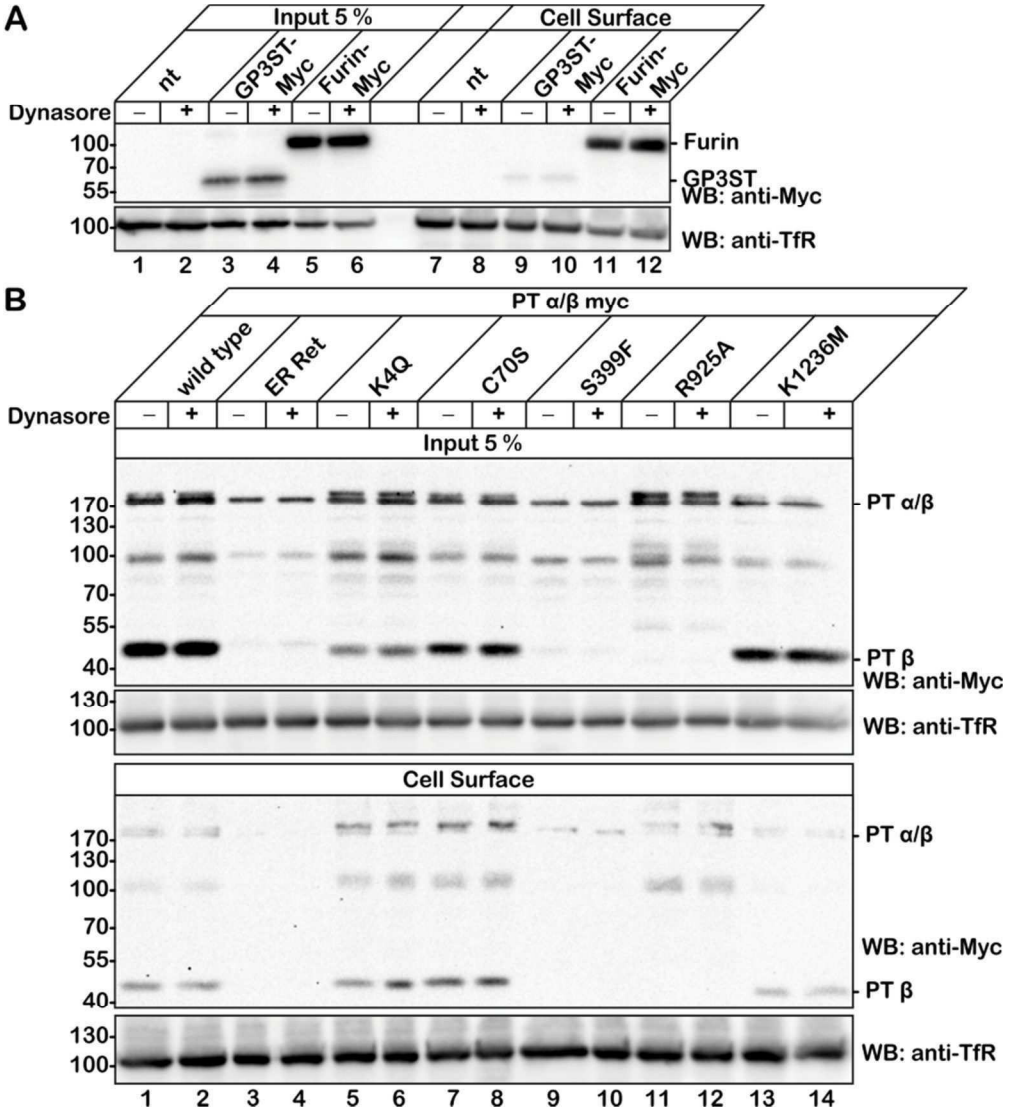

Figure 3.26: Wild type and mutant PT α/β-Myc precursor and β-subunit Myc proteins are not located at the cell surface. (A/B) Cells were transfected with GP3ST-Myc, Furin-Myc, wild type and mutant PT α/β-Myc ER-Ret, K^4Q, $C^{70}S$, $S^{399}F$, $R^{925}A$ and $K^{1236}M$ cDNA constructs. Non transfected cells were used as controls (nt). After 36 hours cells were incubated in the absence (-) or presence (+) of the inhibitor of clathrin-mediated endocytosis dynasore for 3 hours. Subsequently cell surface proteins were labeled with a cell-impermeable NHS-sulfo-biotin at 4°C. Biotinylated proteins were precipitated with streptavidin beads. Input fractions (5% of total) and biotinylated proteins (100%) were subjected to SDS-PAGE and immunoblotting using anti-Myc and anti-TFR antibodies. Expression of endogenous TFR at the cell surface was used as positive control. Positions of molecular mass marker proteins, GP3ST-Myc, Furin-Myc, PT α/β-subunit precursor and PT β-subunit are indicated. Intensities of immunoreactive bands were quantified by densitometry and the amount of cell surface located proteins quantified by comparison with the amounts of protein in the input fraction.

3.2.3.1 The mature PT α- and the PT α-fragment are not released into the medium of cultured HeLa cells

To rule out if lack of detection of PT α- and β-subunits at the cell surface (Fig. 3.26) is due to their rapid shedding by an unknown protease, media were tested for the presence of soluble PT α-subunits. Media of cells expressing wild type and mutant PT α/β-Myc K^4Q

mutant were conditioned in the presence of the proteasomal inhibitor epoxomycin, the cysteine protease inhibitor E64 and the vacuolar H^+-ATPase inhibitor BafA1 for 6 hours. Cell lysates and media were subjected to SDS-PAGE and anti PT α-immunoblotting (Fig. 3.27). To control expression of wild type and mutant PT α/β-Myc K^4Q, cell lysates were also analyzed by Myc immunoblotting.

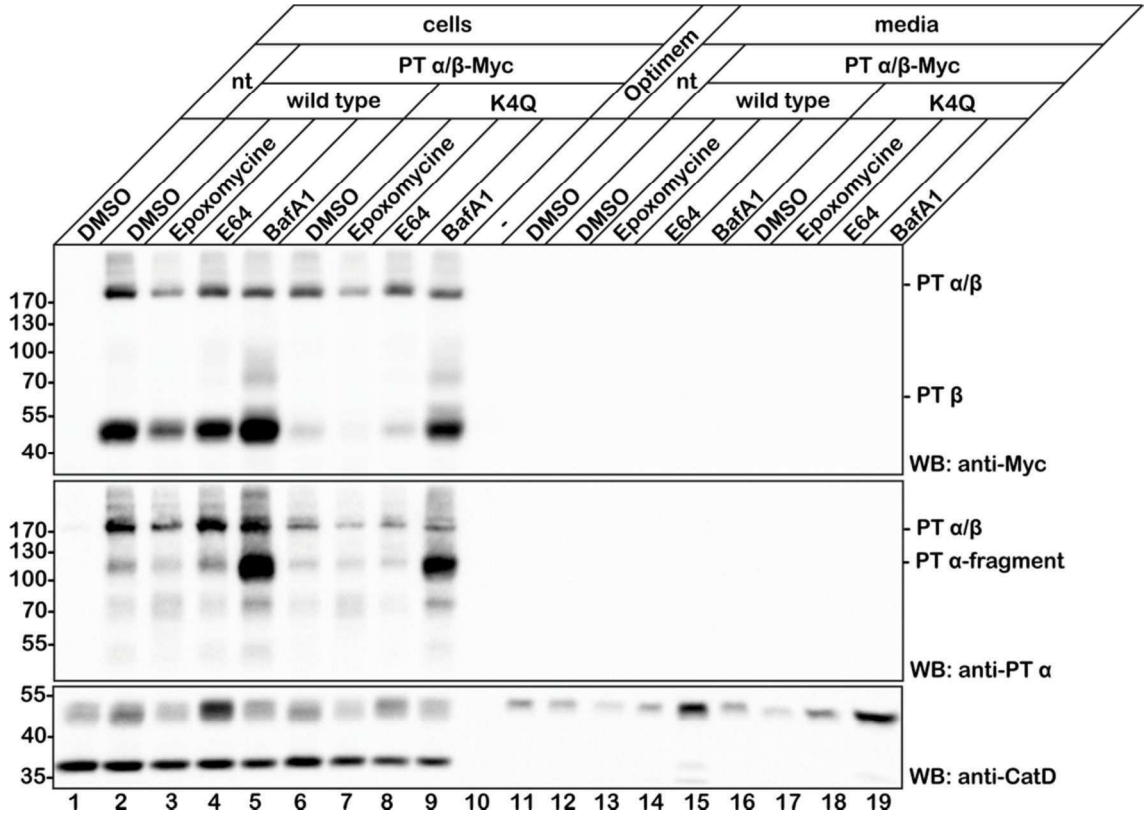

Figure 3.27: Wild type and mutant PT α-fragments are not released into the medium.
Cells were transfected with wild type and mutant PT α/β-Myc K^4Q subunit precursor cDNA constructs. Non-transfected cells were used as controls. After 36 hours cells were washed and incubated with solvent control DMSO or indicated proteasomal and lysosomal protease inhibitors in Optimem for 6 hours. Aliquots of cell lysates (33% of total) and media (66% of total) were separated by SDS-PAGE and analyzed by anti-Myc (upper panel) and anti-PT α (medium panel) western blotting. Equal loading of the gel was verified by anti-cathepsin D immunoblotting (lower panel). Positions of molecular mass marker proteins, the PT α/β-subunit precursor, the PT β-subunit and the PT α-fragment are indicated.

In lysates of cells transfected with wild type and mutant PT α/β-Myc K^4Q, the PT α/β precursor protein, the α-fragment and the β-subunits could be detected by PT α- and Myc-immunoblotting, respectively (Fig. 3.27, lanes 2-9). In media of these cells no secreted α-subunits and α-fragments were observed (Fig. 3.27, lanes 11-19, medium panel). Due to the localization of the Myc-epitope tag in the C-terminal cytosolic tail of the PT β-subunit, the detection of soluble β-subunits in the media was not possible by Myc-immunoblotting (Fig. 3.27, lanes 11-19, upper panel). Cathepsin D was used as a positive control protein secreted into the medium. In cell lysates the 45 kDa precursor and the 37 kDa mature forms of cathepsin D were detected (Fig. 3.27, lower panel). Incubation of cells with the cysteine

protease inhibitor E64 resulted in an increase of cathepsin D precursor forms accompanied by unchanged levels of the mature form (Fig. 3.27). In the media only the cathepsin D precursor form was detected, indicating the absence of intracellular protein in the media. The results are in agreement with data obtained by cell surface biotinylation (Fig. 3.26) indicating the absence of wild type and mutant PT α/β-Myc K^4Q at the cell surface. The data suggest that the PT complex is not localized at the cell surface in HeLa cells and that α-subunits are not shedded and released as soluble forms into the medium.

3.3 Role of cellular folding and trafficking components for M6P-biosynthesis

The organization of the Golgi compartments in *cis*-, *medial*- and *trans*-cisternae with different concentrations of Golgi-resident proteins in specialized cisternae is essential for the selectivity of posttranslational processing across Golgi membranes. The organization of the Golgi apparatus into functional cisternae is also important for the biosynthesis of the M6P recognition marker on newly synthesized soluble lysosomal enzymes, because transport of UDP-GlcNAc from the cytosol to the Golgi lumen, transfer of GlNAc-1-phosphate and removal of GlcNAc are performed in a sequential manner. In the course of an internship in the laboratory of Dr. William Balch, Scripps Research Institute La Jolla, I used an siRNA library directed against genes coding for ER, Golgi and cytosolic proteins to analyze the role of cellular folding and trafficking components in generating *cis*-, *medial*- and *trans*- Golgi compartments and their role for the M6P pathway. Most of the genes used for siRNA-mediated down-regulation encode proteins important for folding and degradation of proteins (Fig. 3.28). The second major group of genes is required for protein transport. Finally genes important for glycosylation, for example processing and modification of *N*- and *O* -linked oligosaccharides were included in the siRNA library (Fig. 3.28).

To identify genes which are involved in the biosynthesis of the M6P-recognition marker on soluble lysosomal proteins and their sorting from ER through the Golgi apparatus to lysosomes, secretion of the highly abundant soluble lysosomal enzyme β-hex activity was used as a marker. Newly synthesized β-hex is transported in a M6P-dependent pathway to lysosomes. Impairment of M6P-biosynthesis and trafficking to lysosomes may lead to hypersecretion of β-hex into the medium (Jessup et al, 1982).

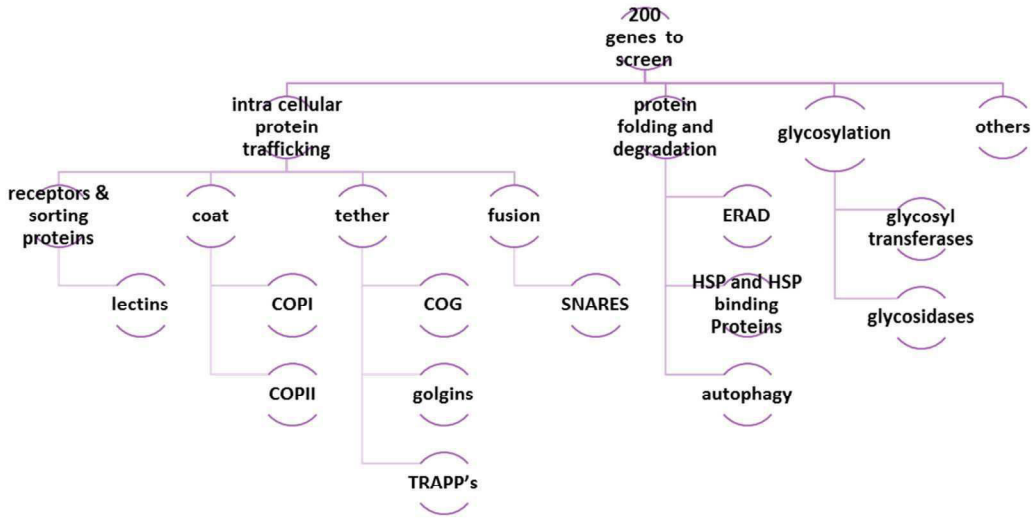

Figure 3.28: Target genes of the used siRNA library. 200 different mRNAs encoding proteins involved in intra cellular protein trafficking, protein folding/degradation and glycosylation were down-regulated by siRNA in cultured HeLa and CFBE cells. Secretion of β-hexosaminidase into the medium was used as criterion to identify genes required for M6P biosynthesis, trafficking and degradation of lysosomal enzymes.

First the protocol to measure β-hex enzyme activity was optimized to a screening applicable micro scale. Therefore different concentrations of NH_4Cl were used to enhance the secretion of β-hex. NH_4Cl neutralizes the pH of endosomes and lysosomes, hence MRPs cannot dissociate from their cargo in the endosomes and are blocked, leading to hypersecretion of lysosomal enzymes into the medium.

For siRNA screens, HeLa or CFBE cells were plated onto 96 well plates and transfected with siRNA in quadruplicates. 47 hours after the start transfection, medium was changed and secreted enzymes collected for another 24 hours. Subsequently activities of secreted β-hex were measured in the media. Downregulation of the *GNPTAB* gene by siRNA and incubation of cells with NH_4Cl were performed as positive controls for impaired M6P-biosynthesis and trafficking to lysosomes (Jessup et al, 1982; Kollmann et al, 2010). Values were normalized to activities in media from non-treated and scrambled control siRNA transfected cells (set as 0). Activities of β-hex in media of positive control cells transfected with siRNA against *GNPTAB* or treated with NH_4Cl ranged from 0.3 to 0.9 fold increase.

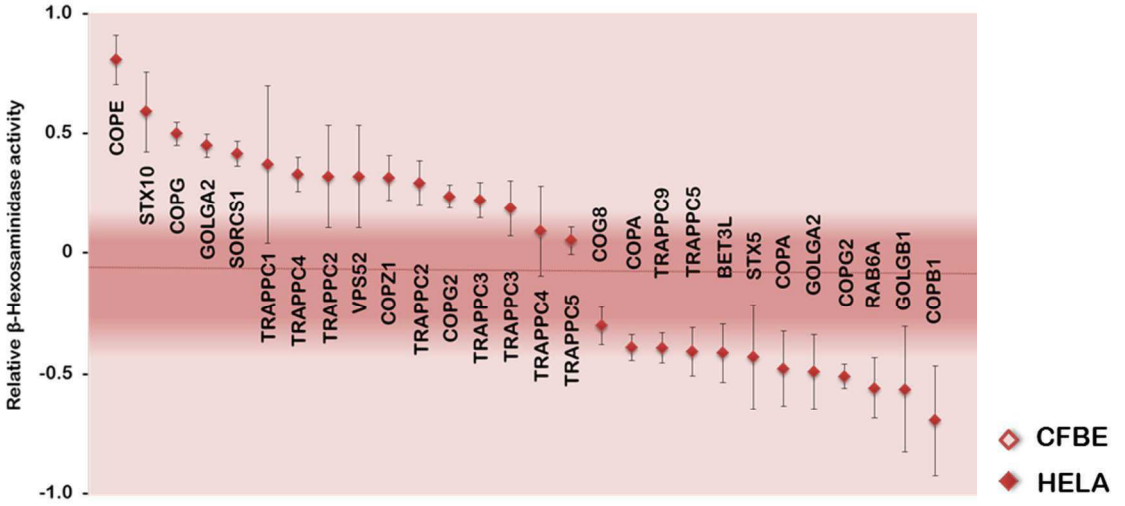

Figure 3.29: Knockdown of genes related to intracellular trafficking leads to altered secretion of lysosomal hydrolase β-hex into the medium. CFBE and HeLa cells were transfected in quadruplicates with siRNAs against genes encoding proteins involved in intracellular trafficking, protein folding and degradation, glycosylation and some others. Forty-eight hours after transfection cells were cultivated in fresh medium for 24 hours. Relative activity of β-hex in the media was measured and selected hits plotted in a diagram.

Most hits were genes encoding for proteins involved in ER-Golgi and intra Golgi transport. In CFBE cells knockdown of most components of the COPI coat and the multisubunit tethering complex TRAPP, as well as the SNARE VPS52 and the cargo receptor SorCS1 resulted in a hypersecretion of β-hex. In contrast, knockdown of the COG8 subunit of the COG complex resulted in decreased β-hex in the medium, compared to control cells. In HeLa cells knockdown of *TRAPPC1* and *TRAPPC2* also resulted in a hypersecretion. A number of genes also led to reduced secretion of β-hex, including genes encoding Golgins, COP coat components, Rab6A and the SNARE syntaxin 5. These preliminary results demonstrate the importance of trafficking and Golgi organization for the M6P-pathway. Further investigations are required to show the specific role of these hits for the activity of the PT-complex and the M6P-pathway.

4 Discussion

The hexameric Golgi-resident PT complex is composed of three different *N*-glycosylated subunits (α2β2γ2) and catalyzes the formation of the M6P-marker on newly synthesized soluble lysosomal proteins (Braulke et al, 2013). The membrane-bound PT α/β-subunit precursor protein is transported from the ER to the Golgi apparatus where it is cleaved by the site-1 protease generating the mature, catalytically active α- and β-subunits (Marschner et al, 2011). ER export and transport to the Golgi apparatus of the PT α/β-subunit precursor protein is therefore essential for enzymatic activity of the PT complex. Mutations in the *GNPTAB* gene coding for the PT α/β-subunit precursor protein lead to the childhood onset lysosomal storage diseases MLII and MLIII (Braulke et al, 2008). The first part of this work was aimed to identify structural requirements for efficient ER export of the PT α/β-subunit precursor protein. The role of luminal, transmembrane, cytosolic domains and of posttranslational modifications of the PT α/β-subunit precursor protein for ER to Golgi transport was investigated. The second part of the study analyzed mechanisms contributing to the turnover of wild type and mutant Golgi-localized PT α- and β-subunits. Finally the effects of mutations identified in MLIII alpha/beta on the ER export, intracellular localization and the turnover of the PT α/β-subunit precursor protein were studied.

4.1 Structural requirements for efficient ER export of the PT α/β-subunit precursor protein

Sorting signal-mediated ER export of Golgi-resident type I and type II membrane proteins is well characterized (Barlowe, 2003). However the anterograde transport of Golgi-resident polytopic type III membrane proteins, for example nucleotide sugar transporters, the Golgi pH-regulator or the PT α/β-subunit precursor protein is less understood (Hirschberg et al, 1998; Maeda et al, 2008). To study structural requirements contributing to efficient ER export whole luminal and TMDs of the PT α/β-subunit precursor protein were substituted by domains of transmembrane proteins bearing type III membrane topology with two TMDs. In addition, the complete cytosolic tails or selected residues of the PT α/β-subunit precursor protein were substituted by alanines. ER export of the wild type, mutant and chimeric PT α/β-subunit precursor proteins and arrival in the Golgi apparatus were

monitored using proteolytic cleavage by S1P, acquisition of complex type *N*-linked oligosaccharides and co-localization with the *cis*-Golgi marker protein GM130 (Franke et al, 2013). As a positive control for defective ER export PT α/β-subunit precursor protein fused to the ER retention motif of the human α_{2C}-adrenergic receptor, potent in retention of type III membrane proteins in the ER, was used.

Expression analyses and localization studies showed that PT α/β is transported as a non-cleaved precursor protein from the ER to the Golgi apparatus (Fig. 3.3). ER export of the PT α/β-subunit precursor protein required the type III membrane topology and the presence of both cytosolic domains. In agreement, the S1P cleavage-deficient mutant PT α/β-R^{925}A was efficiently exported from the ER (Fig. 3.1). Coexpression of the type II α-subunit with the type I β-subunit membrane protein failed to form a subunit complex competent to be sorted into ER-Golgi transport vesicles (Fig. 3.3). ER export was required for proteolytic cleavage as shown by the lack of cleavage of the ER-retained PT α/β-subunit precursor protein (Fig. 3.1).

4.2 ER export of the PT α/β-subunit precursor protein is mediated by a combinatorial sorting motif

The short, well conserved cytosolic domains of the PT α/β-subunit precursor protein are important for efficient ER exit (Fig. 3.8 and 3.9). Alanine scanning mutagenesis revealed the presence of a critical combinatorial ER export motif, which is composed of a dileucine motif, ^{5}LL^{6} and a dibasic ^{1253}RIR^{1255} sorting signal localized in the cytosolic N-terminal domain and the extreme C terminus of the α/β-subunit precursor protein, respectively (Fig. 3.10 and 3.11). Alanine substitution of the ^{5}LL^{6} motif in the N-terminal domain significantly reduced the transport of the PT α/β-subunit precursor protein to the Golgi, whereas mutations of single, double or all three dibasic motifs in the C-terminal domain moderately affected the ER transport (Fig. 3.10). However, the alanine substitution of the N-terminal dileucine motif ^{5}LL^{6} in combination with the C-terminal dibasic motif ^{1253}RIR^{1255} of the PT α/β-subunit precursor strongly inhibited ER export (Fig. 3.10 and 3.11). The data suggest that the N-terminal dileucine motif is the dominant motif and that both motifs are required for efficient ER export of the PT α/β-subunit precursor protein. Combinatorial signal structures required for efficient ER export have also been identified in other multisubunit transmembrane proteins. Signals in both, Erv41p and Erv46p tail

sequences are required in a specific orientation for efficient ER export of the Ev41p-Erv46p complex (Otte & Barlowe, 2002). A combination of di-isoleucine and C-terminal valine residues is required for ER export of the *medial*-Golgi-resident CMP-sialic acid transporter (Zhao et al, 2006). ER exit of the adiponectin receptor 1 containing seven TMDs is dependent on a combinatorial signal composed of $F(X)_3F(X)_3F$ and $D(X)_3LL$ motifs (Juhl et al, 2012).

The identified dileucine and the dibasic (R/K) X (R/K)-based RIR motifs are 13 and 17 amino acids, away from the TMDs and thus located close to the ends of the N- and C-termini of the PT α/β-subunit precursor protein (Fig. 3.10). The two ^{1236}KRK^{1238} and ^{1242}RRR^{1244} motifs located close or seven residues away from the TMD were less effective to promote ER export than the distal RIR motif. This suggests that the sorting motifs have to be positioned in a correct distance to the TMDs to be recognized by the COPII components. Analyses of the crystal structure of the COPII cargo adapter Sec24 revealed that the A- and B-binding sites interacting with ER export signals are situated in a distance of approximately 20 Å from the membrane bilayer (Mossessova et al, 2003). Cytosolic domains of transmembrane cargo would need to extend 20-25 amino acids residues into the cytoplasm to span this distance (7-10 residues) and occupy the binding site (10-15 residues). The N- and C-terminal cytosolic domains of the PT α/β-subunit precursor protein which consist of 19 and 21 amino acids, respectively, would be large enough to reach the binding sites of Sec24 (Fig. 3.8). In contrast, the N-terminal cytosolic domains of type II membrane glycosyltransferase proteins, like galactosyltransferase II (GalT2), are shorter than the 20 amino acids required to reach the Sec24 binding sites. Type II glycosyltransferases, like GalT2, containing (R/K)X(R/K) motifs in their N-terminal cytosolic domains have been shown to directly interact with the A-binding site of Sar1 (Quintero et al, 2010).

The present results indicate that the dileucine and dibasic RIR motifs of the PT α/β-subunit precursor protein are sequence and position specific. Two identical dileucine or dibasic motifs in the N- and C-terminal domains are not sufficient to mediate efficient ER exit of the PT α/β-subunit precursor protein. Substitution of the C-terminal ^{1253}RIR^{1255} motif by dileucine residues, in combination with a dileucine motif or with a dialanine substitution in the N-terminus (^{5}LL^{6}/^{1253}LL^{1254}) (^{5}AA^{6}/^{1253}LL^{1254}) prevented the ER exit of the PT α/β-subunit precursor protein and subsequently its proteolytic processing (Fig.

3.12). In summary, the PT α/β-subunit precursor requires a combinatorial sorting motif composed of the ^{5}LL^{6} and ^{1253}RIR^{1255} motifs in defined positions of the N- and C-terminal domains, which are not interchangeable.

Besides sorting signal-mediated ER export, the masking of arginine-based ER localization signals after assembly of multisubunit complexes in the ER leading to transport to the Golgi apparatus has been described (Michelsen et al, 2005). These ER localization signals conform to the consensus sequence (Φ/Ψ/R)RXR, where Φ/Ψ is an aromatic or bulky hydrophobic residue and X is any amino acid. The C-terminal domain of the PT α/β-subunit precursor protein also contains a highly conserved, arginine-based motif (P^{1242}RRR^{1244}), which could act as a functional ER retention motif. A similar, functional ER localization motif (KRRR) was identified in the NR1-1 subunit of the N-methyl D-aspartate (NMDA) receptor (Michelsen et al, 2005). Expression analyses revealed that triple alanine substitution of the ^{1242}RRR^{1244} motif did not increase ER export of the precursor protein suggesting that the C-terminal arginine-based motif is not a functional ER retention motif (Fig. 3.10). In agreement, triple alanine substitution of the ^{1242}RRR^{1244} motif or deletion of the complete cytosolic tail in the isolated PT β-subunit did not prevent ER retention (Fig. 3.4). The data suggest that ER export of the PT α/β-subunit precursor protein is not mediated by the masking of the C-terminal arginine-based P^{1242}RRR^{1244} motif after assembly of the hexameric multisubunit PT complex in the ER.

4.3 Role of the luminal domain and dimerization for ER export of the PT α/β-subunit precursor protein

The highly glycosylated LD of the PT α/β-subunit precursor protein has a modular structure, which is required for different functions including I.) the binding of lysosomal enzymes via the DNA methyltransferase associated protein (DMAP) interaction domain, II.) the catalytic activity of the PT complex mediated by the cleaved α- and β-subunits, III.) the complex formation with the homodimeric PT γ-subunits and IV.) the binding of the substrate UDP-GlcNAc (Qian et al, 2013; Qian et al, 2010). It is unknown whether the LD and *N*-linked oligosaccharides are required for efficient ER export of the precursor protein. To study the role of the PT α/β-subunit precursor protein LD, chimera were generated composed of the cytosolic and TMDs of PT and the LD of LIMP-2. Similar to the PT α/β-subunit precursor protein, LIMP-2 is a homodimeric type III membrane protein

containing two TMDs (Neculai et al, 2013). Expression analyses in HeLa cells revealed the complete retention of the PT α/β-LIMP-2 chimera in the ER as shown by the absence of endo H-resistant *N*-glycans (Fig. 3.6). Since no severe misfolding and degradation of the PT-LIMP-2 chimera was observed, it is likely that substitution of the LD may impair the proper presentation of the combinatorial cytosolic ER export motif. Alternatively the absence of the PT γ-subunit, which cannot associate with the LIMP2-PT chimera, might also contribute to impaired ER export.

The bovine PT complex was suggested to form a hexameric complex containing two homodimeric, disulfide bridged α- and γ-subunits complexed with two monomeric β-subunits (Bao et al, 1996). To analyze whether dimerization of the PT α/β-subunit precursor protein is required for ER exit, serine substitution of cysteine residue in position 70 was introduced. Expression analyses revealed that the $C^{70}S$ substitution prevented covalent dimerization of two precursor proteins. Amounts of monomeric and dimeric PT α/β-subunit precursor proteins were comparable indicating proper folding of the monomeric PT (Fig. 3.5B). However concentrations of cleaved PT β-subunit were reduced by 40% compared to the dimeric PT α/β-subunit precursor protein indicating impaired ER export of the monomeric PT α/β-subunit precursor protein. Dimerization has been shown to be required for efficient ER export of the type I membrane proteins P-selectin glycoprotein ligand-1 (Miner et al, 2011), ERGIC53 (Nufer et al, 2003) and the polytopic transmembrane proteins human calcium receptor (Zhuang et al, 2010), β2 adrenergic receptor (Salahpour et al, 2004) and prenylin (Liang et al, 2004). In addition, a large number of Golgi *N*-glycosyltransferases exist as homodimeric complexes (Hassinen et al, 2010). Dimerization of the PT α/β-subunit precursor protein could be required for the presentation of multiple combinatorial motifs at the cytosolic part and high affinity binding of COPII components. Oligomerization of the type I ERGIC53 membrane protein is required to present the cytoplasmic targeting motifs for efficient ER export (Nufer et al, 2003). Serine substitution of the cysteine residue 70 prevented covalent dimerization, but additional factors like ionic interactions, hydrogen bonds, hydrophobic effects or van der Waals dispersion forces may contribute to the association of two PT α/β-subunit precursor proteins or two PT α-subunits, which cannot be excluded. Therefore there might be still dimerization to a certain extent and dimerization itself might be much more important for the ER export and stability of the protein as the obtained results suggest (Fig. 3.5B).

TMDs play a critical role in the ER export of membrane proteins and multisubunit complexes by mediating oligomerization and by carrying ER retention motifs, which are demasked upon proper assembly in the ER (Fässler et al, 2010; Horak et al, 2008; Nufer et al, 2003). TM sorting determinants are not conserved amino acid sequences, but physical properties such as the length and the hydrophilicity of the transmembrane span (Cosson et al, 2013). The two putative TMDs of the PT α- and β-subunits have a predicted length of 23 amino acids (N-terminus: amino acids 20-42; C terminus: amino acids 1213-1235, Krogh et al, 2001), which is larger than the average length of Golgi-localized membrane proteins of 20.6 amino acids (Sharpe et al, 2010). A TMD length of 21 amino acids was shown to be most efficient for ER export of ERGIC53 and extension up to 26 amino acids decreased ER exit (Nufer et al, 2003). To analyze whether the single TMDs of the PT α/β-subunit precursor protein mediate ER export, they were exchanged by TMDs of the lysosomal membrane protein LIMP-2. Both LIMP-2 TMDs have a length of 23 amino acids. The exchange of the second TMD did not impair ER export. However, substitution of the first TMD led to reduced ER export of the PT α/β-subunit precursor protein (Fig. 3.7). The first TMD might contribute to the dimerization of two PT α/β-subunit precursor proteins, as it is the case for the subunits of the γ-secretase and ERGIC53 (Fässler et al, 2010; Horak et al, 2008; Nufer et al, 2003). In addition, TMDs are required for Golgi retention of membrane proteins, like for β-1,4-galactosyltransferase (Masibay et al, 1993), Golgi phosphoprotein 2 (GOLPH2, Hu et al, 2011) and syntaxin 10 (Watson & Pessin, 2001). Golgi-resident membrane proteins (average TMD: 20.8 amino acids) tend to have shorter membrane-spanning regions than plasma membrane proteins (average TMD: 24.8 amino acids) with an average difference of 4 amino acids (Sharpe et al, 2010). It remains to be investigated whether the TMDs of the PT α- and β-subunits are needed for proper retention of the PT complex in the Golgi apparatus.

4.4 COPII-mediated ER export of the PT α/β-subunit precursor protein

The COPII coat is composed of the small GTPase Sar1 in its GTP-bound form, and the heterodimeric protein complexes Sec23-Sec24 and Sec13-Sec31, which sequentially mediate the membrane curvature, cargo binding and vesicle fission (Brandizzi & Barlowe, 2013). Sar1 initiates the assembly of the COPII coat on ER membranes and exists in an inactive, GDP-bound, cytosolic form and an active GTP-bound, membrane-associated form (Sato & Nakano, 2007). In the dominant-negative Sar1 $H^{79}G$ mutant GTP-hydrolysis is blocked

(Stroud et al, 2003). Coexpression with the dominant-negative Sar1 $H^{79}G$ mutant inhibited ER export of the PT α/β-subunit precursor protein indicating its transport in COPII-coated vesicles (Fig. 3.15). At present it is unknown which COPII component binds to the combinatorial LL/RIR motif of the PT α/β-subunit precursor protein and how LL and RIR determinants cooperatively interact with distinct coat proteins. To identify interaction partners of the PT α/β-subunit precursor protein coprecipitation experiments were performed with protein extracts from HEK293 cells overexpressing PT α/β-GFP. Mass spectrometric analyses of interacting proteins identified COPII-coat components Sar1 and Sec23A confirming COPII-mediated ER export of the PT (Table 3.1). Interestingly, none of the four Sec24 paralogs present in eukaryotic cells were identified as interaction partner (Wendeler et al, 2007). However, since Sec23 and Sec24 are recruited as heterodimers onto ER membranes, the presence of Sec24 would be very likely (Gillon et al, 2012). Cytosolic proteins and lipids potentially interacting with the N-terminal dileucine and the C-terminal RIR motifs remain to be investigated. It was shown that ERGIC53 tail peptides with a C-terminal dileucine motif specifically interacted with Sec24A *in vitro* and that ER export of an ERGIC53 reporter protein carrying a C terminal dileucine motif was dependent on the presence of Sec24A (Wendeler et al, 2007). It is unknown whether COPII-coat components directly interact with the C-terminal RIR motif. Dibasic (RK)X(RK) ER export motifs present in the N-terminal cytoplasmic domains of type II membrane glycosyltransferase proteins located proximal to the transmembrane border have been reported to interact directly with Sar1 (Giraudo & Maccioni, 2003). ER export of the multispanning serotonine transporter (SERT) is mediated by an RI-motif in its C-terminal cytosolic domain. siRNA-mediated down-regulation of *Sec24C* mRNA resulted in ER retention of SERT (Sucic et al, 2011). Preliminary data from *in vitro* GST pulldown experiments suggest that the C-terminal domain of the PT α/β-subunit precursor protein, which contains two RI motifs (^{1244}RI^{1245} HK and ^{1253}RIR^{1255}V), may interact with Sec24C (Ahmadi, Bachelor Thesis 2013). Further experiments are required to find out which RI motif interacts with Sec24C and whether ER export of the PT α/β-subunit precursor protein is impaired in Sec24C or Sec24C/D downregulated cells. An *in vitro* vesicle budding assay using a membrane bound PT α/β-subunit precursor protein in the presence of recombinant COPII coat components would identify the COPII component which is recognizing the combinatorial sorting motif (Aridor et al, 1998).

4.6 MLIII alpha/beta patient mutation K^4Q impairs ER export of the PT α/β-subunit precursor protein

The present study demonstrated the requirement of two independent sorting motifs present in the N- and C-terminal cytosolic domains of the PT α/β-subunit precursor protein for its efficient ER export. Almost all MLII patients have nonsense, frameshift, or splice site alterations in *GNPTAB*, which lead to a truncation of the PT α/β subunit precursor protein (Braulke et al, 2013). The data suggest that truncation of the PT α/β-subunit precursor protein in the luminal or in the second TMD resulting in the loss of the C-terminal tail will impair ER export of the precursor protein due to the absent targeting information in the C-terminal domain. Besides the ER export defect, misfolding of the mutant PT α/β-subunit precursor proteins will likely increase ER retention. In agreement, MLII alpha/beta patients have complete loss of enzyme activity.

Two homozygous missense mutations, p.K^4Q (exon 1, c.10A>C) and p.$K^{1236}M$ (exon 21, c.3707A>T), have been identified in *GNPTAB* MLII/III intermediate patients, which could possibly disturb the recognition of the sorting motifs (Kudo et al, 2006; Tiede et al, 2006). Intermediate patients demonstrate a phenotype similar to MLII in physical and radiographic features and to MLIII in psychomotor development and life expectancy (Leroy et al, 2013). The non-conservative mutation K^4Q affects the highly conserved, positively charged lysine residue in the N-terminal cytosolic domain, which is positioned proximal to the N-terminal $^5LL^6$ sorting motif. The K^4Q mutation reduced the proteolytic processing of the PT α/β-subunit precursor protein by 60-70% due to impaired ER export (Fig. 3.13). Since the efficiency of ER export strongly depends on the three dimensional orientation of the combinatorial motif and the context of the surrounding amino acids, replacement of the lysine residue at position 4 affects the recognition by COPII components more dramatically than the $^5LL^6$ alanine substitution alone. The reduced amounts of proteolytically activated PT α/β-subunit precursor K^4Q is in agreement with the PT activity of 12% in fibroblasts of patients and 20-40% of wild type after transient expression in HEK293 cells (Kudo et al, 2006; Leroy et al, 2013). Both the non-conservative alanine substitution and the conservative arginine substitution of K^4 impaired ER export comparable with mutant K^4Q suggest that the identity of the residue in position 4 rather than the presence of a positively charged residue is required for ER exit. In contrast, mutation $K^{1236}M$ in the PT α/β-subunit precursor protein did not affect its ER export (Fig. 3.13). The lysine residue mutation $K^{1236}M$ is positioned right behind the second

TMD, close to the C-terminal ^{1253}RIR^{1255} sorting motif (Fig. 3.13). The intermediate phenotype of the patient who survived to the age of 14 years suggests that the mutant PT complex exhibits residual activity (Tiede et al, 2006). Recently it was reported, that introduction of this mutation into the PT α/β-subunit precursor mini cDNA construct leads to an instable *mRNA*, which is rapidly degraded and results in reduced biosynthesis of the mutant protein (De Pace, unpublished data). Further studies are needed to examine whether the K^{1236}M substitution impairs the assembly of the hexameric complex in the ER which might be important for proper phosphorylation of all lysosomal hydrolases. In summary expression analyses of mutant PT α/β-subunit precursor proteins containing missense mutations found in patients with MLII/III alpha/beta revealed that distinct forms of the disease might be due to impaired transport to the Golgi apparatus and subsequent lack of PT activation.

4.7 Turnover of wild type and mutant PT α/β-subunit proteins

The consequences of MLIII alpha/beta mutations on the stability, posttranslational modifications, assembly of the complex and proteolytic processing of the PT α/β-subunit precursor protein are poorly understood. In the present study the consequences of three missense mutations in *GNPTAB* leading to MLIII, located in cytosolic domains (K^{4}Q, K^{1236}M) and LDs (S^{399}F), respectively (Cury et al, 2013; Encarnacao et al, 2009; Kudo et al, 2006; Tiede et al, 2005a), on protein stability and turnover were analyzed. All affected residues are conserved across mammals except residue K^{4}, which is not conserved in *Bos taurus*. Golgi-localized, type II membrane protein GP3ST and the TGN-localized type I membrane proteins Furin and GlcNAc-1-phosphodiesterase (GlcNAc-1-PD) were used as controls to study turnover of Golgi membrane proteins (Fig. 3.17).

To analyze the half-life time of the PT α/β-subunit precursor protein and the cleaved β-subunit, [^{35}S]-methionine pulse-chase and cycloheximide (CHX)-chase analyses were performed using HeLa cells (Fig. 3.2 and 3.18). Both analyses showed the gradual cleavage of the PT α/β-subunit precursor protein to the mature β-subunits. Quantifications revealed a half-life time for the PT α/β-subunit precursor protein of 3 hours and 15 hours using [^{35}S]-methionine pulse-chase and CHX-chase analyses, respectively. The discrepancy of the half-life times obtained by the two methods is unclear. For the pulse-chase analyses PT α/β fused to a GFP and for the CHX-chase analyses PT α/β fused to Myc were used.

Furthermore it is possible that the block of protein biosynthesis during CHX-chase could limit the amount of proteins required for ER export and proteolytic cleavage of the PT α/β-subunit precursor protein in the Golgi. For the ER-retained PT α/β-subunit precursor protein a much larger half-life time of more than 15 hours was observed in CHX-chase analyses suggesting that the half-life time of wild type PT α/β-subunit precursor protein is mainly determined by its S1P-mediated proteolytic cleavage to the mature α- and β-subunits. The half-life times of the cleaved PT β-subunits were 9 hours and more than 15 hours using [^{35}S]-methionine pulse-chase and CHX-chase analyses, respectively. The data indicate that the cleaved PT β-subunits are quite stable with a half-life time > 15 hours comparable to the half-life times of other Golgi-resident membrane proteins like GlcNAc-1-PD (t ½ > 15h) and α-1,4-galactosyltransferase 1 (t ½ = 20h, Strous, 1986).

Expression analyses revealed that the stability of MLIII mutant PT α-and β-subunits were reduced in a mutation-dependent manner. The most dramatic phenotype was observed in cells expressing mutant PT α/β-Myc K^{4}Q. The mutant PT α/β-subunit precursor protein was relatively stable with half-life times of > 15 hours, whereas the cleaved mature PT β-subunit was rapidly degraded with a half-life time of 3 hours (Fig. 3.19D). Expression studies in cells transfected with wild type and mutant PT α/β-Myc K^{4}Q, which were treated with proteasomal and lysosomal protease inhibitors, revealed that the amounts of cleaved PT β-subunit could be increased by the inhibitor of vacuolar H$^+$-ATPase BafA1, but not by inhibitors of the proteasome. This suggests that both wild type and mutant PT α/β K^{4}Q are degraded in acidic compartments. Decreased turnover of PT α/β-Myc K^{4}Q in cells treated with leupeptin and E64, but not by pepstatin, suggests that lysosomal degradation is mediated by cysteine proteases. Further experiments in gene-targeted mouse embryonic fibroblasts deficient for the lysosomal cysteine proteases cathepsin L and B are needed to identify the cleaving protease (Turk & Guncar, 2003). The data suggest that the presence of the mature, mutated α-K^{4}Q subunit in the PT complex subunit leads to increased turnover of the wild type β-subunit. Treatment of the cells with the proteasomal inhibitor epoxomycin increased the amounts of mutant PT α/β-Myc K^{4}Q precursor protein indicating its degradation by ERAD (Fig. 3.21). In contrast, mutant PT α/β-Myc K^{1236}M subunit precursor protein and the cleaved PT β-subunit showed a comparable stability as the wild type protein (Fig. 3.19). Expression analyses revealed strongly decreased amounts of cleaved β-subunit in cells expressing mutant PT α/β-Myc S^{399}F indicating impaired ER export (Fig.3.20). CHX-chase analyses showed a decreased half-life time of 3 hours for the

precursor protein compared to an ER-retained, wild type PT α/β-subunit precursor protein (t ½ > 15h) suggesting degradation by ERAD (Fig. 3.20). In agreement, degradation of the mutant p.$S^{399}F$ precursor protein could be inhibited by treatment of cells with the proteasomal inhibitor epoxomycin (Fig. 3.21). The data indicate that mutant PT α/β $S^{399}F$ is retained in the ER and degraded by the ERAD machinery most likely due to misfolding of the mutant protein. It is unknown, why the mutant protein still exhibits residual enzymatic activity leading to an MLIII alpha/beta phenotype in patients (Encarnacao et al, 2009).

Next, the importance of dimerization and proteolytic cleavage for the half-life time of the PT α/β-subunit precursor and the cleaved α- and β-subunit proteins was analyzed. Both the monomeric PT α/β-$C^{70}S$ subunit precursor protein and the PT β-subunit had shorter half-life times compared to the dimeric wild type precursor protein suggesting that the mature β-subunit complexed to the monomeric α-subunit is degraded more rapidly. Increased amounts of monomeric α-$C^{70}S$ (2.5-fold) and β-subunits (2-fold) in extracts of cells treated with BafA1 suggest that the PT complex containing monomeric α-subunits and complexed β-subunits is degraded in lysosomes. The cleavage-resistant PT α/β-$R^{925}A$ subunit precursor protein was relatively stable with a half-life time of 12 hours. In contrast to the wild type precursor protein, its half-life time is mainly determined by its degradation because of lacking proteolytic cleavage to the mature subunits. Degradation of the cleavage-resistant PT α/β-$R^{925}A$ subunit precursor protein could be inhibited by bafilomycin A1, NH_4Cl, E64 and leupeptin suggesting its turnover in lysosomes mediated by cysteine proteases.

In summary we could show that ER export of mutant PT α/β-K^4Q and $S^{399}F$ precursor proteins was decreased leading to their degradation by ERAD. In addition, mutant PT β-subunits generated by residual ER export of the mutant PT α/β-K^4Q precursor protein were rapidly degraded in lysosomal compartments. In contrast, in cells expressing mutant PT α/β-$K^{1236}M$ proteins no major differences in half-life times of the precursor protein and of the β-subunit compared to the wild type protein were observed, suggesting that increased turnover of this protein is not the cause for reduced PT activity in MLIII patients carrying this mutation.

In addition to the main S1P-mediated cleavage of the PT α/β-subunit precursor protein, an alternative cleavage of the PT α/β-subunit precursor protein was observed, resulting in a 120 kDa PT α-fragment (Fig. 3.22). The glycosylated 120 kDa and degylcosylated 80 kDa PT α-fragments had apparent smaller molecular masses compared to the glycosylated 140 kDa and the deglycosylated 110 kDa PT α-Myc proteins (Fig. 3.22B). The presence of the PT α-fragments both in wild type and S1P-cleavage deficient PT α/β-subunit precursor proteins suggests that the precursor protein is cleaved in the LD generating a 120 kDa PT α-fragment, which is independent of prior cleavage by S1P. In agreement, a 55 kDa PT β-subunit was detected in extracts of cells expressing the S1P-cleavage deficient PT α/β-subunit precursor protein (Fig. 3.24). The absence of the cleaved 120 kDa PT α-fragments in cells expressing ER-retained precursor proteins (PT α/β-ER-Ret and $S^{399}F$) suggests that S1P-independent cleavage of the precursor proteins occurs in post-ER compartments most likely prior to lysosomes (Fig. 3.24). The decreased turnover of the 120 kDa PT α-fragments in BafA1-treated cells indicated that the generated fragments are finally degraded in lysosomes. In cells expressing a PT α/β-subunit precursor protein lacking amino acids 431 to 848 (Marschner et al, 2011), no smaller PT α-fragment was detected suggesting that the alternative cleavage occurs in the LD between amino acids 700 and 850. Further analyses are required to identify the localization of the cleavage event, the cleavage site and the responsible protease.

4.8 The PT α/β-subunit precursor and β-subunit proteins are not transported to the plasmamembrane

Transport to the plasmamembrane, shedding and release of soluble forms into the medium have been shown to contribute to the turnover and the regulation of activity of several membrane-bound Golgi glycosyltransferases (El-Battari et al, 2003; Strous, 1986). Proteolytic cleavage and secretion into the medium generates soluble forms of type II membrane glycosyltransferase proteins (Varki A, 2009), e. g. β-galactoside α 2,6-sialyltransferase (Weinstein et al, 1987), α-1,4-galactosyltransferase 1 (Strous, 1986) and β-1,4-galactosyltransferase (D'Agostaro et al, 1989). Furthermore, tumor cells secrete or shed glycoproteins and glycosyltransferases into the surrounding medium and into serum (Weiser & Wilson, 1981). Finally it was reported that the soluble PT γ-subunit is secreted into the medium of cultured cells and into the human serum (Encarnacao et al, 2011). Double immunofluorescence indicated that the PT α- and β-subunits are not located at the

cell surface (Franke et al, 2013). In agreement, cell surface biotinylation experiments in transfected HeLa cells clearly showed the absence of the PT α/β precursor and β-subunit proteins at the plasma membrane (Fig. 3.26). Cell surface localization of wild type PT was not detected as for the ER-retained, negative controls PT α/β-ER-Ret and S399F. In contrast, the positive controls Furin and the TfR, known to cycle via the cell surface, could be observed at the plasma membrane (Lee et al, 2002; Warren et al, 1997). To rule out that lacking cell surface localization is due to the shedding of membrane-bound PT α/β-subunit precursor protein at the plasma membrane, media were analyzed for the presence of cleaved, soluble α-subunits. Expression analyses revealed the absence of soluble α-subunits in the medium of cells expressing wild type and mutant PT α/β-K^4Q subunits in the medium as observed by immunoblotting (Fig. 3.27). The absence of wild type and mutant PT α/β-K^4Q complexes at the cell surface and of soluble α-subunits in the medium that transport to the plasma membrane and shed into the medium do not contribute to the turnover of PT α- and β-subunits in HeLa cells.

4.9 Role of cellular folding and trafficking components for M6P-biosynthesis

The biosynthesis of the M6P-recognition marker on newly synthesized soluble lysosomal glycoproteins depends on the functionality and localization of the multisubunit PT complex, the site-1 protease (S1P) and the GlcNAc-1-PD in different Golgi cisternae (Braulke et al, 2013). In addition, four different Golgi-resident transporters for UDP-GlcNAc, the monospecific SLC35A3 transporter (Guillen et al, 1998) and the multisubstrate SLC35-B4, -D1 and -D2 transporters (Ashikov et al, 2005; Furuichi et al, 2009; Ishida et al, 2005), have been identified which most likely are critical for M6P biosynthesis. Thus the integrity and organization of the Golgi apparatus into *cis*-, *medial*-, *trans*-cisternae and the TGN is required for the sequential generation of the M6P recognition marker on newly synthesized soluble lysosomal enzymes. To identify genes, which are important for M6P-biosynthesis on soluble lysosomal proteins and their sorting from ER via the Golgi apparatus to lysosomes, 200 genes coding for ER-, Golgi- and cytosolic proteins, which are important for intracellular trafficking, protein folding and degradation, vesicle tethering, glycosylation and others were down-regulated by silencing RNAs in cultured HeLa and CFBE cells. Cells transfected with siRNAs against *GNPTAB* or cultured in the presence of the weak base ammoniumchloride were used as positive controls for increased secretion of lysosomal enzymes into the medium. The highly abundant, soluble lysosomal enzyme β-hex was used as marker protein because its targeting to lysosomes depends on the presence of the M6P marker and increased secretion into the medium indicates impaired M6P biosynthesis or biosynthetic sorting to lysosomes. Down-regulated genes, which resulted in increased β-hex secretion, were considered as hits and grouped into functional pathways. They included proteins involved in retrograde transport of mannose 6-phosphate receptors, tethering complexes, COPI-coat components and sorting receptors (Fig. 3.29).

Missorting of β-hex could be caused by deficient binding of the hydrolase to MPRs in the TGN or to the MPR300 at the cell surface (Braulke & Bonifacino, 2009). As expected, the syntaxin 10 (STX10) and the vacuolar protein sorting 52 homolog (Vps52) gene products involved in the biosynthetic trafficking of the mannose 6-phosphate receptors between the Golgi and endosomes were identified in cells hypersecreting β-hex. STX10 is part of a SNARE complex composed of STX16, Vti1a, and VAMP3, which is required for the retrograde transport of the MPR300 from endosomes to the TGN (Ganley et al, 2008). In agreement with results obtained in this study, Ganley and co-workers showed that

depletion of STX10 leads to hypersecretion of β-hex into the medium caused by MPR missorting and enhanced MPR degradation. Vps52 is part of the Golgi-associated retrograde protein (GARP) complex, which is critical for the recycling of MPRs from the endosome to the TGN (Perez-Victoria et al, 2008). Knockdown of Vps52 by RNAi has been shown to impair sorting of the acid hydrolase cathepsin D to lysosomes and leads to its secretion into the culture medium.

Missorting of β-hex into the medium could be due to depletion of receptors, which recapture missorted lysosomal enzymes at the plasmamembrane (Braulke & Bonifacino, 2009). Knockdown of the type I membrane protein SorCS1 increased β-hex secretion. SorCS1 has been shown to target internalized cargo to lysosomes but is not required for the transport from the TGN to the endosomal compartments to a significant degree (Nielsen et al, 2008).

Increased secretion of β-hex was observed in cells depleted for several subunits (C1, C2, C3, C4 and C6) of the Transport Protein Particle I (TRAPPI)-tethering complex. The *cis*-Golgi localized, multisubunit TRAPPI complex is composed of seven subunits and is required for the docking of COPII vesicles (Lord et al, 2011). The reason for increased β-hex secretion due to deficient transport of COPII vesicles between the ER and the Golgi apparatus is unclear. Missorting of β-hex in cells with down-regulated genes coding for COPI-coat components and subunits of the COG complex was observed. β1, β2, ε, γ1, and γ2-subunits of the COPI complex and the COG2-subunit of the COG complex were found, which are required for the formation and docking of COPI-coated vesicles, respectively, in the Golgi apparatus (Miller & Ungar, 2012; Popoff et al, 2011). It is possible that deficient retrograde transport could affect steady state localization of the PT subunits, S1P and UDP-GlcNAc-monosaccharide transporters in early Golgi compartments. Since knockdown of COPI and COG-subunits will likely influence the integrity of the Golgi and lead to non-specific effects by perturbation of the *N*-glycosylation machinery and intra-Golgi sorting, specificity of down-regulated genes on M6P biosynthesis and biosynthetic sorting of lysosomal enzymes remains to be investigated.

It is unknown whether the knockdown of single genes specifically affects the M6P-biosynthesis on newly synthesized lysosomal proteins by altering for instance localization, protein stability, posttranslational modifications of the PT α/β-subunit precursor protein,

the site-1 protease, transporters for UDP-GlcNAc (SLC35-A3, -B4, -D1, -D2) and the GlcNAc-1-PD. M6P-biosynthesis can be measured by M6P western blotting using antibodies specifically detecting terminally located M6P-residues on glycoproteins (Müller-Loennies et al, 2010). In addition, down-regulation of genes coding for proteins required for localization, protein stability and trafficking of MPRs between the TGN and endosomal compartments will lead to impaired secretion independent of M6P biosynthesis. Down-regulated genes leading to defects in Golgi structure and organization will most likely also perturb sorting of lysosomal enzymes by interfering with *N*-glycosylation of proteins and sorting in the TGN in an unspecific manner (Lowe, 2011; Nilsson et al, 2009).

5 SUMMARY

In the present study structural requirements for efficient ER export of the PT α/β-subunit precursor protein were analyzed. Expression analyses and co-localization studies showed that both wild type and a cleavage-resistant PT α/β-subunit precursor protein were exported from the ER, whereas coexpressed separate α- and β-subunits failed to reach the Golgi indicating that the presence of type III membrane topology is required for ER exit. Mutational analyses revealed that both the N- and C-terminal cytosolic tails are critical for ER export. Alanine scanning analyses of putative ER export signals showed that ER export of the precursor protein is mediated by a combinatorial signal composed a N-terminal dileucine signal (^{5}LL^{6}) and a C-terminal dibasic (R/K)X(R/K)-type RIR (^{1242}RIR^{1244}) motif. These sorting motifs are not interchangeable and have to be exposed in a defined orientation with respect to the TMDs to be recognized by the COPII machinery. In the presence of a dominant-negative Sar1 mutant, ER exit of the precursor protein was inhibited indicating its transport via COPII-coated vesicles. In addition, expression analyses of PT-LIMP-2 chimera revealed that the presence of the dimerized, highly glycosylated LD of the PT α/β-subunit precursor protein is critically required for ER export, whereas the TMDs are not important.

In the second part of the study the turnover of wild type and mutant precursor and mature PT α- and β-subunits were studied. CHX-chase analyses revealed an approximate half-life time of 15 h for the precursor protein and of > 15 h for the mature β-subunit. Expression analyses in the presence of proteasomal and lysosomal protease inhibitors showed that both wild type and mutant PT complexes containing mature, cleaved α- and β-subunits are degraded in lysosomal compartments. Transport to the plasma membrane and shedding into the medium did not contribute to the turnover of wild type PT α and β-subunits. Expression analyses of MLIII mutant precursor proteins revealed that both impaired ER export and increased turnover in lysosomes contribute to reduced amounts of catalytically active PT α- and β-subunits. Mutation S^{399}F located in the LD led to ER retention and ER-associated degradation of the mutant precursor protein. Mutation K^{4}Q in the cytosolic domain resulted in impaired ER export of the mutant precursor protein and rapid degradation of the residual PT β-subunit in lysosomes. Mutation K^{1236}M did not impair ER export of the precursor and stability of the cleaved PT β-subunit. Mechanisms contributing to decreased enzymatic activity of mutant K^{1236}M remain to be investigated.

siRNA-mediated downregulation of genes coding for ER and Golgi-resident and associated proteins identified several genes required for M6P-biosynthesis, MPR-receptor trafficking and intra-Golgi transport. Downregulation of subunits of Golgi-localized SNARES, the GARP and COG-complexes resulted in increased β-hex secretion into the medium. The specific role of these genes for the catalytic activity of the PT α- and β-subunits and MPR trafficking remains to be investigated. The data stress the importance of Golgi-localized tethering complexes for M6P-biosynthesis and MPR-mediated sorting of lysosomal proteins.

6 ZUSAMMENFASSUNG

In der vorliegenden Arbeit wurden die strukturellen Vorausetzungen für den Export des PT α/β-Vorläuferproteins des hexameren, Golgi-residenten GlcNAc-1-Phosphotransferase Komplexes aus dem endoplasmatischem Reticulum (ER) untersucht. Expressionstudien, *N*-Glykosilierungs- und Kolokalisierungsanalysen belegen, daß das Vorläuferprotein und eine Site1-Protease Spaltungs-defiziente Mutante vom ER zum Golgi Apparat transportiert wurden, während die koexprimierten isolierten α- und β-Untereinheiten im ER zurückgehalten wurden. Diese Analysen ergaben, dass die Typ III Membrantopologie und die Dimerisierung des ungespaltenen Vorlauferproteins für den effizienten ER Export notwendig ist. Mutationsanalysen zeigten, daß beide cytosolische Domänen wichtig für den ER Export des Vorläuferproteins sind. Expressionsanalysen von Vorläuferproteinen mit mutierten potentiellen ER Export Motiven belegen, daß der ER Export durch ein kombinatorisches Sortierungssignal vermittelt wird, das aus einem N-terminalen Dileucin Signal (^{5}LL^{6}) und einem C-terminalen dibasischen RIR (^{1242}RIR^{1244}) Motiv zusammengesetzt ist. Die Lokalisation und Sequenz der identifizierten Sortierungssignale in den cytosolischen Domänen waren nicht austauschbar. Koexpressionsstudien mit einer dominant-negativen Sar1-Mutante ergaben, daß das PT α/β-Vorläuferproteins in COPII-beschichteten Vesikeln vom ER zum Golgi Apparat transportiert wird. Expressionsanalysen von chimären Proteinen, die aus der luminalen Domäne von LIMP-2 und den cytosolischen und Transmembrandomänen der PT α/β zusammengesetzt waren, zeigten, daß die luminale PT-Domäne ebenfalls essentiell für den ER Export ist.

Im zweiten Teil der Arbeit wurden Abbauwege von Wild Typ und mutanten PT α-und β-Proteinen in kultivierten Zellen untersucht. CHX-Chase Analysen ergaben für das PT α/β Vorläuferprotein und die gespaltene β-Untereinheit Halbwertszeiten von 15 Stunden bzw. > 15 Stunden. Expressionsanalysen in Anwesenheit von proteasomalen und lysosomalen Inhibitoren zeigten, dass die Wildtyp α- and β-Untereinheiten der PT durch lysosomale Cystein-Proteasen in sauren Kompartimenten abgebaut werden. Expressionsanalysen der mutierten PT-K^{4}Q und -S^{399}F Vorläuferproteine, die bei Patienten mit Mukolipidose Typ III alpha/beta identifiziert wurden, zeigten stark verminderte Halbwertszeiten im Vergleich zum Wild Typ Protein. Verminderter ER Export (S^{399}F, K^{4}Q), ER-assoziierter Abbau der Vorläuferproteine im Proteasom (S^{399}F, K^{4}Q) und erhöhter lysosomaler Abbau (K^{4}Q) führten zur Verminderung gespaltener, katalytisch aktiver α- and β-Untereinheiten im

Golgi Apparat. Die Untersuchungen zeigten, dass Mutationen in der α-Untereinheit der PT (K^4Q) zum gesteigerten lysosomalen Abbau der β-Untereinheiten und möglicherweise des gesamten hexameren PT-Komplexes führen. Biotinylierungsexperimente und Analyse gespaltener α- and β-Untereinheiten der PT im Medium zeigten, dass der Transport an die Plasmamembran und die Sekretion löslicher Formen ins Medium nicht zum Abbau von Wild Typ und mutanten (K^4Q) α and β-Untereinheiten der PT beitragen. Bei einer weiteren MLIII alpha/beta Mutation $K^{1236}M$, die in der C-terminalen cytsoslischen Domäne lokalisiert ist, waren weder der ER Export gehemmt noch der Abbau im Proteasom/Lysosom erhöht.

Durch silencing RNA-vermittelte Herunterregulierung von 200 Genen, die für Proteine des endoplasmatischen Reticulums, des Golgi Apparats und cytosolischer Proteine kodieren, wurde Proteine identifiziert, die für die Phosphorylierung von Mannoseresten und/oder den intrazellulären Transport neusynthetisierter löslicher lysosomaler Enzyme wichtig sind. Die Daten unterstreichen die Bedeutung von Golgi-lokalisierten Tethering Komplexen, wie SNARE-, GARP- and COG-Komplexen, für die Mannose 6-Phosphat Biosynthese an löslichen lysosomalen Enzymen und den intrazellulären Transport der Mannose 6-Phosphat Rezeptoren.

7 Literature

Aebi M (2013) N-linked protein glycosylation in the ER. *Biochim Biophys Acta* **1833:** 2430-2437

Anitei M, Hoflack B (2011) Exit from the trans-Golgi network: from molecules to mechanisms. *Curr Opin Cell Biol* **23:** 443-451

Aridor M, Weissman J, Bannykh S, Nuoffer C, Balch WE (1998) Cargo selection by the COPII budding machinery during export from the ER. *J Cell Biol* **141:** 61-70

Ashikov A, Routier F, Fuhlrott J, Helmus Y, Wild M, Gerardy-Schahn R, Bakker H (2005) The human solute carrier gene SLC35B4 encodes a bifunctional nucleotide sugar transporter with specificity for UDP-xylose and UDP-N-acetylglucosamine. *J Biol Chem* **280:** 27230-27235

Ballabio A, Gieselmann V (2009) Lysosomal disorders: from storage to cellular damage. *Biochim Biophys Acta* **1793:** 684-696

Bao M, Booth JL, Elmendorf BJ, Canfield WM (1996) Bovine UDP-N-acetylglucosamine:lysosomal-enzyme N-acetylglucosamine-1-phosphotransferase. I. Purification and subunit structure. *J Biol Chem* **271:** 31437-31445

Bargal R, Zeigler M, Abu-Libdeh B, Zuri V, Mandel H, Ben Neriah Z, Stewart F, Elcioglu N, Hindi T, Le Merrer M, Bach G, Raas-Rothschild A (2006) When Mucolipidosis III meets Mucolipidosis II: GNPTA gene mutations in 24 patients. *Mol Genet Metab* **88:** 359-363

Barlowe C (2003) Signals for COPII-dependent export from the ER: what's the ticket out? *Trends Cell Biol* **13:** 295-300

Beers MF, Zhao M, Tomer Y, Russo SJ, Zhang P, Gonzales LW, Guttentag SH, Mulugeta S (2013) Disruption of N-linked glycosylation promotes proteasomal degradation of the human ATP-binding cassette transporter ABCA3. *Am J Physiol Lung Cell Mol Physiol*

Blanz J, Groth J, Zachos C, Wehling C, Saftig P, Schwake M (2010) Disease-causing mutations within the lysosomal integral membrane protein type 2 (LIMP-2) reveal the nature of binding to its ligand beta-glucocerebrosidase. *Hum Mol Genet* **19:** 563-572

Boncompain G, Perez F (2013) The many routes of Golgi-dependent trafficking. *Histochem Cell Biol* **140:** 251-260

Bonifacino JS, Glick BS (2004) The mechanisms of vesicle budding and fusion. *Cell* **116:** 153-166

Bonner WM, Laskey RA (1974) A film detection method for tritium-labelled proteins and nucleic acids in polyacrylamide gels. *Eur J Biochem* **46:** 83-88

Bosshart H, Humphrey J, Deignan E, Davidson J, Drazba J, Yuan L, Oorschot V, Peters PJ, Bonifacino JS (1994) The cytoplasmic domain mediates localization of furin to the trans-Golgi network en route to the endosomal/lysosomal system. *J Cell Biol* **126:** 1157-1172

Brandizzi F, Barlowe C (2013) Organization of the ER-Golgi interface for membrane traffic control. *Nat Rev Mol Cell Biol* **14:** 382-392

Braulke T, Bonifacino JS (2009) Sorting of lysosomal proteins. *Biochim Biophys Acta* **1793:** 605-614

Braulke T, Pohl S, Storch S (2008) Molecular analysis of the GlcNac-1-phosphotransferase. *J Inherit Metab Dis* **31:** 253-257

Braulke T, Raas-Rothschild A, Kornfeld S (2013) I-cell disease and pseudo-Hurler polydystrophy: Disorders of lysosomal enzyme phosphorylation and localization. *In The Online Metabolic and Molecular Bases of Inherited Disease, Valle D, Beaudet A, Vogelstein B, Kinzler K, Antonarakis S, Ballabio A, Scriver C, Sly W, Childs B, Bunz F, et al (eds) New York City, NY: McGraw Hill*

Bravo R, Parra V, Gatica D, Rodriguez AE, Torrealba N, Paredes F, Wang ZV, Zorzano A, Hill JA, Jaimovich E, Quest AFG, Lavandero S (2013) Endoplasmic reticulum and the unfolded protein response: dynamics and metabolic integration. *Int Rev Cell Mol Biol* **301:** 215-290

Brown MS, Ye J, Rawson RB, Goldstein JL (2000) Regulated intramembrane proteolysis: a control mechanism conserved from bacteria to humans. *Cell* **100:** 391-398

Budnik A, Stephens DJ (2009) ER exit sites--localization and control of COPII vesicle formation. *FEBS Lett* **583:** 3796-3803

Cathey SS, Leroy JG, Wood T, Eaves K, Simensen RJ, Kudo M, Stevenson RE, Friez MJ (2010) Phenotype and genotype in mucolipidoses II and III alpha/beta: a study of 61 probands. *J Med Genet* **47:** 38-48

Chakrabarti A, Chen AW, Varner JD (2011) A review of the mammalian unfolded protein response. *Biotechnol Bioeng* **108:** 2777-2793

Cosson P, Perrin J, Bonifacino JS (2013) Anchors aweigh: protein localization and transport mediated by transmembrane domains. *Trends Cell Biol* **23:** 511-517

Csala M, Kereszturi E, Mandl J, Banhegyi G (2012) The endoplasmic reticulum as the extracellular space inside the cell: role in protein folding and glycosylation. *Antioxid Redox Signal* **16:** 1100-1108

Cury GK, Matte U, Artigalas O, Alegra T, Velho RV, Sperb F, Burin MG, Ribeiro EM, Lourenco CM, Kim CA, Valadares ER, Galera MF, Acosta AX, Schwartz IV (2013) Mucolipidosis II and III alpha/beta in Brazil: analysis of the GNPTAB gene. *Gene* **524:** 59-64

D'Agostaro G, Bendiak B, Tropak M (1989) Cloning of cDNA encoding the membrane-bound form of bovine beta 1,4-galactosyltransferase. *Eur J Biochem* **183:** 211-217

Dell'Angelica EC, Mullins C, Caplan S, Bonifacino JS (2000) Lysosome-related organelles. *Faseb J* **14:** 1265-1278

Dong C, Nichols CD, Guo J, Huang W, Lambert NA, Wu G (2012) A triple arg motif mediates alpha(2B)-adrenergic receptor interaction with Sec24C/D and export. *Traffic (Copenhagen, Denmark)* **13:** 857-868

El-Battari A, Prorok M, Angata K, Mathieu S, Zerfaoui M, Ong E, Suzuki M, Lombardo D, Fukuda M (2003) Different glycosyltransferases are differentially processed for secretion, dimerization, and autoglycosylation. *Glycobiology* **13:** 941-953

Ellgaard L, Helenius A (2003) Quality control in the endoplasmic reticulum. *Nature reviews Molecular cell biology* **4:** 181-191

Encarnacao M, Kollmann K, Trusch M, Braulke T, Pohl S (2011) Post-translational modifications of the gamma-subunit affect intracellular trafficking and complex assembly of GlcNAc-1-phosphotransferase. *J Biol Chem* **286:** 5311-5318

Encarnacao M, Lacerda L, Costa R, Prata MJ, Coutinho MF, Ribeiro H, Lopes L, Pineda M, Ignatius J, Galvez H, Mustonen A, Vieira P, Lima MR, Alves S (2009) Molecular analysis of the GNPTAB and GNPTG genes in 13 patients with mucolipidosis type II or type III - identification of eight novel mutations. *Clin Genet* **76:** 76-84

Fässler M, Zocher M, Klare S, de la Fuente AG, Scheuermann J, Capell A, Haass C, Valkova C, Veerappan A, Schneider D, Kaether C (2010) Masking of transmembrane-based retention signals controls ER export of gamma-secretase. *Traffic (Copenhagen, Denmark)* **11:** 250-258

Forgac M (1999) Structure and properties of the vacuolar (H+)-ATPases. *J Biol Chem* **274:** 12951-12954

Franke M, Braulke T, Storch S (2013) Transport of the GlcNAc-1-phosphotransferase alpha/beta-subunit precursor protein to the Golgi apparatus requires a combinatorial sorting motif. *J Biol Chem* **288:** 1238-1249

Fujita H, Takata Y, Kono A, Tanaka Y, Takahashi T, Himeno M, Kato K (1992) Isolation and sequencing of a cDNA clone encoding the 85 kDa human lysosomal sialoglycoprotein (hLGP85) in human metastatic pancreas islet tumor cells. *Biochem Biophys Res Commun* **184:** 604-611

Furuichi T, Kayserili H, Hiraoka S, Nishimura G, Ohashi H, Alanay Y, Lerena JC, Aslanger AD, Koseki H, Cohn DH, Superti-Furga A, Unger S, Ikegawa S (2009) Identification of loss-of-function mutations of SLC35D1 in patients with Schneckenbecken dysplasia, but not with other severe spondylodysplastic dysplasias group diseases. *J Med Genet* **46:** 562-568

Futerman AH, van Meer G (2004) The cell biology of lysosomal storage disorders. *Nature reviews Molecular cell biology* **5:** 554-565

Ganley IG, Espinosa E, Pfeffer SR (2008) A syntaxin 10-SNARE complex distinguishes two distinct transport routes from endosomes to the trans-Golgi in human cells. *J Cell Biol* **180:** 159-172

Ghosh P, Dahms NM, Kornfeld S (2003) Mannose 6-phosphate receptors: new twists in the tale. *Nature reviews Molecular cell biology* **4:** 202-212

Gidalevitz T, Stevens F, Argon Y (2013) Orchestration of secretory protein folding by ER chaperones. *Biochim Biophys Acta* **1833:** 2410-2424

Giraudo CG, Maccioni HJ (2003) Endoplasmic reticulum export of glycosyltransferases depends on interaction of a cytoplasmic dibasic motif with Sar1. *Molecular biology of the cell* **14:** 3753-3766

Glick BS, Luini A (2011) Models for Golgi traffic: a critical assessment. *Cold Spring Harb Perspect Biol* **3:** a005215

Guillen E, Abeijon C, Hirschberg CB (1998) Mammalian Golgi apparatus UDP-N-acetylglucosamine transporter: molecular cloning by phenotypic correction of a yeast mutant. *Proc Natl Acad Sci U S A* **95:** 7888-7892

Hagiwara M, Nagata K (2012) Redox-dependent protein quality control in the endoplasmic reticulum: folding to degradation. *Antioxid Redox Signal* **16:** 1119-1128

Hassinen A, Rivinoja A, Kauppila A, Kellokumpu S (2010) Golgi N-glycosyltransferases form both homo- and heterodimeric enzyme complexes in live cells. *J Biol Chem* **285:** 17771-17777

Hirschberg CB, Robbins PW, Abeijon C (1998) Transporters of nucleotide sugars, ATP, and nucleotide sulfate in the endoplasmic reticulum and Golgi apparatus. *Annu Rev Biochem* **67:** 49-69

Honke K, Tsuda M, Koyota S, Wada Y, Iida-Tanaka N, Ishizuka I, Nakayama J, Taniguchi N (2001) Molecular cloning and characterization of a human beta-Gal-3'-sulfotransferase that acts on both type 1 and type 2 (Gal beta 1-3/1-4GlcNAc-R) oligosaccharides. *J Biol Chem* **276:** 267-274

Horak M, Chang K, Wenthold RJ (2008) Masking of the endoplasmic reticulum retention signals during assembly of the NMDA receptor. *The Journal of neuroscience : the official journal of the Society for Neuroscience* **28:** 3500-3509

Hu L, Li L, Xie H, Gu Y, Peng T (2011) The Golgi localization of GOLPH2 (GP73/GOLM1) is determined by the transmembrane and cytoplamic sequences. *PLoS One* **6:** e28207

Hutagalung AH, Novick PJ (2011) Role of Rab GTPases in membrane traffic and cell physiology. *Physiol Rev* **91:** 119-149

Ishida N, Kuba T, Aoki K, Miyatake S, Kawakita M, Sanai Y (2005) Identification and characterization of human Golgi nucleotide sugar transporter SLC35D2, a novel member of the SLC35 nucleotide sugar transporter family. *Genomics* **85:** 106-116

Jakobsen MK, Cheng Z, Lam SK, Roth-Johnson E, Barfield RM, Schekman R (2013) Phosphorylation of Chs2p regulates interaction with COPII. *J Cell Sci* **126:** 2151-2156

Jessup W, Leoni P, Bodmer JL, Dean RT (1982) The effect of weak bases on lysosomal enzyme secretion by mononuclear phagocytes. *Biochem Pharmacol* **31:** 2657-2662

Juhl C, Kosel D, Beck-Sickinger AG (2012) Two motifs with different function regulate the anterograde transport of the adiponectin receptor 1. *Cell Signal* **24:** 1762-1769

Klumperman J (2011) Architecture of the mammalian Golgi. *Cold Spring Harb Perspect Biol* **3**

Koch GL (1990) The endoplasmic reticulum and calcium storage. *Bioessays* **12:** 527-531

Kollmann K, Damme M, Markmann S, Morelle W, Schweizer M, Hermans-Borgmeyer I, Rochert AK, Pohl S, Lübke T, Michalski JC, Kakela R, Walkley SU, Braulke T (2012) Lysosomal dysfunction causes neurodegeneration in mucolipidosis II 'knock-in' mice. *Brain* **135:** 2661-2675

Kollmann K, Pohl S, Marschner K, Encarnacao M, Sakwa I, Tiede S, Poorthuis BJ, Lübke T, Müller-Loennies S, Storch S, Braulke T (2010) Mannose phosphorylation in health and disease. *Eur J Cell Biol* **89:** 117-123

Kornfeld R, Bao M, Brewer K, Noll C, Canfield W (1999) Molecular cloning and functional expression of two splice forms of human N-acetylglucosamine-1-phosphodiester alpha-N-acetylglucosaminidase. *J Biol Chem* **274:** 32778-32785

Krogh A, Larsson B, von Heijne G, Sonnhammer EL (2001) Predicting transmembrane protein topology with a hidden Markov model: application to complete genomes. *J Mol Biol* **305:** 567-580

Kudo M, Brem MS, Canfield WM (2006) Mucolipidosis II (I-cell disease) and mucolipidosis IIIA (classical pseudo-hurler polydystrophy) are caused by mutations in the GlcNAc-phosphotransferase alpha / beta -subunits precursor gene. *Am J Hum Genet* **78:** 451-463

Kudo M, Canfield WM (2006) Structural requirements for efficient processing and activation of recombinant human UDP-N-acetylglucosamine:lysosomal-enzyme-N-acetylglucosamine-1-phosphotransferase. *J Biol Chem* **281:** 11761-11768

Lazzarino DA, Gabel CA (1989) Mannose processing is an important determinant in the assembly of phosphorylated high mannose-type oligosaccharides. *J Biol Chem* **264:** 5015-5023

Lee WS, Rohrer J, Kornfeld R, Kornfeld S (2002) Multiple signals regulate trafficking of the mannose 6-phosphate-uncovering enzyme. *J Biol Chem* **277:** 3544-3551

Leroy JG, Sillence D, Wood T, Barnes J, Lebel RR, Friez MJ, Stevenson RE, Steet R, Cathey SS (2013) A novel intermediate mucolipidosis II/IIIalphabeta caused by GNPTAB mutation in the cytosolic N-terminal domain. *Eur J Hum Genet*

Liang Z, Veeraprame H, Bayan N, Li G (2004) The C-terminus of prenylin is important in forming a dimer conformation necessary for endoplasmic-reticulum-to-Golgi transport. *Biochem J* **380:** 43-49

Lord C, Bhandari D, Menon S, Ghassemian M, Nycz D, Hay J, Ghosh P, Ferro-Novick S (2011) Sequential interactions with Sec23 control the direction of vesicle traffic. *Nature* **473:** 181-186

Lord C, Ferro-Novick S, Miller EA (2013) The highly conserved COPII coat complex sorts cargo from the endoplasmic reticulum and targets it to the golgi. *Cold Spring Harb Perspect Biol* **5**

Lowe M (2011) Structural organization of the Golgi apparatus. *Curr Opin Cell Biol* **23:** 85-93

Lübke T, Lobel P, Sleat DE (2009) Proteomics of the lysosome. *Biochim Biophys Acta* **1793:** 625-635

Macia E, Ehrlich M, Massol R, Boucrot E, Brunner C, Kirchhausen T (2006) Dynasore, a cell-permeable inhibitor of dynamin. *Dev Cell* **10:** 839-850

Maeda Y, Ide T, Koike M, Uchiyama Y, Kinoshita T (2008) GPHR is a novel anion channel critical for acidification and functions of the Golgi apparatus. *Nat Cell Biol* **10:** 1135-1145

Makrypidi G, Damme M, Muller-Loennies S, Trusch M, Schmidt B, Schluter H, Heeren J, Lubke T, Saftig P, Braulke T (2012) Mannose 6 dephosphorylation of lysosomal proteins mediated by acid phosphatases Acp2 and Acp5. *Mol Cell Biol* **32:** 774-782

Marschner K (2011) Funktionelle Analyse von Modulstrukturen der N-Acetylglukosamin-1-Phosphotransferase. *Dissertation 2011, Universität Hamburg, FB Chemie*

Marschner K, Kollmann K, Schweizer M, Braulke T, Pohl S (2011) A key enzyme in the biogenesis of lysosomes is a protease that regulates cholesterol metabolism. *Science* **333:** 87-90

Martinez-Menarguez JA, Geuze HJ, Slot JW, Klumperman J (1999) Vesicular tubular clusters between the ER and Golgi mediate concentration of soluble secretory proteins by exclusion from COPI-coated vesicles. *Cell* **98:** 81-90

Masibay AS, Balaji PV, Boeggeman EE, Qasba PK (1993) Mutational analysis of the Golgi retention signal of bovine beta-1,4-galactosyltransferase. *J Biol Chem* **268:** 9908-9916

Michelsen K, Yuan H, Schwappach B (2005) Hide and run. Arginine-based endoplasmic-reticulum-sorting motifs in the assembly of heteromultimeric membrane proteins. *EMBO reports* **6:** 717-722

Miller EA, Beilharz TH, Malkus PN, Lee MC, Hamamoto S, Orci L, Schekman R (2003) Multiple cargo binding sites on the COPII subunit Sec24p ensure capture of diverse membrane proteins into transport vesicles. *Cell* **114:** 497-509

Miller VJ, Ungar D (2012) Re'COG'nition at the Golgi. *Traffic (Copenhagen, Denmark)* **13:** 891-897

Miner JJ, Shao B, Wang Y, Chichili GR, Liu Z, Klopocki AG, Yago T, McDaniel JM, Rodgers W, Xia L, McEver RP (2011) Cytoplasmic domain of P-selectin glycoprotein ligand-1 facilitates dimerization and export from the endoplasmic reticulum. *J Biol Chem* **286:** 9577-9586

Moremen KW, Tiemeyer M, Nairn AV (2012) Vertebrate protein glycosylation: diversity, synthesis and function. *Nat Rev Mol Cell Biol* **13:** 448-462

Mossessova E, Bickford LC, Goldberg J (2003) SNARE selectivity of the COPII coat. *Cell* **114:** 483-495

Müller-Loennies S, Galliciotti G, Kollmann K, Glatzel M, Braulke T (2010) A novel single-chain antibody fragment for detection of mannose 6-phosphate-containing proteins: application in mucolipidosis type II patients and mice. *Am J Pathol* **177:** 240-247

Munro S (2011a) The golgin coiled-coil proteins of the Golgi apparatus. *Cold Spring Harb Perspect Biol* **3**

Munro S (2011b) What is the Golgi apparatus, and why are we asking? *BMC Biol* **9:** 63

Neculai D, Schwake M, Ravichandran M, Zunke F, Collins RF, Peters J, Neculai M, Plumb J, Loppnau P, Pizarro JC, Seitova A, Trimble WS, Saftig P, Grinstein S, Dhe-Paganon S (2013) Structure of LIMP-2 provides functional insights with implications for SR-BI and CD36. *Nature*

Nielsen MS, Keat SJ, Hamati JW, Madsen P, Gutzmann JJ, Engelsberg A, Pedersen KM, Gustafsen C, Nykjaer A, Gliemann J, Hermans-Borgmeyer I, Kuhl D, Petersen CM, Hermey G (2008) Different motifs regulate trafficking of SorCS1 isoforms. *Traffic (Copenhagen, Denmark)* **9:** 980-994

Nilsson T, Au CE, Bergeron JJ (2009) Sorting out glycosylation enzymes in the Golgi apparatus. *FEBS Lett* **583:** 3764-3769

Nufer O, Kappeler F, Guldbrandsen S, Hauri HP (2003) ER export of ERGIC-53 is controlled by cooperation of targeting determinants in all three of its domains. *J Cell Sci* **116:** 4429-4440

Nyathi Y, Wilkinson BM, Pool MR (2013) Co-translational targeting and translocation of proteins to the endoplasmic reticulum. *Biochim Biophys Acta* **1833:** 2392-2402

Otsu W, Kurooka T, Otsuka Y, Sato K, Inaba M (2013) A new class of endoplasmic reticulum export signal PhiXPhiXPhi for transmembrane proteins and its selective interaction with Sec24C. *J Biol Chem* **288:** 18521-18532

Otte S, Barlowe C (2002) The Erv41p-Erv46p complex: multiple export signals are required in trans for COPII-dependent transport from the ER. *Embo J* **21:** 6095-6104

Parodi AJ (2000) Protein glucosylation and its role in protein folding. *Annu Rev Biochem* **69:** 69-93

Patterson GH, Hirschberg K, Polishchuk RS, Gerlich D, Phair RD, Lippincott-Schwartz J (2008) Transport through the Golgi apparatus by rapid partitioning within a two-phase membrane system. *Cell* **133:** 1055-1067

Pendin D, McNew JA, Daga A (2011) Balancing ER dynamics: shaping, bending, severing, and mending membranes. *Curr Opin Cell Biol* **23:** 435-442

Perez-Victoria FJ, Mardones GA, Bonifacino JS (2008) Requirement of the human GARP complex for mannose 6-phosphate-receptor-dependent sorting of cathepsin D to lysosomes. *Molecular biology of the cell* **19:** 2350-2362

Platt FM, Boland B, van der Spoel AC (2012) The cell biology of disease: lysosomal storage disorders: the cellular impact of lysosomal dysfunction. *J Cell Biol* **199:** 723-734

Pohl S, Marschner K, Storch S, Braulke T (2009) Glycosylation- and phosphorylation-dependent intracellular transport of lysosomal hydrolases. *Biol Chem* **390:** 521-527

Popoff V, Adolf F, Brugger B, Wieland F (2011) COPI budding within the Golgi stack. *Cold Spring Harb Perspect Biol* **3:** a005231

Qian Y, Flanagan-Steet H, van Meel E, Steet R, Kornfeld SA (2013) The DMAP interaction domain of UDP-GlcNAc:lysosomal enzyme N-acetylglucosamine-1-phosphotransferase is a substrate recognition module. *Proc Natl Acad Sci U S A* **110:** 10246-10251

Qian Y, Lee I, Lee WS, Qian M, Kudo M, Canfield WM, Lobel P, Kornfeld S (2010) Functions of the alpha, beta, and gamma subunits of UDP-GlcNAc:lysosomal enzyme N-acetylglucosamine-1-phosphotransferase. *J Biol Chem* **285:** 3360-3370

Quintero CA, Giraudo CG, Villarreal M, Montich G, Maccioni HJ (2010) Identification of a site in Sar1 involved in the interaction with the cytoplasmic tail of glycolipid glycosyltransferases. *J Biol Chem* **285:** 30340-30346

Raas-Rothschild A, Cormier-Daire V, Bao M, Genin E, Salomon R, Brewer K, Zeigler M, Mandel H, Toth S, Roe B, Munnich A, Canfield WM (2000) Molecular basis of variant pseudo-hurler polydystrophy (mucolipidosis IIIC). *J Clin Invest* **105:** 673-681

Rabouille C, Klumperman J (2005) Opinion: The maturing role of COPI vesicles in intra-Golgi transport. *Nature reviews Molecular cell biology* **6:** 812-817

Rendon WO, Martinez-Alonso E, Tomas M, Martinez-Martinez N, Martinez-Menarguez JA (2013) Golgi fragmentation is Rab and SNARE dependent in cellular models of Parkinson's disease. *Histochem Cell Biol* **139:** 671-684

Rohrer J, Kornfeld R (2001) Lysosomal hydrolase mannose 6-phosphate uncovering enzyme resides in the trans-Golgi network. *Molecular biology of the cell* **12:** 1623-1631

Saftig P, Klumperman J (2009) Lysosome biogenesis and lysosomal membrane proteins: trafficking meets function. *Nature reviews Molecular cell biology* **10:** 623-635

Salahpour A, Angers S, Mercier JF, Lagace M, Marullo S, Bouvier M (2004) Homodimerization of the beta2-adrenergic receptor as a prerequisite for cell surface targeting. *J Biol Chem* **279:** 33390-33397

Sato K, Nakano A (2007) Mechanisms of COPII vesicle formation and protein sorting. *FEBS Lett* **581:** 2076-2082

Schröder BA, Wrocklage C, Hasilik A, Saftig P (2010) The proteome of lysosomes. *Proteomics* **10:** 4053-4076

Settembre C, Fraldi A, Medina DL, Ballabio A (2013) Signals from the lysosome: a control centre for cellular clearance and energy metabolism. *Nature reviews Molecular cell biology* **14:** 283-296

Sharpe HJ, Stevens TJ, Munro S (2010) A comprehensive comparison of transmembrane domains reveals organelle-specific properties. *Cell* **142:** 158-169

Spranger J, Brill, P., Poznanski, A (2002) Bone dysplasias: An atlas of genetic disorders of the skeletal development. *Oxford University Press***:** 57-79

Stroud WJ, Jiang S, Jack G, Storrie B (2003) Persistence of Golgi matrix distribution exhibits the same dependence on Sar1p activity as a Golgi glycosyltransferase. *Traffic* **4:** 631-641

Strous GJ (1986) Golgi and secreted galactosyltransferase. *CRC Crit Rev Biochem* **21:** 119-151

Sucic S, El-Kasaby A, Kudlacek O, Sarker S, Sitte HH, Marin P, Freissmuth M (2011) The serotonin transporter is an exclusive client of the coat protein complex II (COPII) component SEC24C. *J Biol Chem* **286:** 16482-16490

Thomas G (2002) Furin at the cutting edge: from protein traffic to embryogenesis and disease. *Nature reviews Molecular cell biology* **3:** 753-766

Thor F, Gautschi M, Geiger R, Helenius A (2009) Bulk flow revisited: transport of a soluble protein in the secretory pathway. *Traffic* **10:** 1819-1830

Tiede S, Cantz M, Spranger J, Braulke T (2006) Missense mutation in the N-acetylglucosamine-1-phosphotransferase gene (GNPTA) in a patient with mucolipidosis II induces changes in the size and cellular distribution of GNPTG. *Hum Mutat* **27:** 830-831

Tiede S, Muschol N, Reutter G, Cantz M, Ullrich K, Braulke T (2005a) Missense mutations in N-acetylglucosamine-1-phosphotransferase alpha/beta subunit gene in a patient with mucolipidosis III and a mild clinical phenotype. *Am J Med Genet A* **137A:** 235-240

Tiede S, Storch S, Lübke T, Henrissat B, Bargal R, Raas-Rothschild A, Braulke T (2005b) Mucolipidosis II is caused by mutations in GNPTA encoding the alpha/beta GlcNAc-1-phosphotransferase. *Nat Med* **11:** 1109-1112

Tu L, Banfield DK (2010) Localization of Golgi-resident glycosyltransferases. *Cell Mol Life Sci* **67:** 29-41

Turk D, Guncar G (2003) Lysosomal cysteine proteases (cathepsins): promising drug targets. *Acta Crystallogr D Biol Crystallogr* **59:** 203-213

van Meer G (2005) Cellular lipidomics. *Embo J* **24:** 3159-3165

Varki A CR, Esko JD, et al., editors. (2009) Essentials of Glycobiology. 2nd edition. Cold Spring Harbor (NY): Cold Spring Harbor Laboratory Press.

Vembar SS, Brodsky JL (2008) One step at a time: endoplasmic reticulum-associated degradation. *Nature reviews Molecular cell biology* **9:** 944-957

Venditti R, Wilson C, De Matteis MA (2013) Exiting the ER: what we know and what we don't. *Trends Cell Biol*

Waheed A, Pohlmann R, Hasilik A, von Figura K (1981) Subcellular location of two enzymes involved in the synthesis of phosphorylated recognition markers in lysosomal enzymes. *J Biol Chem* **256:** 4150-4152

Wang W, Malcolm BA (1999) Two-stage PCR protocol allowing introduction of multiple mutations, deletions and insertions using QuikChange Site-Directed Mutagenesis. *Biotechniques* **26:** 680-682

Warren RA, Green FA, Enns CA (1997) Saturation of the endocytic pathway for the transferrin receptor does not affect the endocytosis of the epidermal growth factor receptor. *J Biol Chem* **272:** 2116-2121

Watson RT, Pessin JE (2001) Transmembrane domain length determines intracellular membrane compartment localization of syntaxins 3, 4, and 5. *Am J Physiol Cell Physiol* **281:** C215-223

Weinstein J, Lee EU, McEntee K, Lai PH, Paulson JC (1987) Primary structure of beta-galactoside alpha 2,6-sialyltransferase. Conversion of membrane-bound enzyme to soluble forms by cleavage of the NH2-terminal signal anchor. *J Biol Chem* **262:** 17735-17743

Weiser MM, Wilson JR (1981) Serum levels of glycosyltransferases and related glycoproteins as indicators of cancer: biological and clinical implications. *Crit Rev Clin Lab Sci* **14:** 189-239

Wendeler MW, Paccaud JP, Hauri HP (2007) Role of Sec24 isoforms in selective export of membrane proteins from the endoplasmic reticulum. *EMBO reports* **8:** 258-264

Zanetti G, Pahuja KB, Studer S, Shim S, Schekman R (2012) COPII and the regulation of protein sorting in mammals. *Nat Cell Biol* **14:** 20-28

Zhao W, Chen TL, Vertel BM, Colley KJ (2006) The CMP-sialic acid transporter is localized in the medial-trans Golgi and possesses two specific endoplasmic reticulum export motifs in its carboxyl-terminal cytoplasmic tail. *J Biol Chem* **281:** 31106-31118

Zhuang X, Chowdhury S, Northup JK, Ray K (2010) Sar1-dependent trafficking of the human calcium receptor to the cell surface. *Biochem Biophys Res Commun* **396:** 874-880

8. Abbreviations

AA	Amino acid
Acp2	Acid phosphatase 2
Acp5	Acid phosphatase 5
ADP	Adenosine diphosphate
ALLN	Acetyl-Leu-Leu-Norleucinal
APS	Ammonium peroxydisulfate
ARF	ADP ribosylation factor
ATP	Adenosine triphosphate
BafA1	Bafilomycin A1
BIP	binding immunoglobulin protein
bp	Base pairs
BSA	Bovine serum albumin
°C	Degree celsius
C-terminal	Carboxyl-terminal
cDNA	Complementary DNA
CFBE	Cystic fibrosis bronchial epithelial cells
CFTR	Cystic fibrosis transmembrane conductance regulator
CHX	Cycloheximide
COG	Conserved oligomeric Golgi complex subunits
COPI	Coat protein complex I
COPII	Coat protein complex II
COS-7	CV-1 (simian) in origin, and carrying the SV40 genetic material
DAPI	4',6-Diamidino-2-phenylindole
DMEM	Dulbecco's modified Eagle´s medium
DMSO	Dimethylsulfoxide
DNA	Deoxyribonucleic acid
dNTP	Deoxynucleoside triphosphate
DTT	Dithiothreitol
ECL	Enhanced chemiluminescence
E. coli	Escherichia coli
EDEM	ER degradation enhancing alpha-mannosidase-like proteins
EDTA	Ethylenediaminetetraacetic acid
e.g.	for example
EGFP	Enhanced green fluorescent protein
elF2α	eukariotic initiation factor 2α
Endo H	Endoglycosidase H
ER	Endoplasmic reticulum
ERAD	ER-associated degradation
ERES	ER exit sites
ERGIC	ER-Golgi intermediate compartment
Erp57	ER protein 57
et al	and others
EtBr	Ethidium bromide
E64	L-trans-Epoxysuccinyl-leucylamido(4-guanidino)butane
FBS	Fetal bovine serum

FCS	Fetal calf serum
Fig.	Figure
GARP	Golgi-associated retrograde protein
GDP	Guanosine diphosphate
GEF	guanine nucleotide exchange factor
GFP	Green fluorescent protein
GlcNAc	N-Acetylglucosamin
GlcNAc-1-PD	N-Acetylglucosamin-1-phosphodiesterase
GlcNAc-1-phosphate	N-acetyl-glucosamin-1-phosphate
GM130	Golgi matrix protein 130
GP3ST	β-Gal 3'-sulfotransferase
GPI anchor	Glycosylphosphatidylinositol
GRASP65	Golgi reassembly stacking protein of 65 kDa
GTP	Guanosine-triphosphate
h	Hours
HA	Hemagglutinin
HEK293	Human embryonic kidney cell line 293
HeLa (Henrietta Lacks)	Human cell line from cervical cancer
β-hex	β-hexosaminidase
HRP	Horseradish peroxidase
IB	Immunoblot
IF	Immunofluorescence
IgG	Immunoglobulin G
IP	Immunoprecipitation
IRE1	Inositol requiring kinase 1
kb	Kilo-base pair
kDa	Kilodalton
LB	Lysogeny broth
LD	Luminal domain
LDL	Low density lipoprotein
LIMP-2	Lysosomal integral membrane protein 2
LSDs	Lysosomal storage disorders
M6P	Mannose 6-phosphate
MCS	Multiple cloning site
MEM	Minimal essential medium
ML	Mucolipidosis
µl	Microliters
ml	milliliters
MPR46	Mannose 6-phosphate receptor of 46 kDa
MPR300	Mannose 6-phosphate receptor of 300 kDa
mRNA	Messenger ribonucleic acid
NP40	Nonidet P40
OD	Optical density
PA	Polyacrylamide
PAGE	Polyacrylamide gel electrophoresis
PBS	Phosphate buffered saline
PCR	Polymerase chain reaction
PDI	Protein disulfide isomerase
PERK	PKR-like ER kinase
PFA	Paraformaldehyde

PKR	Double-stranded RNA-activated protein kinase
PMSF	Phenylmethylsulfonyl fluoride
PNGase F	Peptide N-glycosidase F
PPO	2,5-Diphenyloxazole
PT	GlcNAc-1-phosphotransferase
P/S	Penicillin/ streptomycin
RFP	Red fluorescent protein
RNA	Ribonucleic acid
RNC	Ribosome-nascent chain complex
RT	Room temperature
S1P	Site-1 protease
SDS	Sodium dodecyl sulfate
SDS-PAGE	SDS-Polyacrylamide gel electrophoresis
siRNA	Small interfering RNA
SNARE	Soluble N-ethylmaleimide-sensitive factor Attachment Protein REceptor
SOC	Super optimal broth medium with catabolite repression
SR	SRP-receptor
SRP	Signal Recognition Particle
STX10	Syntaxin 10
TAE	Tris-acetate-EDTA buffer
TBS	Tris-buffered saline
TEMED	NNN'N'-Tetramethylethylenediamine
TfR	Transferrin receptor
TGN	Trans-Golgi network
TM	Transmembrane domain
TMD	Transmembrane domain
TRAPP	TRAnsport Protein Particle
Tris	Tris(hydroxymethyl)aminomethane
TRS	TRAPP-subunit
UDP	Uridine diphosphate
UKE	University Medical Center Eppendorf, Hamburg
UPR	Unfolded protein response
UV	Ultraviolet
v/v	volume per volume
Vps52	Vacuolar protein sorting 52 homolog
w/v	weight per volume
×g	Times gravity

9 Appendix

9.1 Results of siRNA screens with CFBE and Hela cells

The results obtained from siRNA knock-down screens in CFBE and HeLa cells are listed in Table 9.1 and 9.2 respectively, with gene names and corresponding relative β-hex activities in media (average of 4 samples, SD: standart deviation). Values are normalized to non-transfected cells set as zero. NH_4Cl-treated and *GNPTAB* down-regulated cells served as positive controls. Medium was used as negative control.

Table 9.1: Enzyme activity of β-hex in media of siRNA-transfected CFBE cells.

Gene	relative activity	relative SD
NH_4Cl	0,908	0,040
COPE	0,815	0,096
NH_4Cl	0,675	0,104
COPG	0,523	0,045
GNPTAB	0,523	0,074
NH_4Cl	0,500	0,060
NH_4Cl	0,491	0,052
GOLGA2	0,477	0,045
GNPTAB	0,477	0,158
SORCS1	0,446	0,049
TRAPPC4	0,364	0,067
COPZ1	0,350	0,087
SCFD1	0,341	0,060
TRAPPC2	0,330	0,089
GNPTAB	0,287	0,072
COPG2	0,277	0,045
B4GALT2	0,262	0,125
TRAPPC3	0,261	0,069
SLC35A1	0,172	0,101
VPS52	0,147	0,100
TRAPPC5	0,136	0,029
HSPA14	0,125	0,051
SORCS3	0,092	0,041
TRAPPC1	0,091	0,085
TRAPPC10	0,091	0,084
STX10	0,086	0,063
STIP1	0,080	0,049
DNAJA1	0,075	0,069
SORCS2	0,062	0,076
SLC35A2	0,046	0,086
HSPA4	0,037	0,027
TRAPPC6A	0,034	0,068
COG2	0,025	0,154
USO1	0,023	0,103
MAN2A2	0,017	0,118
MGAT2	0,017	0,121
B4GALT1	0,015	0,091
SLC35A3	0,015	0,090
HSPH1	0,012	0,060
no siRNA	0,000	0,089
no siRNA	0,000	0,073
no siRNA	0,000	0,116
no siRNA	0,000	0,101
MGAT1	-0,009	0,104
RAB33B	-0,011	0,037
CDC37L1	-0,011	0,035
COG1	-0,013	0,094
ST3GAL2	-0,015	0,069
RAB1B	-0,017	0,118
TRAPPC1	-0,023	0,034
PSMB2	-0,026	0,079
COPB1	-0,031	0,162
GOLGB1	-0,034	0,049
HSPA4L	-0,037	0,027
USE1	-0,043	0,043
STX5	-0,052	0,078
GOLGA5	-0,062	0,057
HSPA8	-0,063	0,028
GORASP1	-0,068	0,029
KIAA1377	-0,068	0,029

RAB6A	-0,068	0,156
COG6	-0,075	0,073
VTI1A	-0,078	0,086
RAB11A	-0,078	0,072
HSPA6	-0,087	0,045
TRAPPC9	-0,091	0,080
COPZ2	-0,100	0,086
PSMC5	-0,112	0,086
BET3L	-0,125	0,079
COG5	-0,125	0,113
RAB1A	-0,129	0,093
HSPA1A	-0,138	0,040
ST3GAL1	-0,147	0,112
HSPA2	-0,163	0,049
VPS53	-0,164	0,143
COG7	-0,167	0,047
HSPB2	-0,169	0,104
COG4	-0,175	0,111
SEC22A	-0,190	0,052
BET1	-0,190	0,085
MAN2A1	-0,198	0,076
STX18	-0,207	0,081
COG3	-0,213	0,152
GOSR2	-0,216	0,141
COG8	-0,238	0,075
ST3GAL3	-0,292	0,165
COPA	-0,323	0,052
HSPA1L	-0,338	0,097
MAN1B1	-0,431	0,130
MAN1C1	-0,492	0,155
FUT8	-0,754	0,148
MAN1A1	-0,785	0,106

Table 9.2: Enzyme activity of β-hex in media of siRNA-transfected HeLa cells.

Gene	relative activity	relative SD
GNPTAB	1,885	0,116
GNPTAB	1,878	0,038
NH_4Cl	1,685	0,148
NH_4Cl	1,663	0,025
GNPTAB	1,658	0,676
NH_4Cl	1,633	0,140
HSPD1	1,604	0,139
GNPTAB	1,581	0,529
NH_4Cl	1,544	0,453
GNPTAB	1,415	0,300
NH_4Cl	1,154	0,401
GNPTAB	0,902	0,373
NH_4Cl	0,704	0,845
DNAJB12	0,682	0,202
SEC63	0,638	0,547
STX10	0,611	0,158
USE1	0,488	0,832
TRAPPC1	0,402	0,312
STUB1	0,367	0,150
ERP44	0,359	0,229
VPS52	0,355	0,202
DNAJB9	0,327	0,096
CANX	0,327	0,037
TMX3	0,309	0,166
EDEM3	0,291	0,237
UGCGL2	0,288	0,210
PDIA5	0,276	0,145
GOSR2	0,267	0,061
DNAJB11	0,232	0,147
VPS53	0,229	0,108
VTI1A	0,223	0,312
TXNDC12	0,221	0,140
HSPA1A	0,214	0,279
MAN1B1	0,208	0,080
CALR	0,187	0,038
FKBP10	0,170	0,202
TXDNC5	0,155	0,062
HSPH1	0,153	0,130
SCFD1	0,139	0,179
PSMB2	0,132	0,197
AGR3	0,127	0,075
ST13	0,123	0,106
DNAJC10	0,122	0,210
TXNDC14	0,120	0,111
HSPA2	0,115	0,109
PDIA2	0,108	0,082
DNAJB8	0,104	0,034
STX18	0,101	0,054
P4118	0,085	0,056
COG1	0,081	0,135
RAB1B	0,076	0,264
HSPA4L	0,076	0,078

DNAJB4	0,056	0,061
LMAN2L	0,051	0,093
COG4	0,050	0,165
HYOU1	0,043	0,073
HSPA1L	0,043	0,199
PDIA6	0,043	0,091
FKBP11	0,037	0,129
DNAJB3	0,034	0,072
HSPA14	0,024	0,191
TRAPPC2	0,023	0,219
KIAA1377	0,022	0,191
FKBP3	0,019	0,234
MAN2A2	0,016	0,145
SLC35A1	0,012	0,188
BET1	0,003	0,126
COG3	0,001	0,324
no siRNA	0,000	0,113
no siRNA	0,000	0,194
no siRNA	0,000	0,036
SCR	0,000	0,364
HSPB8	0,000	0,053
SCR	0,000	0,363
no siRNA	0,000	0,132
COPZ2	-0,003	0,067
SEC22A	-0,004	0,158
MAN2A1	-0,004	0,116
HSPA8	-0,004	0,036
C20RF30	-0,004	0,043
ERO1LB	-0,018	0,102
TRAPPC1	-0,018	0,270
DNAJA2	-0,018	0,061
GORASP1	-0,020	0,326
FKBP6	-0,021	0,132
DNAJB1	-0,025	0,115
HSPA6	-0,026	0,056
ACP5	-0,026	0,039
COPZ1	-0,031	0,083
LMAN2	-0,032	0,151
HSPB2	-0,039	0,040
DNAJB7	-0,040	0,052
CLASP	-0,043	0,043
RAB1A	-0,045	0,097
HSP90B1	-0,045	0,072
DNAJA4	-0,047	0,057
LMAN1	-0,047	0,144
ERP27	-0,054	0,073

DNAJB2	-0,055	0,097
AGR2	-0,057	0,135
DNAJC1	-0,076	0,152
ERP29	-0,083	0,136
MGAT1	-0,089	0,164
HSPA4	-0,092	0,124
RAB11A	-0,094	0,172
COG2	-0,096	0,152
FKBP1B	-0,099	0,067
HSPA5	-0,101	0,114
DNAJB5	-0,101	0,059
ST3GAL1	-0,102	0,238
COG6	-0,107	0,058
COPB2	-0,108	0,199
TXNDC1	-0,115	0,057
B4GALT2	-0,116	0,134
DNAJA3	-0,132	0,096
TRAPPC3	-0,134	0,271
DNAJA1	-0,138	0,085
COG5	-0,150	0,129
USO1	-0,156	0,205
COPE	-0,178	0,197
PSMC5	-0,189	0,088
RAB33B	-0,201	0,209
TMX4	-0,203	0,147
HSPB6	-0,210	0,030
TRAPPC10	-0,212	0,131
MGAT2	-0,216	0,088
MAN1A1	-0,218	0,126
ST3GAL2	-0,227	0,111
MAN1C1	-0,239	0,226
TRAPPC4	-0,249	0,044
COPG	-0,253	0,278
EDEM2	-0,254	0,126
SORCS2	-0,264	0,340
TRAPPC6A	-0,267	0,057
COG7	-0,272	0,059
SLC35A3	-0,275	0,125
ST3GAL3	-0,278	0,083
COG8	-0,280	0,043
GOLGA5	-0,289	0,066
SLC35A2	-0,294	0,085
SORCS3	-0,303	0,157
TRAPPC9	-0,325	0,059
TRAPPC5	-0,339	0,095
BET3L	-0,345	0,114

CDC37L1	-0,358	0,133
STX5	-0,359	0,204
FUT8	-0,374	0,307
B4GALT1	-0,381	0,186
STIP1	-0,381	0,083
EDEM1	-0,403	0,058
COPA	-0,406	0,147
GOLGA2	-0,418	0,147
COPG2	-0,436	0,048
RAB6A	-0,482	0,120
GOLGB1	-0,487	0,248
COPB1	-0,612	0,216
blank	-0,898	0,013
blank	-0,913	0,069
blank	-0,915	0,043
blank	-0,920	0,117
blank	-0,921	0,030
blank	-0,938	0,062

9.2 Publications and conference contributions

9.2.1 Publications

Franke, M., Braulke, T., and Storch, S. (2013) Transport of the GlcNAc-1-phosphotransferase alpha/beta-subunit precursor protein to the Golgi apparatus requires a combinatorial sorting motif. *J Biol Chem* **288:** 1238-1249

9.2.2 Oral presentations

Franke, M., Structural requirements for the anterograde transport of the GlcNAc-1-phosphotransferase α/β-subunit precursor from the ER to the Golgi apparatus, GRK1459 Retreat, Westerland, October 2011.

Franke, M., Structural requirements for the anterograde transport of the GlcNAc-1-phosphotransferase α/β-subunit precursor from the ER to the Golgi apparatus, GRK1459 Retreat Wedel, October.2013

Franke, M., Decreased Golgi retention and lysosomal degradation of mutant GlcNAc-1-phosphotransferase α/β-subunit precursor proteins, GRK1459 Retreat Wismar, 27.10.2013

Stephan Storch, **Franke, M.**, Transport of the GlcNAc-1-phosphotransferase α/β-Subunit Precursor Protein to the Golgi Apparatus Requires a Combinatorial Sorting Motif, "The Multitasking Endoplasmic Reticulum in Health and Disease", Warrenton, Va, USA (presented by Stephan Storch).

9.2.3 Poster presentations

Franke, M., and Storch, S. (2011) Anterograde transport of GlcNAc-1-phosphotransferase to the Golgi apparatus is mediated by a complex sorting motif, 34th Annual Meeting of the German Society for Cell Biology, Bonn, Germany

Franke, M., Braulke, T., and Storch, S. (2011) Anterograde transport of GlcNAc-1-phosphotransferase to the Golgi apparatus is mediated by a complex sorting motif, 18th workshop of European Study Group on Lysosomal Diseases, Långvik, Finland

Franke, M., Braulke, T., and Storch, S. (2012) Transport of the GlcNAc-1-phosphotransferase alpha/beta-subunit precursor protein to the Golgi apparatus requires a combinatorial sorting motif. "Trafficking in Health and Disease", Hamburg, Germany

Franke, M., Braulke, T., and Storch, S. (2013) Transport of the GlcNAc-1-phosphotransferase α/β-Subunit Precursor Protein to the Golgi Apparatus Requires a Combinatorial Sorting Motif, "The Multitasking Endoplasmic Reticulum in Health and Disease", Warrenton, Va, USA

9.2.4 Conference attendance

"Lysosomes", September 2011, Hamburg, Germany.

San Diego Glycobiology Symposium, January 2013, San Diego, CA, USA

Acknonowledgements

Danksagung

Meinem Doktorvater PD Dr. Stephan Storch und Prof. Dr. Thomas Braulke möchte ich für die Bereitstellung des Themas, die hervorragende Betreuung, viele anregende Diskussionen und die kritische Durchsicht meiner Arbeit danken.

Dr. Edgar Kramer danke ich für die Begutachtung meiner Arbeit.

Prof. Dr. William E. Balch und Dr. Chris Baskerville danke ich für das Praktikum und die hervorragende Betreuung. Sowie der gesamten Arbeitsgruppe Balch.

Marcus Wurlitzer vom Institut für Klinische Chemie danke ich für die massenspektrometrische Analyse.

Ich danke meinem Labor für die gute Zeit und ihre Unterstützung. Danke, Angela, Benjamin, Carolin, Jessica, Johannes, Katrin und Katrin, Laura, Lisa, Marisa, Melanie, Pieter, Raffa, Sandra und Sandra und Sarah! Und ganz besonders Gio- Deine immergute Laune hat mich aus manchem Tief gerettet!

Meiner Familie, die immer für mich da war und mich unterstützt hat! Annem, kardesim ve tüm aileme herzaman yanimda ulduklari icin tesekür ederim! Und ganz besonders Klaas!